CRANFIELD UNIVERSITY

SCHOOL OF MECHANICAL ENGINEERING

Department of Fluid Engineering and Instrumentation

TOTAL TECHNOLOGY

PhD THESIS

Academic year 1991-1994

T AMARE

ELECTROMAGNETIC FLOWMETER FOR DIELECTRIC LIQUIDS

Supervisors: Professor M L Sanderson and Dr J Hemp

July 1995

ABSTRACT

Experimental investigation and theoretical analysis of an electromagnetic flowmeter designed for use with dielectric liquids has been carried out.

An extensive survey of the industrial users of flowmeters has been made, involving the participation of over 47 companies, which provides information about the current industrial use, attitudes and attributes of electromagnetic and other types of flowmeters.

The design of the flowmeter is mainly concerned with overcoming the charge noise that is associated with the flow of dielectric liquids so as to effectively detect the weak flow signal. It is shown that the working of the flowmeter depends heavily on the design of the eddy current free electrostatic shield. The result of the mathematical analysis of the design is a simplified formula for predicting the sensitivity of the meter. It is adjusted to take account of such factors as end-effects and electrical properties of the flow conduit of the meter.

Experimental results show that not only an induction flowmeter based on Faraday's principle is possible but also the measured values of the flow signal closely matches those obtained from the formula. It is suggested that the formula can be generalised to include moderately conducting liquids which is supported by results achieved from experiments on water. Finally, recommendations for future work are put forward for further improvement of the design.

ACKNOWLEDGEMENTS

The author is highly indebted to Dr J Hemp for his continuous support throughout the project including the preparation of this thesis.

The author also thanks Professor M L Sanderson for his guidance and input in solving the practical problems encountered during the research.

The author appreciates highly the role played by Engineering and Physical Science Research Council and Schlumberger Cambridge Research Ltd. who, between them, sponsored the work.

Especial thanks are due to D MacLeod who gave considerable assistance to the author with the electronics design part of the project. Dr G Oddie also proved an invaluable source of information particularly in the production of the electrostatic shield.

The author express gratitude to C Evans for his work in building the flow rig and making other bits and pieces associated with the flowmeter. The author also acknowledges the part played by Dr R Dowdeswell to draw illustrative diagrams. In addition, especial thanks are due to J Ovens, Miss K Smith and to members of the department of fluid engineering and instrumentation.

Finally, the author wishes to dedicates this work to his family, in particular to Samuel and Mike Amare for their brotherly love.

CONTENTS

LIST OF TABLES

LIST OF FIGURES

NOMENCLATURE

B	Magnetic flux density
C	Capacitance
D	Diffusion coefficient
D_T	Turbulent diffusion coefficient
E	Electric field
F	Force
f	Frequency
G_o	Open loop gain
H	Magnetic field intensity
I	Direct current (dc)
i	Alternating current
J	Current density
J_n	Bessel function of the n order
$j_{1,n}$	The first zero of J_n
j	Complex variable (= $\sqrt{-1}$)
L	Inductance
M	Magnetization
p	polarization
q	charge
R	Resistance

S_m Magnetic shielding ratio

S_e Electrostatic shielding ratio

U Electric potential (dc)

u Electric potential (ac)

v Velocity

X_C Reactance of a capacitance

X_L Reactance of an inductance

Y Admittance

Z Electromagnetic flowmeter attenuation factor

δ Laminar sublayer

ε Dielectric constant

ε_o Dielectric permittivity of free space

η Dynamic viscosity

Θ Atoms or elements magnetic moment

λ Debye length

λ_T Debye length for a turbulent flow

μ Magnetic permeability

μ_o Magnetic permeability of free space

ρ Resistivity

σ Electrical conductivity

ς Zeta potential

T Friction factor

τ Relaxation time

ϕ	Magnetic scalar potential
ω	Angular frequency
ϱ	Density
φ	Magnetic flux

1.0 INTRODUCTION

1.1 Background to the research

Electromagnetic flowmeters are successfully used in a wide range of applications including in medicine and the water industry. The basis for these applications is Faraday's law of induction (Faraday, 1832), which is the generation of an electric field E within a medium moving at a velocity v across an externally applied magnetic field B. At first, this was thought to apply only to conducting media. However, in 1904, nearly six decades after Faraday's initial observation, Wilson proved that it is equally applicable to dielectric fluids.

The magnitude of the induced effective electric field is $|E| = |v \times B|$ It is therefore directly proportional to the fluid velocity and this is the basis of the flowrate measurement. In practice, though, it is not the electric field which is measured but differences in the associated potential U due to charge redistribution or polarisation.

The potential in an electromagnetic flowmeter varies with the electromagnetic properties of the flowing liquid. For insulating liquids, such as hydrocarbons, it is small compared with the associated noise. As a result an electromagnetic flowmeter suitable for use with these liquids has not yet been designed. However, as it is a non-intrusive device there is great interest in the possibility of electromagnetic flowmeters in particular in the petroleum and petroleum based product industries.

1.2 Objectives

A measure of suitability of an electromagnetic flowmeter for general applications is its

electrical conductivity range. At the moment the lowest possible conductivity (σ) of liquid that can be handled by an electromagnetic flowmeter is that of deionized water ($\sigma \approx 4\times10^{-4}$ Siemens/metre).

The objective of this research has been to design an electromagnetic flowmeter which can be used with dielectric liquids or liquids with $\sigma < 10^{-4}$ S/m. It has involved the investigation of design problems, in particular noise generated by the movement of charges which arise in connection with the flow of these liquids, and looking into ways of overcoming them as well as mathematical analyses. As part of the management programme of the PhD, a survey of industrial flowmeters has also been done to assess the users opinion of reliability and accuracy of electromagnetic flowmeters in comparison with other flowmeters.

Non-polar organic liquids with low dielectric permittivities and very small electrical conductivities are poorly conducting dielectrics. Most commonly such liquids are petroleum based products, such as hydrocarbons, with conductivities less than 10^{-9} S/m. However, liquidified gases or cryogenics (for instance liquid Helium) whose natural electrical conductivity lies between that of polar liquids (such as deionized water) and petroleum based products, are increasingly being used in industry.

1.3 Thesis layout

Chapter 2 starts by describing the aim and general overview of the market survey for flowmeters. A detailed explanation of the questionnaire is followed by the analysis of the results. The chapter ends with concluding remarks on the survey and its relevance to the technical work.

The results of a literature survey on the theoretical and practical design of electromagnetic flowmeters for dielectric liquids are discussed in chapter 3.

Chapter 4 provides an introduction to charge phenomena in a pipe flow. It also examines the effect charges have on electromagnetic flowmeters and possible ways of minimizing the quantity or magnitude of these charges.

Chapter 5 sets out design considerations for a flow rig suitable for dielectric liquids. It also includes description of the experimental flow circuit along with a list of properties of BP dielectric 180 oil.

A device developed to measure the electrical conductivity of BP dielectric 180 is described in detail in chapter 6. A theoretical analysis of the design is offered and comparisons are made with commercially available low conductivity measuring cells. In addition, a technique to determine the permittivity of BP 180 is discussed.

Chapter 7 contains a comprehensive description of the electromagnetic flowmeter designed to be applicable to dielectric liquids. Apart from setting out the general design considerations and a detailed description of each part of the flow meter, it also outlines factors affecting the choice of the frequency of the alternating magnetic field and practical problems encountered during the testing of the flowmeter.

The theoretical analyses of the flowmeter are given in chapter 8. The topics covered in this chapter include estimation of the flowmeter signal, equivalent circuit for the meter and its internal impedance. In all cases mathematical formulas are derived, with the help of realistic assumptions on the geometry as well as on the physical sizes of parts of the meter, to approximate their magnitudes.

Chapter 9 covers the experimental side of the research, describing the procedures which were used and presents the results obtained. The relationship between the theoretical and the experimental work is also discussed.

The 10th and final chapter of the thesis outlines the conclusions drawn from the research and presents recommendations for further work.

2.0 MARKET SURVEY

2.1 Introduction

As part of the management side of the research programme, a letter together with a questionnaire was sent to 110 flowmeter user companies in UK at the end of the second year (see Appendix A).

The response was quite considerable: 47 replies, containing information on a total of about 397,425 flowmeters were received. In the remainder of this chapter, the layout of the questionnaire, the survey results and its relevance to the technical work are discussed. The results are analyzed with the help of tables and graphs; a summary of which has been sent, upon request, to the participating companies.

2.2 The survey questionnaire

The key to a market survey is the setting out of the questionnaire. It should contain all the required questions, yet should also be concise, easy to understand, self explanatory and have as few pages as possible.

The survey questionnaire for this research programme, given in Appendix A, was based around the answers to the following questions:

(i) -What type of liquids were the flowmeters used to measure?

(ii) -Which information on the flowmeters was of interest for the survey?

(iii)-Which features of the flowmeters were the opinion of the users required?

Since the research is in to developing an electromagnet flowmeter suitable for poorly conducting liquids, but with the possibility of adopting it for moderately conducting liquids, the survey had to be on water and water related products (such as waste water), petroleum and petroleum products, and liquid petroleum gases or cryogenics. This meant that the survey would be sent to companies which produce or use these liquids. The survey was anonymous. To encourage companies to reply to the survey, questions regarding their activities were restricted to identifying the sector of industry they were in and the types of liquid for which they monitored the flowrate (refer to question 1 and 2).

To simplify and shorten the questionnaire, a table identifying the main items related to the flowmeters was drawn (see question 2). The companies were persuaded on the questionnaire to provide all the necessary information and, if they could, to elaborate and to add more information on the items.

The most important part of the survey was finding out the users perception of different types of flowmeter. Hence, their opinion was sought on the features of their flowmeter and factors affecting their decision when purchasing (refer to question 4 and 5).

2.3 The survey results

Out of the 47 replies: 42 of the questionnaires were returned with all the questions answered, however, in the remaining 5 only one or two of the questions were completed.

Explanation on the interpretation of the tables and figures referred to in this section, when necessary, is given under the tables and figures sections respectively.

In the analysis of the questionnaire, the users were divided in to three groups depending on the number of flowmeters recorded on the form: There were 15 "small" users having fewer than 50 meters each, 14 "medium-size" users with between 50 and 500 meters each and 13 "large" users owning more than 500 meters each (see table 2.1). It should be noted that, in general, a "user" corresponds to a particular site or to an individual's area of responsibility, rather than to an entire company.

Positive displacement is by far the most widely used flowmeter with 71 %, followed by turbine or rotary inferential with 22 % of the total number of meters in use (see figure 2.1). From the outset, it looks as if these meters have held, even increased, their market share contrary to the predicted decline by a number of previous surveys like Higham (1985) and Halsey (1986). However, the main reason behind the rise of in market share of these flowmeters is the privatization of service industries; especially of water. Three of the nine major regional water companies have started introducing water meters for customer billing and this trend is expected to continue. Since positive displacement and turbine or rotary inferential flowmeter do not need electric power, they are seen to be cheap and ideal for customer billing. As the questioner is about flowmeters in use, without distinguishing between customer billing and industrial flow monitoring, the number of flowmeters recorded proves the effect of privatization (see table 2.2). Even though there were only 10 replies from a single site or sub-section of 6 of the regional water companies, they recorded 95% of the total number flowmeters in the survey (refer to table 2.3 and figure 2.2). Follow up discussions with some of the participants of the survey indicates that the market share of positive displacement, turbine or rotary inferential and differential pressure meters for industrial flow monitoring is still in decline. In the water industry, they are being replaced by electromagnetic and ultrasonic flowmeters.

Differential pressure and positive displacement with 54.6 % and 38.4 % of the total number of meters respectively dominate flow measurement of petroleum and petroleum products. They also hold 45 % and 47 % of the number of flowmeters in use for cryogenics or liquid petroleum gas (see table 2.4 and figure 2.3 (a), (b) and (c)). It is

worth mentioning here that the only other flowmeter type recorded outside of the given choices on the questionnaire was the thermal mass flowmeter.

Positive displacement and turbine or rotary inferential flowmeters are considered to be accurate, reliable, easy to operate and carry great confidence of users (see figure 2.4 (a), (b), (c) and (d)).

Most users do not consider price, brand loyalty or recommendation as critical factors when making decisions to purchase new flowmeters (see figure 2.5). Other factors, in addition to those in the questionnaire, include site compatibility, availability of spare parts if required, the simplicity of maintenance and ease of meter reading.

The commonest diameters and flowrates are 1 to 5 inch and 1 to 20 litres/second respectively. Maintenance is carried out mainly by skilled in house persons on average between 6 to 12 months. Since the majority of the flowmeters have been in use for three or more years, it is difficult to quote the purchase cost. However, the annual running cost on average varies from £200 to £500 each including maintenance, service and power cost depending on the type of flowmeter.

2.4 Conclusions from the market survey

From a detailed analysis of the questionnaire and the follow up discussions with some of the participants of the survey, the following conclusions can be drawn:

(1) - Positive displacement and turbine or rotary inferential meters dominate the market in usage for continuous flow measurement.

(2) - Follow up disscusions indicate that electromagnetic and ultrasonic meters are increasing their market share in industrial flow monitoring.

(3) - Generally, reliability and accuracy are the major factors in meter selection. Although ease of maintenance ranks just as high for proportionally high number of small users.

(4) - Large users have a wide spread variety of flowmeter types.

2.5 Relevance of the survey to the technical work

As all electromagnetic flowmeters are non-intrusive, they are ideal for continuous flow monitoring; hence their increased use in industry, especially for water. Figure 2.4 also shows electromagnetic flowmeters are consistently the second best to the long established positive displacement and turbine or rotary inferential meters in users appraisal on accuracy, reliability, confidence and ease of operation. This is despite the fact that electromagnetic flowmeters are used in water and water related products like spirit, and these industries constitute only 35 % of the survey.

The survey establishes the good base the electromagnetic flowmeter has in industrial flow monitoring, and this could be improved further by the design of an electromagnetic flowmeter suitable for "insulating" liquids. The motivation is clearly to expand the range of electromagnetic flowmeters to cover petroleum, petroleum products and liquid petroleum gases.

3.0 LITERATURE SURVEY

3.1 Introduction

The basic arrangement for an electromagnetic flowmeter is shown in figure 3.1. When a moderately conducting liquid flows at a velocity v across a magnetic field B, any charge q in the liquid experiences the Lorentz force (the total electric and magnetic force):

$$\underline{F} = q(\underline{E} + \underline{v} \times \underline{B})$$

which is the source of the flow related potential (Δu).

A number of papers are available on the general theory of electromagnetic flowmeter (Williams (1930), Kolin (1945), Astely (1952), Bevir (1969)). However, the most comprehensive treatment of the subject is given by Shercliff (1962). The remaining sections of this chapter describe the results of previous attempts, theoretical as well as practical, to develop an electromagnetic flowmeter suitable for dielectric liquids.

3.2 Literature survey

H.A. Wilson (1904) carried out the first experiment of its kind in which a dielectric hollow cylinder (made of ebonite) rotated at high speeds inside a large solenoid designed to produce a strong magnetic field parallel to the axis of the cylinder. The induced signal in the ebonite cylinder was picked up by two metal cylinders attached

to its inner and outer surfaces (the electrodes). The signal generated was measured using a quadrant electrometer. Wilson used direct current to excite the solenoid and he observed the flow induced signal every time he reversed the direction of the field. From the results, he concluded that an induced potential as described by Maxwell and developed by Lorentz should be produced in a dielectric and should be equal to the potential that would be induced in a conductor multiplied by the factor $1 - \varepsilon^{-1}$; Where ε is the dielectric constant..

The relation between the electric potential that arises in connection with the induced electric field of an electromagnetic flowmeter and the electrical properties of the fluid being measured was further investigated by Cushing (1958). For a circular pipe electromagnetic flowmeter with point electrodes and alternating magnetic field B (see figure 3.2) ; he estimated the induced potential u to be governed by

$$\nabla^2 u = ZB\frac{dv(r)}{dr}\cos\theta \qquad 3.1$$

where $v(r)$ is the flow velocity and

$$Z = \beta + j\varsigma, \qquad 3.2$$

$$\beta = \frac{1+(\frac{\omega\varepsilon_o}{\sigma})^2\varepsilon(\varepsilon-1)}{1+(\frac{\omega\varepsilon_o\varepsilon}{\sigma})^2}, \qquad 3.3$$

$$\varsigma = \frac{\frac{\omega\varepsilon_o}{\sigma}}{1+(\frac{\omega\varepsilon\varepsilon_o}{\sigma})^2}. \qquad 3.4$$

for a fluid of dielectric constant ε and conductivity σ.

The boundary conditions and assumptions for the analysis, along with a detailed mathematical derivation of equation 3.1 are given in appendix B.

From equations 3.2 to 3.4 it is noticeable that the flowmeter attenuation factor (Z) is dependent only on the induction frequency ($\omega = 2\pi f$), electrical conductivity and the dielectric constant of the liquid. For a low frequency magnetic field, say $f = 2\ kHz$, Z approximates to $1 - \varepsilon^{-1}$ for poorly conducting liquids; which confirms Wilson's result.

This result was also indirectly confirmed by Head (1959) when he reported that the induced potential of an electromagnetic flowmeter is not dependent on conductivity for poorly conducting liquids following his experiments on a number of types of liquid with different conductivities.

Cushing (1965) proposed a design for an electromagnetic flowmeter based on a capacitive signal pick-off which is suitable for both moderately conducting and poorly conducting liquids. It consisted of a wide area detection electrode placed so as to touch the flowing liquid and a driven shield that is held at the same potential as the detection electrode by a buffer amplifier. Both electrodes were formed within the walls of a fibre glass pipe. In his summary on the experimental results he indicated that he was not satisfied with the zero line stability of the flowmeter. Later, Cushing (1966) patented the design and re-patented an improved version (1967) in which he suggested selection of the induction frequency based on the type of liquid measured to minimize the effect of the flow associated electrostatic charge. The experimental result for the improved design is not available.

Both Cushing (1971) and Hentschel (1973) reported that the movement of electrostatic charges generated by the flow of dielectric liquids appears as a random noise across the electrodes of an electromagnetic flowmeter, and the frequency spectrum of this noise shows a distinct low frequency characteristic. Electrostatic charge noise, they reasoned, is the major obstacle to the development of an effective electromagnetic meter.

Zosimov (1979) published a theoretical and practical design analyses of a combined electric and magnetic field contactless electromagnetic flowmeter for dielectric liquids. In the case of a flow of a dielectric medium in crossed variable electric and magnetic fields there is an energy transfer from the source supplying the magnetic field to the source supplying the electric field. The energy transfer, from Zosimov's description, is proportional to the velocity of the dielectric and to the volume of dielectric in the crossed fields, and depends on the phase relationship between the oscillations of the two fields. He argued that the energy transfer effect can be used to improve the sensitivity of the flowrate measurements. However, no experimental result of any kind for this type of flowmeter is available.

Expanding the work done by Cushing (1958), Bevir (1969) and Engl (1970, 1972); Al-Rabeh, Baker and Hemp (1978) described the governing equations for an electromagnetic flowmeter applicable to poorly conducting liquids. The paper outlines the general expression and condition of validity of potential sensing for the meter in relation to velocity and magnetic field distribution. It is an adequate reference to the theoretical principles behind the design of this type of flowmeter.

Al-Rabeh (1981) repeated Wilson's experiment and arrived at the same conclusion. He then went on to design an axial current geometry type meter. Despite the shortcomings of the design, such as flow obstruction, he recorded a flow related signal for transformer oil. However, the zero line was unstable.

In recent years, two internal reports from Schlumberger suggest experiments carried out on a capacitive signal pick-off meter resulted in mixed results. Codazzi and Mioque (1986) indicated that a flow related signal for transformer oil was observed only for flowrates under 1.5 metre/second because of charge noise; whereas Barnes (1991) reported that no flow induced signal was detected and attributed the failure to the form of the electro-magnetic excitation employed and the flow induced noise.

4.0 CHARGING PHENOMENA IN PIPE FLOW

4.1 Introduction

The electrification of dielectric liquids during pipeline flow is due to the formation and the subsequent separation of the electrical double layer at the interface between the liquid and the pipe wall. This double layer leads to the observation of a streaming current made up of the moving charges, and expressed as

$$I_s = \pi d \int qv dy \qquad 4.1$$

where q is the charge density in the fluid, v is the axial velocity, d is the pipe radius and y is the distance from the wall.

Klinkenberg and Van Der Minne (1958) described the occurrence of a streaming current in hydrocarbons, and the measured value from their experiments shows it to be a few nano amperes. In addition, they illustrated that the type of flow, either laminar or turbulent, affects the size of the streaming current.

4.2 Basic Equations of charging in pipe flow

A simple physical model, but one that contains all the essential phenomena, for charging in pipe flow is given by Abedian and Sonin (1982). This makes various assumptions but is more tractable than models employed by other authors. According to this model, the governing equations are the equation of charge conservation

$$\frac{\partial q}{\partial t}+\nabla\cdot\underline{J}=0 \qquad 4.2$$

the current density $\underline{J}$ being given in the small-charge density approximation by

$$\underline{J}=q\underline{v}-D\nabla q-\sigma\nabla U \qquad 4.3$$

and Poisson's equation for the electric potential

$$\nabla^2 U=-\frac{q}{\varepsilon_o\varepsilon} \qquad 4.4$$

where $\underline{v}$ is the bulk flow velocity, D is the average molecular diffusion coefficient, U is the electric potential, ε and σ are the fluid's dielectric constant and conductivity respectively.

According to Abedian and Sonin (1982) at the wall of the pipe the charge density is constant for a given chemical composition of the liquid and the wall material. Different degrees of absorbtion of the positive and negative ions of the liquid into the wall gives rise to a certain charge density $q = q_w$ = constant on the liquid side of the liquid/wall interface.

Substituting for $\underline{J}$ in equation 4.2 from 4.3 and combining the result with 4.4, the following expression can be obtained for q

$$\frac{\partial q}{\partial t}+\underline{v}\cdot\nabla q-\nabla\cdot(D\nabla q)+\frac{\sigma}{\varepsilon_o\varepsilon}q=0 \qquad 4.5$$

In steady turbulent flow the velocity (v), the charge density (q) and the potential (U) have time averaged and fluctuating parts. For an incompressible fluid (which is true

for most dielectric liquids) $\nabla v=0$, and the turbulent flow introduces its own diffusion represented by D_T (turbulent diffusion factor). If a bar on top (-) is used to represent time averaged quantities and a prime (') the fluctuating part, equation 4.5 can be rewritten as

$$\frac{\partial q'}{\partial t}+\bar{\underline{v}}\cdot\nabla\bar{q}+\bar{\underline{v}}\cdot\nabla q'+\underline{v'}\cdot\nabla\bar{q}+\underline{v'}\cdot\nabla q'-\nabla\cdot(D\nabla\bar{q}+D\nabla q')+\frac{\sigma}{\varepsilon_o\varepsilon}(\bar{q}+q')=0 \qquad 4.6\text{ (a)}$$

and

$$\overline{q'\underline{v'}}=-D_T\nabla\bar{q} \qquad 4.6\text{(b)}$$

4.2.1 The mean charge distribution in fully developed flow

The time averaged parts of equation 4.6 are

$$\bar{\underline{v}}\cdot\nabla\bar{q}-\nabla\cdot((D+D_T)\nabla\bar{q})+\frac{\sigma}{\varepsilon_o\varepsilon}\bar{q}=0 \qquad 4.7\text{(a)}$$

$$\nabla^2\bar{U}=-\frac{\bar{q}}{\varepsilon_o\varepsilon} \qquad 4.7\text{(b)}$$

$$\bar{q}=q_w \text{ , at the wall.} \qquad 4.7\text{(c)}$$

Equations (4.7) have been solved for $\bar{q}$ using simplified expressions for v and D_T representing fully developed velocity profiles and turbulent diffusivities for flow in an infinitely long perfectly smooth cylindrical pipe of uniform material (Abedian and Sonin, 1982). Three characteristic lengths λ, λ_T and δ are important for describing

the form of the charge distribution $\bar{q}(y)$ where y is the distance from the wall (see figure 4.1(a)).

The Debye length (λ) is the characteristic thickness of the charge layer in the liquid near the wall under no flow conditions. It is given by

$$\lambda = \sqrt{\frac{\varepsilon_o \varepsilon D}{\sigma}} \qquad 4.8$$

δ measures the thickness of the laminar sublayer near the wall for which simple order of magnitude expression is

$$\delta = \frac{\eta}{\varrho v_*} \qquad 4.9$$

where η and ϱ are the liquid's viscosity and density respectively and v_* is the friction velocity related to friction factor T and mean pipe velocity $\bar{v}$ by

$$v_* = \bar{v}\sqrt{\frac{T}{2}} \qquad 4.10$$

The charge distribution at the liquid/wall interface is a result of an equilibrium between charge relaxation and diffusion. The relaxation time of a liquid is dependent on its electrical properties, and is expressed as

$$\tau = \frac{\varepsilon_o \varepsilon}{\sigma} \qquad 4.11$$

If $\lambda^2 < \delta^2$ the charge is almost entirely contained to a region within a distance $\sim\lambda$ of

the wall and distributed in the same way as under the conditions of zero liquid velocity (see figure 4.1(b)), *i.e.* according to the expression

$$\bar{q}(y)=q_w e^{-\frac{y}{\lambda}} \qquad 4.12$$

which can be derived from 4.7(a). The electric potential (assumed zero far from the wall) is, from 4.7(b)

$$\bar{U}=-q_w\frac{D}{\sigma}e^{-\frac{y}{\lambda}} \qquad 4.13$$

The value of $\bar{U}$ at the wall (the ζ-potential) is thus related to q_w by

$$\zeta=-\frac{Dq_w}{\sigma} \qquad 4.14$$

If $\lambda^2 \gg \delta^2$, as is the case for most insulating liquids, the charge layer penetrates into the region of eddying flow and charge is mixed into the core of the flow producing a flatter distribution which rises up to q_w approximately according to equation 4.12 within a distance $\sim\delta$ from the wall (see figure 4.1(c)).

For $y > \delta$ the molecular diffusivity D is replaced by the much higher turbulent diffusivity D_T which is in the core of the flow ($\delta < y \leq a$, where a is the tube radius, refer to figure 4.1(a)) . Hence

$$\lambda_T=\sqrt{\frac{\varepsilon_o \varepsilon D_T}{\sigma}} \qquad 4.15$$

which is $> \lambda$.

For a feeling of the order of magnitude of the characteristic lengths and other quantities expressed in this section, refer to a report by Hemp, Spendel and Lochhead (1987).

4.2.2 Fluctuations in the charge distribution and potential

In principle the fluctuations q' in the charge distribution could be found from equation 4.6. Hence subtracting equation 4.7(a) from 4.6

$$\frac{\partial q'}{\partial t}+\bar{\underline{v}}\cdot\nabla q'+\underline{v}'\cdot\nabla\bar{q}+\underline{v}'\cdot\nabla q'-\nabla\cdot(D\nabla q')+\nabla\cdot(D_T\nabla\bar{q})+\frac{\sigma}{\varepsilon_o\varepsilon}q'=0 \qquad 4.16$$

and from equation 4.12

$$q'=0, \quad \text{at the wall.} \qquad 4.17$$

In theory, equations 4.16 and 4.17 could be solved for q' assuming $\bar{\underline{v}}$, $\bar{q}$ and $\underline{v}'$ are given.

Once q' is known the fluctuation potential U' could be found using

$$\nabla^2 U'=-\frac{q'}{\varepsilon_o\varepsilon} \qquad 4.18$$

and suitable boundary conditions.

In practice it is difficult to find q' and U'. This is because of external contaminants such

as oxygen affecting the electrical properties of the liquid, difficulty in obtaining $\underline{v}'$ and the complexity of the equations for either analytical or numerical analysis.

4.3 Effects of charges on an electromagnetic flowmeter

When charge separation occurs in a pipe flow, the "fixed" charge remains at the wall and the "drifting" charge moves with the liquid. The polarity of the "fixed" and the moving charge depends on the electrochemistry between the pipe material and the liquid. However, as yet it is impossible to identify and quantify the deciding parameter(s) or element(s) of the electrochemistry. One of the reasons for this may be because of the fact that conduction in most dielectric liquids, for instance hydrocarbons, is due to the presence of impurities in the liquid. Most impurities, like dissolved oxygen and its ions, are difficult to avoid.

Nakano and Tanaka (1990) reported that for hydraulic oil the liquid and the wall become negatively and positively charged respectively. But it is known that charge reversal can occur. Furthermore, the conductivity of the liquid increases with usage thereby reducing the density of the charge as expressed in equation 4.13.

The electrodes of an electromagnetic flowmeter detect the flow induced charges. These charges appear as a noise signal thereby contaminating the flow signal. The fluctuating part of the charges, particularly, resemble random white noise at low frequencies and are the main cause of the failure of signal purity in electromagnetic flowmeters for dielectric liquids. The lower the conductivity the higher the charge density, hence, the lower the signal to noise ratio. The noise appears to have low frequency and wide bandwidth as will be shown in chapter 7. Clearly this puts constraints on the frequency of excitation of the magnetic field and the operational bandwidth of electromagnetic flowmeters. High frequency and narrow bandwidth will be the obvious choice, but this has its own drawbacks. At high frequencies the eddy current loss is considerable as will

be seen in chapter 7, and driving the coils for the magnetic field can be difficult. A very narrow bandwidth increases the quality factor of the required filter to the point where it is impossible to achieve in practice. Hence realistic compromise design criteria should be set.

4.4 Possible ways of minimizing the tribo-electric noise

For an electromagnetic flowmeter to work with insulating liquids the magnitude of the (processed) tribo-electric noise must be very small compared to (preprocessed) the flow signal. Reducing the noise at the source is preferable as it makes the application of signal processing techniques for further reduction at a later stage easier. Brief descriptions of three possible ways of minimizing the tribo-electric noise are given. The three methods are:

(1)- Charge injection,

(2)- Boundary layer control,

(3)-Chemical additives.

4.4.1 Charge injection

Charge injection is used to measure charge mobility, and investigate breakdown phenomena in dielectric liquids (Gallagher, 1975). Since the "natural" conductivity of dielectric liquids is generally very small and irregular, controlled transient external excitation is applied to enhance the normal charge density to make the measurement of charge mobility easier. For breakdown, charge is injected continuously until a surge of

high current starts to flow or the liquid "conducts" (breaks down). In both cases, the liquid is static, *i.e.* no movement or flow is involved.

Charge injection as a means of minimizing charging in a pipe flow is a slightly different concept. The objective here is to minimize the charges which are detected by the electrodes of an electromagnetic flowmeter. It may be achieved by injecting charges opposite in sign to those flowing with the liquid. For instance, negative charges flowing with the liquid can be "neutralized" by injecting positive ones. A control mechanism to identify not only the polarity of the charges flowing with the liquid but also the magnitude of the charges to be injected is necessary because of charge reversal.

The suitable charge injection technique for a pipe flow configuration is field emission or ionization.

Field emission or ionization

When a fine metal-point or sharp blade edge electrode is raised to a sufficiently high negative or positive potential to produce a field near its tip, electrons or positive ions, respectively can be created in the vicinity of the point or edge, see figure 4.2. The etched tip or blade edge radius is dependent on the voltage applied and the amount of charge needed to be injected. Although it is usually less than 1000 Å. The opposite electrode is normally flat. The injecting electrode (with the fine metal-point) should be made of a metal with less tendency to oxidization and with high stability at high temperature and electric field (*e.g.* Tungsten).

Depending on the quantity of the charge to be injected and the distance between the two electrodes a very high potential field is required. The choice between the point and blade electrode is related to the quantity of the charge to be injected. The blade may be used for high quantity injection.

4.4.2 Boundary layer control

Industrial flow meters are used with both laminar and turbulent flow, although the latter is the most common. The density of charges flowing with the liquid increases with the flow velocity. Hence, more charges flow with the liquid in turbulent than in laminar flow. As expressed in equation 4.9, a turbulent flow has a laminar sublayer close to the wall. Charges flowing with the liquid in a turbulent flow can therefore be reduced by expanding the laminar sublayer; *i.e.* by increasing the laminar sublayer thickness (δ).

Operating an electromagnetic flowmeter at relatively higher value of δ is possible by either measuring the flow close to a reservoir or manipulating the turbulent boundary layer using passive techniques. At the outlet of a reservoir or a settling tank, the static liquid starts to move and the flow begins to develop. This takes place in comparatively small distance from the reservoir, approximately under 10 times the diameter of the pipe. Across this distance the laminar sublayer thickness is higher than it is during steady turbulent flow and hence there will be a lower charge density in the liquid. Alternatively, internal manipulators like rings and inner pipe grooves can be fixed inside a pipe to delay transition from laminar to turbulent thereby increasing the laminar sublayer thickness (Coustols, 1990). The exact effect of these passive devices on a turbulent flow, however, is still under investigation.

4.4.3 Chemical additives

Wall stress or skin friction is the cause of charge movement in a pipe flow. Skin friction determines the thickness of the laminar sublayer which in itself governs the distribution of charges in a flow. The laminar sublayer can be increased or the transition from laminar to turbulent delayed by reducing skin friction so as to minimize charges

flowing with the liquid. This can be achieved by dissolving small quantities of a chemical additive in the flowing liquid.

Chemical additives are used both for moderately conducting and dielectric liquids. However, the emphasis on the reason for the usage is different. In water, for instance, chemical additives are employed purely to minimize flow resistance whereas in the petroleum industry it is used to reduce charge concentration. Klinkenberg and Van Der Minne (1958) reported how the occurrence of massive explosions during oil flow prompted the Shell Company to initiate research into developing effective chemical additives. He also indicated that his research team came up with such a product which is the basis for the current petroleum additives used in the petroleum industry.

Chemical additives, mostly polymer solutions, are chemically characterised by: flexible, well dissolving and very long chain like molecules (McComb and Rabie, 1982). For a liquid flowing at a certain volumetric flow rate and pressure, when appropriately selected additives are dissolved in to the liquid, the pressure drop needed to maintain the same flow rate is very much reduced (by up to 25 %). This effect is more remarkable because the laminar flow behaviour of the dilute solution is very little different from that of the liquid on its own, *i.e.* the density and viscosity of the polymer solution are not different from those for the liquid.

Dielectric liquids flowing in a pipe have very high charge density fluctuating at low frequencies (mainly 0 to 300 hertz depending on the type of liquid). That additives can reduce these charges enabling an electromagnetic flowmeter to work at these frequencies is very doubtful. It is, however, feasible at higher frequencies where charge reduction might reduce the random noise to ensure a more stable flow related signal.

5.0 FLOW-RIG DESIGN

5.1 Introduction

A single phase flowmeter is usually tested on a flow circuit set up for the type or types of liquid it is designed for. This is particularly critical in the case of electromagnetic flowmeter suitable for dielectric liquids as the electrical properties of these liquids are affected by impurities. Polar liquids in general, for instance, leave charged molecules behind which could alter (depending on the degree of absorption) the conductivity and dielectric permittivity of low viscosity dielectric liquids (Gallagher, 1975). This in turn could alter the sensitivity of an electromagnetic flowmeter as set out in chapter 3 if used in the same flow rig. Moreover, the design of a flow loop suitable for dielectric liquids must take in to account the flow associated charge density. This is on top of the other common factors such as temperature and flow loop pressure.

Just as important is the choice of the dielectric liquid. For this project BP dielectric 180 oil was selected. A list of its properties along with a description of the flow rig designed to handle the experiments are given in the sections below.

5.2 Design considerations

When designing a flow loop for dielectric liquids which will be used to test an electromagnetic flowmeter, two special considerations dictate the process: minimizing the excess charges and a stable earth or ground.

Designing to keep the excess charges to the minimum possible affects not only the

choice of pumps, filters and valves but also the placement of these devices in the flow rig. The impeller of a pump generates excess charges where it contacts high speed dielectric liquid. These are likely to constitute the majority of the total excess charges in the flow and as such they should be kept to the lowest possible level. This may be achieved by connecting a tank to the outlet of the pump to reduce the flow rate to near zero so as to give more time for the excess charges to relax to ground; hence the name "relaxation tank". Selecting the power rate and pressure head of a pump to match the size of the flow rig also helps. Another source of excess charges are intrusive devices like control valves, filters and reference flowmeter. These must be installed, only if they have to be, downstream of the test point in order not to interfere with the measurement. A large reservoir which holds at least 4 to 5 times the total loop volume is essential as it restricts the chances of a continuous circulation of the same section of liquid thereby removing excess charges and limiting the liquid's temperature rise to only a fraction of a degree centigrade from the normal room temperature for each circulation in the loop. If allowed to rise, the temperature could increase the conductivity and dielectric permittivity of the dielectric liquid.

To avoid charge building up in the flow, the flow rig must be grounded. Grounding minimizes excess charges and stabilizes the flow signal reference point of the electromagnetic flowmeter. The more charge that flows to ground the less charge density there will be in the flowing liquid. Therefore, a flow loop suitable for dielectric liquid must be made from conducting pipe materials in order to have a common earth point.

5.3 Description of the flow rig

Figure 5.1 shows the design drawing of the flow circuit. The flow circuit was made from 2 inch (50 millimeter) outside diameter mild steel pipes. The reservoir was a cylindrical tank. It was 1.5 m high with a base radius of 0.5 m and was made from 1.5

mm thick mild steel sheet. It was capable of containing about 1130 litres (1.13 m^3) of liquid, which was 7 times the total volume of the flow loop. The dielectric liquid was drawn out of one side of the tank and was returned (eventually) to the other end. To lengther the life of the liquid, a mild steel cap (made to fit tightly) was used to cover the tank to reduce the amount of contaminants entering the liquid.

A 2 horse power centrifugal pump (LOWARA CEK 370/2 type) was chosen to pump the liquid round the circuit. The duty point of the pump was a volumetric flowrate of 4 litres/second and a total head of 40 feet (10.5 m) of water at a pressure of 1.75 bar. Considering the various hydraulic losses in the circuit and taking into account the density and viscosity of the BP dielectric 180 oil, a maximum mean velocity in the circuit of 3.25 metre/second (equivalent to a volumetric flowrate of 6.5 litre/second) was expected to be attained. The inlet and outlet of the pump were fitted to ball valves (normally open) in the flow circuit so as to make disconnecting the pump easier in case of a fault occurring during experiments.

The outlet of the pump was raised to a height of 725 mm from ground via a straight pipe and directed to a horizontal level by a 90° bend pipe which was connected to a cylindrical relaxation tank with a conical inlet and outlet. The conical entrance and exit shape was chosen for smooth transition of the flow. The relaxation tank was designed to reduced the flowrate of the liquid by $\frac{1}{20}$ (i.e the liquid flowed 20 times faster at the entrance and exit than it did inside the relaxation tank). It was supported by two metal frames and was fitted to ball valves (normally open) at its up- and downstream ends. It had a drain at the bottom side for draining the liquid and a vent at the top side to let air out of the flow circuit.

A long straight pipe of about 60D, which was more than enough to provide fully developed flow, was used to join the relaxation tank to the test section (the electromagnetic flowmeter). The downstream side of the test section was followed by

temperature and pressure monitoring instruments. An insertion platinum resistance thermometer and a pressure gauge were used to monitor the temperature of the liquid and the line pressure respectively. A vertical pipe brought the line back down to the floor level via two 90° bends. A straight pipe, with a drain on its side for the circuit, lead to a 2 inch rotary turbine reference flowmeter (type: KDG MOBREY M2/2000/250). The downstream end of the reference meter was connected to the reservoir via a diaphragm flow control valve to complete the circuit.

5.4 BP Dielectric 180

BP dielectric 180 (commonly known as BP 180) is a hydrocarbon oil designed for spark-erosion processes in electro-discharge machines. It is additive-treated to have long service life and avoid the generation of unpleasant odours in service. BP 180 has been in use in the Department of Fluid Engineering for experimental purposes since 1987, and has been found to have very stable physical properties. It also has stable electrical properties as will be shown in the next chapter.

The following is a list of some of the physical properties of BP 180:

Physical properties of BP 180

Density, 15.5 °C	0.749 g/cm^3
Viscosity, 20 °C	1.75 cSt
Flash point	70 °C
Pour point	-24 °C
Boiling point	230 °C
Electric strength	18 kV/mm
Appearance	Clear bright fluid

6.0 MEASUREMENT OF DIELECTRIC PERMITTIVITY & CONDUCTIVITY

6.1 Introduction

It is noticeable that the electrical properties of BP 180 are absent from the list given in the last section of the previous chapter. This is because the manufacturer's data quotes the conductivity and permittivity values of petroleum and petroleum products in general, which are $\sigma \approx 1\times10^{-16}$ S/m and $\varepsilon \approx 2.2$ (-0.001/^{0}C), rather than a specific set of figures for each type of product. This is rectified in this chapter, at least for BP 180, with a determination of its permittivity and conductivity.

For practical and, more significantly, theoretical analysis of the design of an electromagnetic flowmeter, identifying the exact (within a reasonable tolerance) values of the electrical conductivity and dielectric permittivity of the liquid is important. Apart from the sensitivity of the flowmeter, these parameters affect the magnitude of the charge noise and distribution of charges in the flow as described in chapter 4.

6.2 Measuring dielectric permittivity of BP 180

To determine the permittivity of BP 180, a simple but effective technique was used. The procedures adopted for the measurement method were as follows:

1 - A variable air capacitor, 4 cm long, 4 cm high and 3 cm wide, was fixed at its highest value. A 0.5 m long insulated copper wire of 0.5 mm diameter was attached to the two terminals.

2 - This capacitance was measured in an empty cylindrical plastic bucket of 25cm

diameter and 30 cm high (*i.e.* using air as the dielectric).

3 - Then, the bucket was filled with BP 180 with the capacitor inside. The capacitance was measured and recorded (*i.e.* using BP 180 as the dielectric).

4 - The ratio of the measured capacitance in 3 (above) to the one in 2 resulted with the dielectric constant of 2.0 for BP180.

The capacitances in 2 and 3 were measured with in a tolerance of 1 % using a Bridge (Wayne Kerr B641 type) at the frequency of 1592 Hz. The extraneous capacitance does not affect the result as it is a ratio measurement. To illustrate this, let C_a and C_o be the capacitances of air and BP 180 respectively, and the extraneous capacitances are in parallel in both cases; Then,

$$C_a=\frac{\varepsilon_o A}{d}+\frac{\varepsilon_o A_1}{d_1} \qquad 6.1$$

$$C_o=\frac{\varepsilon_o \varepsilon A}{d}+\frac{\varepsilon_o \varepsilon A_1}{d_1} \qquad 6.2$$

where ε and ε_o are dielectric constant of BP 180 and dielectric permittivity air respectively, A is the total area of the electrodes of the variable capacitor, d the total distance between the electrodes of the variable capacitor, and A_1 and d_1 are equivalent total area and distance of the extraneous capacitances respectively. The ratio, therefor,

$$\frac{C_o}{C_a}=\frac{\varepsilon(\frac{\varepsilon_o A}{d}+\frac{\varepsilon_o A_1}{d_1})}{\frac{\varepsilon_o A}{d}+\frac{\varepsilon_o A_1}{d_1}}=\varepsilon \qquad 6.3$$

Since the extraneous capacitances have the same area and distance in both air and BP 180, the result will be unchanged for series or series-parallel combinations with the main capacitor.

6.3 Measuring conductivity of BP 180

During experiments on the electromagnetic flowmeter, the conductivity of BP dielectric 180 had to be monitored to estimate its deterioration due to contaminants and usage. Hence, there was a need for a consistent, repeatable and easy to use system for measuring conductivity.

The common method of measuring conductivity of dielectric liquids is a two terminal cell in which the liquid is placed and its resistance measured. As the cell geometry, including the distance between the two electrodes (terminals), is pre-determined, the resistivity, hence the conductivity, is easily determined. The conductivity measuring device used in this project was designed on the same principle. However, to improve its accuracy and sensitivity a new geometrical configuration was adopted.

6.3.1 The conductivity measuring device

The conductivity measuring device and its equivalent circuit are shown in figures 6.1(a) and (b). The device has two parts: the conductivity cell and the charge amplifier.

The conductivity cell

The two electrodes of the conductivity cell were arranged as shown in figure 6.2. The outer electrode was made from a 76 mm long copper pipe of inside diameter of 32 mm and pipe-wall thickness of 1mm (*i.e.* the outside diameter was 34 mm). A copper plate of the same thickness and outside diameter as those of the pipe was welded on to one side so as to close it. This allowed the pipe to be used as an electrode as well as a

container for the liquid to be measured (in this case BP 180). The inner electrode was a solid cylindrical copper rod of 70 mm in length and 26 mm in diameter. It was supported to stand in the centre and insulated electrically from the outer electrode by a total of 7 circular PTFE rods of 2.5 mm in diameter and 4.5 mm long (of which 1.5 mm was screwed into the cylinder). One rod was placed at the centre of the bottom circular area and three each way at a distance 5 mm along the length of the cylinder. A PTFE insulated copper wire, 2.5 mm in diameter, was connected to the top of the inner electrode for the power supply. A cap, with a hole at the centre for the electrical wire, was made from a 3 mm thick copper sheet and fitted tightly to the outer electrode. Because the surfaces of the rods and the inner side of the outer electrode were smooth, it was possible to remove the inner electrode and replace it after cleaning both electrodes whenever necessary. When measuring the conductivity, the cell was placed on a PTFE disc 20mm thick and 55 mm in diameter in order to minimize charge leakage.

The charge amplifier

When a d.c. voltage was applied to the inner electrode of the conductivity cell, it induced a leakage current due to the high resistance of the BP 180. This leakage current was measured using a charge amplifier (refer to figure 6.1(a)). A coaxial cable soldered onto the outer electrode of the cell was connected to op-amp AD-515 via a 10 kΩ resistor. The shielding mesh of the coaxial cable was grounded. To convert the very small current to a reasonable voltage at the output, a high resistance value (= 10^8 Ω) resistor was connected in parallel with a capacitor in the feed-back loop. The capacitor was added to filter out noise. The noise sources were the oil resistance (the main contributor), the resistors in the circuit and the op-amp. The time constant for the circuit, τ = 2.2 seconds, was chosen because it offered a good stability when reading the output voltage. The op-amp AD-515 was selected due to its low noise (4 micro volt (μV) peak to peak), ultra low bias current (75 femto amperes (fA)), low offset voltage

(0.2 mV), low drift (10 $\mu V/^0C$) and high input impedance ($10^{13}\Omega$).

6.3.2 Analysis of the design

The leakage current, I_l in figure 6.1(a), can be calculated from

$$I_l = \frac{U_{out}}{R_b} \qquad 6.4$$

where U_{out} is the output voltage and R_b the feedback resistance. The resistance (R) of BP 180 for the applied d.c. voltage (U_c) is found from

$$(R+R_a) = \frac{U_c}{I_l} = \frac{U_c}{U_{out}} R_b \qquad 6.5$$

In practice, since R_a (= 10 kΩ) « R, it can be ignored. The resistivity (ρ) of BP 180, therefore, can now be determined from the basic resistance formula:

$$\rho = \frac{RA}{d} \qquad 6.6$$

where A is the equivalent area of the electrodes and d is the equivalent distance between them. Since conductivity (σ) is the inverse of resistivity, equation 6.6 can be rewritten for the conductivity of BP 180 as

$$\sigma = \frac{d}{RA} \qquad 6.7$$

However, because of the cylindrical nature of the design of both electrodes, determining A and d from the geometry of the conductivity cell is difficult. The solution to this problem is to find the ratio $\frac{d}{A}$ by measuring the capacitance of the conductivity cell with BP 180 as the dielectric material. If the capacitance is known, then, from the expression $C=\frac{\varepsilon_o \varepsilon A}{d}$, the ratio can easily be calculated; $\frac{d}{A}=\frac{\varepsilon_o \varepsilon}{C}$ where ε is the dielectric constant of BP 180 (measured as explained in section 6.2).

6.3.3 Estimation of the capacitance of the conductivity cell

Approximate capacitance of the conductivity cell as that of 3 capacitors C_1, C_2 and C_3 in parallel representing capacitances across regions U_1, U_2 and U_3 respectively (see figure 6.3) are given by

$$C_1=\frac{\varepsilon_o \varepsilon \pi (a^2-c^2)}{d} \qquad 6.8(a)$$

$$C_2=\frac{2\pi l \varepsilon_o \varepsilon}{\ln(\frac{b}{a})} \qquad 6.8(b)$$

$$C_3=\frac{\varepsilon_o \varepsilon \pi a^2}{g} \qquad 6.8(c)$$

By geometrical design $d = g = b - a$. The capacitance of the conductivity cell, therefore, is the sum of the three; *i.e.* $C = C_1 + C_2 + C_3$. For the dimensions given in section

6.3.1, the capacitance of the conductivity cell with BP 180 in it was calculated to be 36 pF.

6.3.4 Result of measurement

After removing the cap, the conductivity cell was filled with BP 180. The cap was replaced and the capacitance of the cell was measured, using a Wayne Kerr Bridge, from which the ratio $\frac{d}{A}$ was determined. A variable d.c. supply was connected to the cell. The input voltage and the corresponding leakage current was recorded. Figure 6.4 shows a graph obtained for the conductivity of BP 180 from equation 6.7. As the straight line indicates the conductivity of BP 180 is 5.7×10^{-11} S/m; hence by definition the resistivity is $1.75\times10^{10}\ \Omega$ /m.

The measured capacitance of the conductivity cell with BP 180 in it was 38 pF, which is a difference of about 5 % from the theoretically estimated value (in section 6.3). The estimated value of conductivity is also out by 5 % from the measured value. This is mainly because of impurities entering the liquid when transferring the liquid from the reservoir to the conductivity cell and charge leakage. In addition, in the theoretical analysis the surfaces of the conductivity cell were assumed to be smooth, however, in reality some roughness is to be expected as the conductivity cell was hand-made.

The maximum conductivity of BP 180 recorded in two and half years of continuous monitoring was 9.12×10^{-11} S/m (an increase of about 1.6 times). This confirms the high stability of BP 180.

6.3.5 General remarks on the design

From experiments carried out with brass-copper and copper-copper inner-outer electrode combinations, it was observed that the brass-copper combination generated a proportionally high level of drift (up to 10% of the full scale input voltage (2mv) compared to 1% for copper-copper combination) at the output. This was because of the difference in absorption (between brass and copper) of ions in to the BP 180.

PTFE was chosen for insulation due to its high resistivity ($\approx 10^{18}$ S/m). The PTFE circular rods used in the conductivity cell had no bearing on the output voltage as the ratio $\frac{A}{d}$ for them was minimal compared to that for the electrodes.

The cap had to fit tightly to prevent dust particles from entering the cell. It was also important that the legs of the op-amp were fixed onto PTFE to minimize charge leakage.

The small input voltage range on the result graph in figure 6.4 (from 0 to 2mV) was because of the copper electrodes. Copper easily oxidizes and oxygen is the major impurity in dielectric liquids. The oxidization tendency increases with the applied voltage which in turn increases drift (hence unstable readings) at the output of conductivity measuring devices of the type used here. This is the main reason behind the use of precious metals like gold and platinum as electrodes in commercial conductivity cells.

6.4 Electrical properties of BP 180

As a summary, the chapter is concluded with a list of the electrical properties and

charging constants of BP 180 .

Conductivity	5.7×10^{-11} S/m
Dielectric constant	2.0
Relaxation time	0.312 sec
Debye length	5.69 micro meter (μm)

For the Debye length, the molecular diffusivity (D) was taken to be 10^{-10} m^2/s (calculated from the general formula $D=\frac{kT}{6\pi\eta r_i}$, where k is Boltzmann`s constant, T absolute temperature, η dynamic viscosity and r_i the radius of the ion (Walmsley and Woodford, 1981)).

7.0 DESIGN OF THE ELECTROMAGNETIC FLOWMETER

7.1 Introduction

The schematic diagram in figure 7.1 illustrates the electromagnetic flowmeter designed for use with dielectric liquids. The main parts of the meter are the flow conduit, electrodes, sensing and processing electronics, coils for magnetic field and electrostatic shield. The design of each part and the practical problems associated with it are described and discussed in the remaining sections of the chapter.

7.2 The flow conduit

The flow conduit of the electromagnetic flowmeter was made from a 375 mm long (measured from flange to flange) 2 inch (OD) perspex pipe (see figure 7.2). Perspex was chosen because it is an insulator.

A pipe wall made from an insulator does not give rise to eddy currents in the alternating magnetic field.. Eddy currents affect the distribution of the magnetic field of the meter (refer to section 7.3 below). The low conductivity of the pipe wall also ensures that the flow signal does not get shorted. Another advantage of a non-conducting wall, particularly to electromagnetic flowmeters applicable to dielectric liquids, is the similarity between its electrochemical properties and those of dielectric liquids themselves. Electronegativity is one of the electrochemical properties of a medium. Charge separation, in quantity as well as polarity, is partly dependent on the relative electronegativity of the liquid and the pipe wall (Walmsley and Woodford, 1981). If the liquid and the pipe wall have similar electronegativities, the charge

generated is smaller than in the case when they have differing electronegativities. Nakano and Tanaka (1990), for instance, reported a difference of at least 2 % between metallic and non-metallic pipes when used with transformer oil.

7.3 The electrodes

Figure 7.3 shows the two sides of the capacitive-type electrodes used for the flowmeter. The two copper electrodes (in fish-bone conductor layout to reduce eddy currents) were manufactured, courtesy of Schlumberger, on a flexible printed circuit board. Figure 7.4 shows the schematic of the top, under and side view of the electrodes. Each electrode was in the form of a detection electrode of large area behind which was a driven shield electrode (often referred to as "a guard electrode") of even greater area, the two being isolated from one another by the flexible board. The detection electrode was 52 mm wide and 72 mm long (along the flow axis), and the shielding electrode, on the other hand, was 75 mm wide and 100 mm long. The detection electrode was enclosed by an additional guard electrode, on the same side, which was connected to the main shield electrode on the other side (see underside view on figure 7.4). The purpose of the additional guard and the large area of the main guard electrode was for effective shielding of the detection electrode. PTFE insulated output leads for the two sides were soldered onto the central heavy tracks and routed through a hole (see top side view on figure 7.4). Each of the ribbing copper tracks were 0.7 mm wide and were separated by 0.9 mm gap. Both the detection and shielding sides were covered with insulator to protect the copper tracks from damage and dirt. The flexible board and the insulator were made from a 125 micro meter thick Kapton film (polyamide type). Kapton was selected for its physical and electrical properties. It can stand high temperature (250 °C), important for soldering, has low electrical conductivity (1×10^{-16} S/m), for good insulation and is a stable dielectric material ($\varepsilon = 3.4$). The value of the capacitance formed by the detection and the shield electrodes was 870 pF at 1592 Hz.

The flexible board for the two electrodes was 160 mm in width and 102 mm in length (along the flow axis). It was designed to encircle the 2 inch perspex pipe on the out side. When the electrodes (the flexible boards) were placed on the flow conduit of the meter, the central heavy tracks were positioned parallel to the flow axis (on the central plane perpendicular to the magnetic field) so as to average the flow related voltage over each side of the duct.

7.4 Choice of the frequency of operation

The formation of a double layer and the subsequent separation of charges that are associated with the flow of dielectric liquids rule out d.c. excitation of the magnetic circuit of the electromagnetic flowmeter. Hence, an alternating wave form had to be used. For the reason which becomes clear in section 7.7, a sinusoidal waveform was used for the magnetic field. The choice of the exact frequency of operation was a compromise between the following design factors:

(1) charge noise bandwidth,

(2) magnitude of the quadrature voltage,

(3) eddy currents in the electrostatic shield,

(4) voltage on the magnetic field coils.

7.4.1 Charge noise bandwidth

To determine the charge noise bandwidth, the following experiment was carried out.

The electrodes of the meter were connected to the electronics described in section 7.5 below. The flowmeter, then, without the coils and shielded with aluminium foil (which was grounded) to reduce external interference was inserted at the test section of the flow rig (refer to figure 5.1). The pump on the flow rig was switched on to start the flow of BP 180. The output voltage of the detection electronics was stored on a digital oscilloscope (ONO S0KKI CF-930 type) and plotted. The experiment was repeated at different flowrates.

Figure 7.5(a) and (b) show the result of the experiment for flowrates (mean flow velocities) of 1 m/s and 3 m/s. As observed by others before (see literature survey), the noise seems to be mainly of low frequency. As expected, the magnitude of the charge noise increased with the flowrate. Particularly important was the starting frequency for the normal (*i.e.* base line noise) 20 db/dec roll-off after the charge noise bandwidth. For a flowrate of 1 m/s it was about 700 Hz, and for the 3 m/s around 1 kHz, *i.e.* the charge noise extended from 0 to 700 Hz for 1 m/s and to 1 kHz for 3 m/s. The magnitude of the charge noise at 600 Hz for a mean velocity of 3 m/s (assuming a bandwidth of 10 Hz) is about 0.4mV; which is more than the expected signal level of 0.3mV. As the maximum flowrate achievable from the pump was 3.25 m/s, the frequency of excitation for the coil had to be over 1 kHz in order to avoid the charge noise.

7.4.2 Magnitude of the quadrature voltage

The quadrature voltage is a transformer effect. The detection circuit of the electromagnetic flowmeter forms a loop constituting the fluid, the electrodes, electrode wires and associated circuits. There is an electromotive force induced in this loop. This is independent of the flowrate and its magnitude depends on the projected area of the loop in the direction of the magnetic field. From Faraday's induction law, the relation

between the electric field (E) around the loop and the magnetic field (B) in the projected area is given by

$$\oint E \cdot dl = -\frac{d}{dt}\int B \cdot da \qquad 7.1$$

Hence, the magnitude of the induced quadrature voltage for a sinusoidal magnetic field of $B = B\sin\omega t$ is

$$u = \omega BA\cos\omega t \qquad 7.2$$

where $\omega = 2\pi f$, f is frequency, and A is the total effective projected area of the loop. The magnitude of the quadrature voltage is proportional to the frequency of the magnetic field. This voltage can be minimized by careful manufacture of the device so as to reduce the projection area. However, if the frequency is high even a small projection area can induce a quadrature voltage many times bigger than the flow signal.

7.4.3 Eddy currents

When the electrostatic shield is traversed by an alternating magnetic field, eddy currents are generated. Eddy currents represent a power loss as well as a disturbance to the applied magnetic field.

A schematic of the magnetic circuit used in the flowmeter is shown in figure 7.6(a). The magnetomotive force that arises as a result of a current i flowing through the combined turns of the two coils, $N = 2n$, is the integral of the uniform magnetic field intensity H across the total length of the main field lines. Therefore,

$$\int H \cdot dl = Ni \qquad 7.3$$

If the magnetic coils are placed on an outer non-conducting pipe of diameter D, the uniform magnetic field strength inside the flow conduit is given by

$$H_g = \frac{Ni}{2D} \qquad 7.4$$

The flux density B associated with H_g is

$$B = \mu_o H_g \approx \mu_o \frac{Ni}{2D} \qquad 7.5$$

where μ_o is the magnetic permeability of air.

Now suppose a continuous aluminium shield is placed over the outer insulating pipe. The magnetic field B, induces a circulating electric field in the aluminium shield, which in turn gives rise to eddy currents. The relationship between this electric field and the magnetic flux can be obtained from Faraday's law. Hence,

$$\int E \cdot dl = -\frac{d\varphi}{dt} \qquad 7.6$$

where the integration is conducted over the total path of the electric field and $\frac{d\varphi}{dt}$

stands for the rate of change of magnetic flux with time. For a sinusoidal excitation $\frac{d\varphi}{dt}$

can be replaced by ωBA. If the area a covered by one of the coils of the magnetic circuit is considered, equation 7.6 gives

$$E \approx \frac{\omega B a}{l} \qquad 7.7$$

where $l = 2\pi R$, is the circumference of the circular path under the coil, and $a = 2\pi R^2$, the area encircled by the path of radius R.

The eddy current can be expressed as

$$i_e = JA_e \qquad 7.8$$

where the current density $J = \sigma E$, and the area fluxed by the eddy current $A_e \approx tR$, see figure 7.6 (b). t and σ stand for the aluminium shield thickness and conductivity respectively. Using equation 7.7 and substituting for J and A_e in 7.8 we get

$$i_e \approx \frac{\sigma \omega B R^2 t}{2} \qquad 7.9$$

This eddy current induces a magnetic field, in phase quadrature to the main field, whose flux density B', by similar analysis as in equations 7.4 and 7.5, is given by

$$B' \approx \mu_o \frac{i_e}{D} \qquad 7.10$$

Hence, from equations 7.9 and 7.10

$$\frac{B'}{B} \approx \mu_o \frac{\sigma \omega R^2 t}{2D} \qquad 7.11$$

The vectorial directions of B, i_e and E are shown in figure 7.6(b). The secondary field

B' is uniform and 90° out of phase with B. Although it is a power loss, B' does not cause a change in the flow related potential after phase sensitive detection. However it induces a further eddy current in the shield which generates a magnetic field B'' which is in anti-phase with B and therefore does affect the flow related signal. Using the same analysis as for B',

$$\frac{B''}{B} \approx (\frac{\mu_o \sigma \omega R^2 t}{2D})^2, \qquad 7.12$$

The third order field B''' ,which is anti-phase with B', can be expressed as

$$\frac{B'''}{B} \approx (\frac{\mu_o \sigma \omega R^2 t}{2D})^3 \qquad 7.13$$

The magnitude and the significant number of regenerated fields depends on the magnitude of the applied field B and the quantity $\mu_o \frac{\sigma \omega R^2 t}{2D}$.

To compensate for the loss of some of the main magnetic field by the opposing fields, more current is needed; which in turn increases the opposing fields. This is why eddy currents can cause a power loss. Since eddy currents are proportional to frequency (equation 7.9), as low a frequency as other design considerations allowed had to be selected.

7.4.4 Voltage on the magnetic field coils

For two coils in series with a combined inductance of L, the magnitude of the reactance of the coils is given by $X_L = \mid \omega L \mid$ The reactance is directly proportional to the

frequency. If an alternating current i flows through the coils, the voltage on the coils, is $u_L = i \times X_L$. The voltage on the coils increases with the frequency. A high voltage on the coils of an electromagnetic flowmeter introduces a capacitively coupled voltage at the electrodes and in the associated electronics. Hence, minimizing this voltage had to be an important design consideration.

After careful analyses of the main factors described in the above sections 7.4.1 to 7.4.4 it was decided that the frequency of the sinusoidal magnetic field was to be 1.5 kHz.

7.5 The electronics

Figure 7.7 shows the circuit diagram of the electronics employed in the flowmeter. It consisted of signal detection and processing parts. The output of the signal processing electronics was fed to a lock-in amplifier to obtain the flow related potential.

7.5.1 Detection electronics

The signal sensing electronics was made up of two follower amplifiers and a differential amplifier, as shown in figure 7.8. The detection electrode was connected to the non-inverting input and the shielding electrode to the output of AD549 amplifier. This particular way of connection (usually refereed as "bootstrapping") keeps the detection and shielding electrodes at the same potential since the gain of the follower amplifier is close to 1. This reduces the capacitance between the electrode and external interference as well as ground; i.e capacitive loading from external sources and ground is minimized. A 500 MΩ resistor was connected between each electrode and ground. The purpose of this resistor was to allow the input bias current of the follower to flow

to ground, and to protect the op-amp from static build up. Because of the high input impedance of the flowmeter, op-amp AD549 was chosen for the follower circuit. AD549 has a high input impedance ($10^{13}\,\Omega \parallel 1$ pF) to match that of the flowmeter, an ultralow input bias current (50 fA) and low offset drift (2 μV/°C).

The difference between the signal voltage on the two electrodes was determined using a differential amplifier. Since the liquid (BP 180) was grounded, the voltages on each electrode were opposite in sign. The gain of the differential amplifier was 1. The op-amp AD OP-27 was selected because of its ultralow noise (2 nano volt /√ Hz at 1.5 kHz), ultralow offset voltage drift (0.2 μV/°C) and high common mode rejection ratio (126 db).

7.5.2 Signal processing electronics

The signal processing electronics comprised of a reference voltage amplitude and phase control circuit, and an instrumentation amplifier.

To reduce the quadrature voltage, which has the same frequency as the flow signal but out of phase by 90°, a synchronous deduction technique was used. In this method, a reference voltage is generated and its amplitude and phase is adjusted to equal that of the quadrature so that it is subtracted from the quadrature contaminated flow signal (the detection circuit output). A small 40 turns search coil, made from 0.2 mm diameter insulated copper wire, was placed in the centre of one of the flowmeter's coils to generate the reference voltage. In the circuit, a variable resistor R_c was used to control the amplitude (see figure 7.9). The reference voltage was then split in to u_1 and u_2 which were equal in magnitude but 180° apart in phase. C_p and R_p were combined to set the phase of the output voltage u_p.

Applying the super-imposing method in electrical circuit analysis, the output voltage (

u_p) of the phase shifter can be expressed as

$$u_p = \frac{u_2 - j\omega C_p R_p u_1}{1 - j\omega C_p R_p} \qquad 7.14$$

where $j = \sqrt{-1}$. By altering the value of C_p or R_p, in this case fixed C_p and variable R_p, the phase of the output voltage can be shifted from 0° to 180°, i.e. from phase of u_1 to u_2.

The difference between the phase shifter and the detection circuit output was obtained using an instrumentation amplifier. The instrumentation amplifier was built from TL072 (dual op-amp package) and OP27 op-amps and designed for a gain of 7 (see figure 7.7). The output of the instrumentation amplifier is fed to a lock-in amplifier (refer to section 7.5.3 below) to give the final result signal.

7.5.3 Lock-in amplifier

To separate the remaining quadrature voltage and to capture the flow related signal a lock-in amplifier was used. Lock-in amplifiers use a technique known as phase-sensitive detection to single out the component of the signal at a specific reference frequency and phase. Noise signals at frequencies other than the reference frequency are rejected and do not affect the result.

Let a square wave, from a sync output of a function generator with frequency $\omega = 2\pi f$ be the reference, and the resulting signal for an experiment excited using the sine output of the function generator be $u_s = U_s \sin(\omega t + \theta_s)$, where U_s is the signal amplitude and θ_s is the signal's phase. Lock-in amplifiers generate their own internal reference signal using a phase-locked-loop locked to the external reference. Let this internal reference be $u_r = 2\sin(\omega t + \theta_r)$, where θ_r is the phase of the internal reference.

Figure 7.10 illustrates the waveforms and respective phase angles of the external reference , the signal and the internal reference of the lock-in amplifier. The output of the phase-sensitive detector is simply the product of the two sine waves u_s and u_r, *i.e.*

$$u_{psd}=2U_s\sin(\omega t+\theta_s)\sin(\omega t+\theta_r) \qquad 7.15$$

writing the product of two sines in sum and difference form yields:

$$u_{psd}=U_s(-\cos(2\omega t+(\theta_s+\theta_r))+\cos(\theta_s-\theta_r)) \qquad 7.16$$

If this voltage is passed through a low pass filter, the alternating signals are removed; hence,

$$u_{psd}=U_s\cos(\theta_p) \qquad 7.17$$

where $\theta_p = \theta_s - \theta_r$. This is a d.c. signal proportional to the signal amplitude. θ_p is the phase difference between the signal and the lock-in reference oscillator. By adjusting θ_r , θ_p can be made to equal zero, in which case only the full experimental signal is measured (since $cos\theta_p = 1$). Conversely, if θ_p is 90°, there will be no output. A lock-in with a single phase-sensitive detector is called a single-phase lock-in and its output is $U_s cos\theta_p$ (*i.e.* signal only, the quadrature is rejected). The low pass filter bandwidth and roll-off determine the bandwidth of detection and the attenuation of noise signals. Only the signal at the reference frequency will result in a true d.c. output and so be unaffected by the low pass filter. Noise signals at frequencies far from the reference are attenuated at the phase-sensitive detector output by the low pass filter (neither (ω_{noise} + ω) nor (ω_{noise} - ω) are close to d.c.). The low pass filters are designed up to fourth order, although the most common is second order with 40 db/dec roll-off, to minimize noise at frequencies very close to the reference. The lock-in amplifier used in this project was a single-phase output (type: Brook-deal AORTIC-9401).

7.5.4 Flow simulator

A test, similar to that of Codazzi and Mioque (1986), was carried out using a flow simulator in order to check *in situ* the operation of the detection electronics of the flowmeter. The flow simulator basically consisted of two thin (100 μm) copper sheets of the same size as the detection electrodes of the meter. These sheets were fixed with a double sided adhesive tape on to a perspex tube that exactly fitted the inside of the flow conduit of the meter. Two grounded electrodes were installed upstream and downstream in order to simulate the correct boundary conditions. The two simulation electrodes, which were placed parallel to the detection electrodes of the flowmeter, were driven at a floating potential difference u (see figure 7.11) and the system output u_o was measured. At the operating frequency of 1.5 kHz, u_o was found to be (0.76 × u), and the phase shift between u and u_o was 3°; *i.e.* the gain of the front end or the follower amplifier was 0.76. It was possible to increase the gain to approach 1 by using a higher value resistor than the 500 MΩ resistor. However, the increase was wiped out by the Johnson noise (refer to section 7.6 below), hence, the 500 MΩ, on balance, was a good compromise. As the phase of both the flow signal and quadrature voltages were expected to be shifted by 3°, phase sensitive detection was still applicable.

7.6 Noise sources

Apart from the charge and quadrature noise, the following were the other possible sources of noise or unwanted signals.

7.6.1 Johnson noise

Random thermal motion of charge carriers gives rise to fluctuating fields and hence a

fluctuating voltage within a conductor. The fluctuating voltage appears as wide band white noise. For a resistor in thermal equilibrium with its surroundings, the Johnson noise it generates is given by the expression:

$$\overline{u}_{nj}^{\,2}=4kTR\Delta f \qquad 7.18$$

where k is the Boltzmann constant ($\approx 1.38\text{x}10^{-23}$ J/K), T is the temperature in K, Δf is the bandwidth of the measuring system and R is the resistance.

Figure 7.12 shows the equivalent circuit for the flowmeter as a voltage source. R_o and C_o are the internal resistance and capacitance respectively. As it will be described in chapter 8, R_o is around 10^{11} Ω . Both R_o and the 500 MΩ biasing resistor generate Johnson noise, and account for the majority of the total random noise in the system. The noise bandwidth was set by the low pass filter of the lock-in amplifier.

7.6.2 Capacitive coupling

Unless two conductors are at the same potential, there exists a capacitive coupling between them. Under alternating current conditions, this coupling will give rise to current loops within a circuit when there appears to be no conducting means. Examples of this might be a wire running close to the metal lid of an earthed box or just two wires running alongside one another. This generally is a concern in high impedance or small signal systems as is the case here. Capacitive coupling can be prevented by proper shielding of wires and electrodes, which is explained further in section 7.8.

7.6.3 Pick-up noise

Stray pick-up constitutes a form of interference. The spectrum and amplitude depend on the source. For instance 50Hz mains has a relatively constant amplitude whereas other impulsive interference from electrical systems (like motors and heating systems) tend to be spikey in amplitude and have a broad spectrum. Since the working frequency for the flowmeter was 1.5 kHz, the mains frequency was not a problem, and other pick-ups were rejected at the phase-sensitive detector stage of the lock-in amplifier.

7.6.4 Temperature variation

Generally the resistance of a medium, in this case the liquid and the electrodes, alters with fluctuations in temperature. This gives rise to a randomly varying potential (Barnes, 1991), *i.e.* random noise. This noise is usually very small and it is insignificant when compared with say Johnson noise. If u_{nJ} is Johnson noise, u_{nt} noise due to temperature variation and $u_{nJ} \gg u_{nt}$, then, since the mean squares of noise are added, total noise $= (u_{nJ})^2 + (u_{nt})^2 \approx (u_{nJ})^2$.

7.6.5 Ground loops

Earth potential can be highly localised. If two conductors are driven into ground only a few meters apart, it is possible that differences in potential of a few mV will be observable. If shielding, measuring and supply equipment are individually earthed at different points in space then it is possible that earth-loop currents driven by these differences in potential will occur. This can then degrade a signal (especially in long

cables) giving rise to spurious readings. To avoid ground-loop generated noise, a star type connection was used in this project (see figure 7.13). The earth point was the flange of the meter at the upstream side of the flow. The earth flange was made from a stainless steel for good contact with the liquid to provide a stable reference. The other flange, at the downstream side of the flow, was perspex.

7.6.6 Shot and flicker noise

Since current consists of the arrival of a finite number of electrons per second and the flow of electrons is a random process, there will be a fluctuation in the number arriving at any one place in any one period. These fluctuations give rise to noise in the circuit. By Fourier analysis (Jones, 1985) of the pulse of current due to arrival of a single electron of charge e (= 1.602×10^{-19} coulombs), the mean square value of shot noise is given by,

$$\bar{i}_{sn}^{\,2} = 2eI\Delta f \qquad 7.19$$

where I is the current flow as a result of the moving electrons and Δf the noise bandwidth as determined by the low pass filter of the lock-in amplifier.

In addition, devices have various sources of noise due to many factors having to do with their construction. In an op-amp for example this will depend on the semiconductor's internal and external connection leads. Device noise has an approximately 1/f spectrum, that is, equal power per decade of frequency, hence, the name 1/f or flicker noise. The shot and flicker noise, like Johnson noise, cannot be removed completely. However, they can be cut to the minimum possible by choosing operational amplifiers with low or ultralow noise. This was one of the reasons behind the choice of AD549 and ADOP-27 for use in the electronics of the flowmeter.

7.6.7 Microphonic noise

The mechanical vibration of the flexible electrodes of the meter caused by the pump and the movement of the liquid can produce an electrical signal. The bandwidth of this noise signal depends on the frequency of vibration which in turn is determined by the flowrate. Hence, a thin (10μm) but very strong double sided tape was used to tightly fix the electrodes on to the flow conduit of the flow meter in order to minimize this noise source.

7.6.8 Common mode signal

A common mode signal is associated with dual input circuits like differential and instrumentation amplifiers. Common mode is measured by the ratio of the differential gain to common mode gain which is known as common mode rejection ratio (CMRR). The CMRR of an amplifier is obtained by applying the same signal to both of its inputs as in figure 7.14. The CMRR of the differential and the instrumentation amplifiers of the flowmeter at 1.5 kHz was found to be 70 db (which is good considering that the circuits were made up of discrete devices).

7.6.9 The total random noise

The flowmeter, with the electronics connected, was inserted at the test section of the flow rig. The flow was started by switching the pump on. Once the flow loop was filled with BP 180, the pump was switched off. The recorded output of the flowmeter at zero flow in the rig is shown in figure 7.15. This illustrates the noise spectrum of the flowmeter at no flow. Assuming a bandwidth of 10 Hz, the amplitude of the random

noise at 1.5 kHz was about 70 micro volt.

7.7 Coil design

The 1.5 kHz frequency of the magnetic field made the use of metal-cored coils very difficult due to eddy currents, *i.e.* only air-cored coils could be used. This meant that iron magnetic circuits could not be employed to channel the field lines to increase the strength of the magnetic field at the centre.

7.7.1 Estimation of field distribution

For a steady current (I) flowing in a circular loop of radius R, the magnetic flux density at a vertical distance z from the centre (see figure 7.16) can be determined from the Biot-Savart law (Corson and Lorrain, 1962) and is given by

$$B_1 = \frac{\mu_o I R^2}{2(R^2+z^2)^{\frac{3}{2}}} \qquad 7.20$$

where μ_o is the magnetic permeability of air. The graphs in figure 7.17(a) and (b) show the distribution of the magnetic flux density for variations in R and z. As expected, B_1 decreases as z increases. The field strength is maximum at $R = z\sqrt{2}$ (found by solving $\frac{\partial B_1}{\partial R} = 0$); which is the design criterion for circular coils. Based on this analysis, it was possible to estimate the magnetic flux density at the centre of the flow pipe of the flowmeter (see figure 7.18).

For ease of flow signal measurement it was decided to aim for a magnetic flux density of about 100 Gauss (0.01 T) at the centre of the flow conduit. This meant that each coil of the meter had to be designed to deliver a field strength of around 50 Gauss. Following the common rule of thumb of 1000 ampere / (inch) ^{2} to prevent over heating in copper wire coils, the thickness and width of the coil was determined to be 25 mm by 25 mm respectively (see figure 7.19). Insulated copper wire of 0.8 mm diameter was used capable of carrying an r.m.s. current of 2 A. z was taken to be the radius of the shield supporting pipe (= 42 mm) plus half the thickness of the coil, and R was chosen for maximum field strength. Using a computer program written for the task, the codes of which are given in appendix C, the field strength and the number of turns required were found to be 51 Gauss and 475 turns respectively.

The low frequency approximate value of the inductance of a coil (L) (Terman, 1943) is

$$L=\frac{3.2R^2N^2}{12R+9t+10w} \qquad 7.21$$

where N is the number of turns, R the radius, t the thickness and w the width of the coil (all in inches). Substituting for the values of these quantities, the inductance of the coil was estimated to be 30 mH.

7.7.2 The resonant circuit

The two coils of the flowmeter are shown in figure 7.20. Each coil was made from 475 turns and the measured value of the inductance of the two coils, connected in series for voltage drive, was 65 mH. The series coils were connected to a capacitance to form a series resonance circuit (see figure 7.21).

In a series resonant circuit, the reactance of the capacitance is equal to the reactance of the inductance and as a result the resonance frequency (f_r) is expressed by

$$f_r = \frac{1}{2\pi\sqrt{LC}} \qquad 7.22$$

where L is the inductance of the coil and C is the capacitance. To achieve the resonance frequency of 1.5 kHz the required series capacitance for the inductance of the coils of the meter was 0.17 μF. Six 1μF capacitors in series were used to provide the correct value.

The resistance R_L of the coils was 8.7 Ω and the resistance part R_C of the capacitance was 5.6 Ω (from the manufacturer's data). For a 2 amperes (rms) sinusoidal current in the resonant circuit the rms supply voltage required was the sum of the voltage across the two resistors R_C and R_L, which was 28.6 volt rms (= 81 volts peak to peak). This voltage was supplied from a hybrid power amplifier.

The power amplifier (RS MOS 248 type) was an audio amplifier operating from ± 55 volts d.c. supply rails and was capable of delivering 120 watts of continuous power in to an 8 Ω load. Its input was connected to a programable function generator (type: ENERTEC 4431). When connected to the resonant circuit of the meter, the power amplifier was able to supply a maximum of 2.25 amperes of sinusoidal current at its maximum voltage of 110 volts peak to peak.

The rms voltage across the coil is given by $U_L = i_{ms} \times X_L$, where $X_L = \mid \omega L \mid$. For the 2 amperes rms current $U_L = 1225$ volt. This very high voltage was the main reason why a sinusoidal waveform was preferred to other waveform types, in particular square, trapezoidal and dc key-field. Since these waveforms do not resonate, the coil current is not as high as in the case of the sinusoidal wave and depends on the rise time of the selected waveform. As it was decided on a minimum signal to noise ratio of 5, the size of the current could not be reduced to alter significantly the voltage required. In

addition, with the exception of square wave, trapezoid and dc key-field waves need multiple sources to realize because of their shapes. The application of these waveforms in electromagnetic flowmeters is described in the papers by Yanof, Slaz and Rosen (1963) and Wyatt (1977).

7.7.3 Measuring the magnetic field

To measure the alternating sinusoidal magnetic field of the meter, a wood-cored search coil was used. The coil was made from 50 single-layer turns of 0.1mm diameter insulated copper wire wound on a 5 mm thick square piece of wood of area 225 mm^2. From Faraday's induction law, the voltage (u) generated in the coil is given by

$$u=-N\frac{d\varphi}{dt} \qquad 7.23$$

where N is the number of turns of the coil and φ is the magnetic flux. Inside the area A of the wooden core $\varphi = BA$, where B is the magnetic flux density. Since $\frac{d\varphi}{dt}=\omega BA$ for a sinusoidal wave , the amplitude of the field strength (B) is

$$B=\frac{u}{N\omega A} \qquad 7.24$$

The resonant circuit of the magnetic field of the meter was excited. The wooden-cored coil was placed inside the flow conduit. By measuring the voltage across the coil the rms magnetic flux density at the centre was determined to be 104 Gauss.

Using a ruler, the flow conduit of the meter was marked in cm. Then, the coil was

moved across the flow conduit in the flow direction. Figure 7.22 shows the recorded distribution of the magnetic field in the axial direction. It fell off gradually as the distance from the centre was increased.

7.8 Electric and magnetic field shielding

Electronic devices and circuits or signal cables are shielded from electric fields in order to minimize coupling. Magnetic shielding, for electromagnetic flowmeters, is required to prevent the field from interfering with any other systems nearby.

7.8.1 Electrostatic shield

An electrostatic shield is a metal case or sheet. In most applications the choice of the physical size and the electrical conductivity of the shielding metal is arbitrary and based mainly on availability. For electromagnetic flowmeters, however, the conductivity and the thickness of the shield is dependent on the level of tolerance of the system to eddy currents and capacitive coupling voltage. A thick metal sheet with high electrical conductivity may be an ideal shield for the attenuation of the capacitive coupling voltage, but it is also a good source of eddy currents as described in equation 7.9. Hence, a compromise must be made between capacitive coupling and eddy current generation when designing an electrostatic shield.

The attenuation of an electrostatic shield can be approximated theoretically from an analysis of simple geometries. One such geometry is a hollow cylinder.

If a long conducting hollow cylinder of inside radius a and outside radius b is placed in a transverse uniform electric field (a.c.), the penetration of the field inside the

cylinder can be estimated from the following three basic equations:

$$\underline{E} = -\nabla u \qquad 7.25(a)$$

$$\underline{i} = \underline{J} + \frac{d\underline{D}}{dt} \qquad 7.25(b)$$

$$\nabla^2 u = 0 \qquad 7.25(c)$$

where u is potential, $\underline{i}$ is the total current, $\underline{J}$ is conduction current and $\underline{D}$ is displacement current. Since $\underline{J} = \sigma \underline{E}$ and $\underline{D} = \varepsilon_o \varepsilon \underline{E}$, if the transverse electric field takes the form $\underline{E} = E e^{j\omega t}$, then the Ohm's law of equation 7.25(b) can be written as

$$\underline{i} = (\sigma + j\omega \varepsilon_o \varepsilon) E e^{j\omega t} \qquad 7.26$$

where σ is conductivity, E is the magnitude of the electric field, $\omega = 2\pi f$ is the angular frequency, $\varepsilon_o \varepsilon$ is dielectric permittivity of a medium and $j = \sqrt{-1}$. The term ($\sigma + j\omega\varepsilon_o\varepsilon$) is often referred to as the complex conductivity of a medium. For the hollow cylinder, there are three regions of electric distribution (see figure 7.23): Outside (at infinity), on the walls ($a < r < b$) and inside ($r < a$) of the cylinder. Outside and inside the cylinder there is only the displacement current, *i.e.* since $\omega\varepsilon_o \gg (\sigma_1 = \sigma_3)$, where σ_1, σ_2 and σ_3 are conductivities for the three regions corresponding to E_1, E_2 and E_3 respectively, $\underline{i} = j\omega\varepsilon_o E e^{j\omega t}$. The conduction current is dominant in the walls of the cylinder, *i.e.* since $\sigma_2 \gg \omega\varepsilon_o\varepsilon_2$, $\underline{i} = \sigma_2 E e^{j\omega t}$.

The corresponding potentials for the three regions are u_1 outside the cylinder, u_2 in the walls of the cylinder and u_3 inside the cylinder. u is a function of polar coordinates r and θ. As the total charge is zero, $\nabla^2 u = 0$ applies for all regions. The boundary conditions for a two dimensional analysis are:

(A)- continuity of the electric field in the direction of θ

$$u_1(b,\theta)=u_2(b,\theta)$$

$$u_2(a,\theta)=u_3(a,\theta)$$

(B)-continuity of current in the direction of r

$$j\varepsilon_o\omega\left(\frac{\partial u_1(b,\theta)}{\partial r}\right)=\sigma_2\left(\frac{\partial u_2(b,\theta)}{\partial r}\right)$$

$$\sigma_2\left(\frac{\partial u_2(a,\theta)}{\partial r}\right)=j\varepsilon_o\omega\left(\frac{\partial u_3(a,\theta)}{\partial r}\right)$$

solving for u_3 by routine analysis (Panofsky and Phillips, 1955),

$$u_3=\left(\frac{4s}{(1+s)^2-\left(\frac{b}{a}\right)^2(1-s)^2}\right)r\cos\theta \qquad 7.27$$

where $s=\frac{\sigma_2}{j\omega\varepsilon_o}$. The ratio of the field inside to the field outside by the definition is the

coefficient of u_3 , which is

$$S_e = \frac{4s}{(1+s)^2 - (\frac{b}{a})^2 (1-s)^2} \qquad 7.28$$

S_e is commonly known as electric shielding ratio. For a relatively thin conducting wall shield, $\frac{b}{a}$ is close to 1 and $\sigma \gg \omega\varepsilon_o\varepsilon$, hence S_e can be simplified to

$$S_e \approx \frac{1}{1 + \frac{\sigma_2}{j2\omega\varepsilon_o}(\frac{a-b}{a})} \qquad 7.29$$

for good screening, $S_e \ll 1$ or $\frac{\sigma_2}{\omega\varepsilon_o}\frac{(a-b)}{a} \gg 1$.

7.8.2 Eddy current free electrostatic shield

Eddy currents would disturb (both in magnitude and phase) the transverse magnetic field and make it difficult to apply synchronized reduction of the quadrature voltage. Hence, the design of an eddy current free shield not only reduces power loss but also stabilizes the technique of quadrature voltage minimization.

Eddy currents circulate in a loop around the lines of the applied transverse magnetic field. The circular loops range from small to large depending on the magnitude and spread of the magnetic field lines. The total eddy current is the sum of all the circulating currents in the area fluxed by the field lines. The principle behind the design of eddy current free shield is the breaking of the circular loops. This can be accomplished by constructing the shield from a grid-like arrangement (see figure 7.24

). Each of the metal grid lines are separated from one another by insulating material in order to break the continuity. All the grids are joined at one end so as to ground the shield.

The main electrostatic shield of the meter was made by lining up insulated copper wires side by side on a stick-back plastic film and soldering them together at one end (see figure 7.25). The diameter of each wire was 0.3 mm and the area of the shield was 300 mm by 300 mm. The shield was tested both for eddy current and electric field attenuation. To determine the size of eddy current indirectly, the magnetic field generated by 2 amperes (rms) sinusoidal current flowing through the flowmeter coils was measured at the centre of the supporting perspex pipe with and without the shield. The field strength at 1.5kHz found to be the same in both cases, proving that the eddy current on the shield was very minimal (negligible quantity). To test the effectiveness in electric field attenuation, the shield was wrapped around the supporting pipe and grounded. A sinusoidal voltage source was placed on top of the shield and the resulting capacitive coupling voltage inside the supporting pipe was measured using copper wire of 2 mm in diameter. The attenuation of the shield at 1.5 kHz was found to be about 60 db, *i.e.* for the source voltage of 1000 volt, the coupling voltage was 1 volt. A complete shielding was not achieved due to the insulation on the copper wires which let alternating electric field through. As the frequency decreased the attenuation of the shield increased (at 50 Hz for instance it was 75 db). In order to minimize the coupling voltage further, an additional shield, a polycarbonate mylar coated with 0.09 micron thick aluminum, was used. The magnitude of the quadrature magnetic field due to eddy currents was estimated to be around 0.05 % of the applied field (*i.e.* $\frac{B'}{B}$ in equation 7.11) which was tolerable.

7.8.3 Magnetic shielding

The magnetic field of an electromagnetic flowmeter needs to be shielded in order for it not to interfere with other systems. The common magnetic shields are metals, such as iron and its alloys, with a relatively high magnetic permittivity. The required thickness of a shield is determined by its magnetic permeability. A magnetic shield can only be effective until it saturates. Hence, selecting a shield thickness appropriate to the strength of the applied field is essential.

By applying the same analysis as in the case of electric field and a hollow cylinder, it is possible to approximate the shielding ratio of a magnetic shield. The equivalent basic equations for a magnetic field are:

$$\underline{B}=\mu H \qquad 7.30(a)$$

$$\underline{H}=-\nabla\phi \qquad 7.30(b)$$

$$\nabla^2\phi=0 \qquad 7.30(c)$$

where ϕ is magnetic scalar potential and is a function of r and θ, μ is magnetic permeability, B is magnetic flux density and H is magnetic field intensity.

The boundary conditions for two dimensional analysis of the three regions (see figure 7.26) are:

$$\phi_1(b,\theta)=\phi_2(b,\theta)$$

$$\phi_2(a,\theta)=\phi_3(a,\theta)$$

for continuity of H in the θ direction, and

$$\mu_o\left(\frac{\partial\phi_1(b,\theta)}{\partial r}\right)=\mu_2\left(\frac{\partial\phi_2(b,\theta)}{\partial r}\right)$$

$$\mu_2\left(\frac{\partial\phi_2(a,\theta)}{\partial r}\right)=\mu_o\left(\frac{\partial\phi_3(a,\theta)}{\partial r}\right)$$

for continuity of B in the r direction.

The magnetic potential inside the cylinder, therefore, is

$$\phi_3=\left(\frac{4\mu_r}{(1+\mu_r)^2-\left(\frac{b}{a}\right)^2(1-\mu_r)^2}\right)r\cos\theta \qquad 7.31$$

where $\mu_r=\frac{\mu_2}{\mu_o}$. ϕ_3 is uniform and in the same direction as the field outside. Therefore,

by definition, the magnetic shielding ratio is

$$S_m=\frac{4\mu_r}{(1+\mu_r)^2-\left(\frac{b}{a}\right)^2(1-\mu_r)^2} \qquad 7.32$$

If $\frac{b}{a}$ is close to 1 and $\mu \gg 1$, S_m can be simplified to

$$S_m \approx \frac{1}{1+\frac{\mu_r}{2}(\frac{a-b}{a})} \qquad 7.33$$

for good screening, the requirement is $S_m \ll 1$ or $\frac{\mu_r}{2}(\frac{a-b}{a}) \gg 1$.

The magnetic field of the flowmeter described in this chapter, which was strong so as to provide a detectable signal, was not shielded mainly because of eddy currents. In a simple experiment where a box made of mumetal (distance 5 cm from the coils in all directions) was fitted on the meter, the phase of the net magnetic field was observed to shift by 20° as a direct consequence of the eddy currents generated in the mumetal. The other reason for not having the magnetic shielding was harmonic distortion which is the next topic of discussion.

7.9 Harmonic distortion

At first, the AD549 op-amps were placed very near to the electrodes of the meter so as to use short wires for connection. It was thought this would reduce noise that can be picked up due to the leakage capacitance of long wires. However, during the final test of the whole assembly of the flowmeter before it was fitted onto the flow rig, the applied magnetic field was found to be distorted the result of which is a distorted quadrature signal (before synchronous detection). As shown in the time domain graph of figure 7.27(a), the alternating applied magnetic field was distorted severely. Step by step elimination of possible causes revealed that the source of the distortion was the metal shielding, an iron alloy, of the AD549 op-amp. Further investigation confirmed that the applied magnetic field of the meter was distorted whenever a highly magnetic material was placed inside the flow conduit. Weak-magnetic and non-magnetic metals have no distorting effect on the field.

Figure 7.27(b) shows the frequency spectrum of the distorted magnetic field. The distortion was a result of contamination with mainly odd harmonics, particularly the third and fifth, and to some extent by a few even harmonics. The second harmonic was indistinguishable from the random noise level and the fourth harmonic was about 25 db lower than the centre frequency. The third and fifth harmonics, on the other hand, were only 1.84 db and 5 db respectively adrift in magnitude from the centre frequency. The higher odd and even harmonics decrease in magnitude, although the rate of fall of the odd harmonics was significantly slower than that of the even harmonics.

This harmonic distortion phenomenon can be explained in terms of the non-linear magnetization curve (see figure 7.28). For ferromagnetic and to a lesser degree for paramagnetic materials, the magnetic field (B) is not linearly related to the magnetic field intensity (H). Highly magnetic metals such as Iron, Cobalt and Nickel are ferromagnetic. Metals like Aluminium and Tin are paramagnetic. How non-linear the magnetization curve of a ferromagnetic metal is, is partly dependent on the production technique involved, *i.e.* cold or hot working.

The exact mechanism by which harmonic distortion occurs in ferromagnetic materials is not yet well understood. The closest to a reasonable theoretical analysis of the phenomena that the author has found is the classical theory of paramagnetism of Langevin (Cullity, 1972). He assumed a paramagnetic material to consist of atoms, or molecules, each of which has the same net magnetic moment Θ, arising because all the spin and orbital magnetic moments of the electrons do not cancel out. In the absence of an applied field, these atomic moments point at random and cancel one another, so that the magnetization of the specimen is zero. When a field is applied, there is a tendency for each atomic moment to turn toward the direction of the field; if no opposing force acts, complete alignment of the atomic moments would be produced and the specimen as a whole would acquire a very large magnetic moment in the direction of the field. But thermal agitation of the atoms opposes this tendency and tends to keep the atomic moments pointed at random. The result is only partial alignment in the field direction.

For a unit volume of material containing n atoms, each having a magnetic moment Θ, under a magnetic field intensity (H), Langevin found the ratio of the partial alignment (M) to perfect alignment (M_o), referred to as relative magnetization, to be

$$\frac{M}{M_o}=\coth(a)-\frac{1}{a} \qquad 7.34$$

where $a=\frac{\Theta H}{kT}$, k is Boltzmann constant, T is temperature in K. The expression on the right is called the Langevin function, usually abbreviated by $L(a)$. Expressed as a series, it is

$$L(a)=\frac{a}{3}-\frac{a^3}{45}+\frac{2a^5}{945}-... \qquad 7.35$$

Although the Langevin analysis is based on paramagnetic materials, it is by and large equally applicable to ferromagnetic materials. From the physics aspect of magnetism, the complete theory is the quantum theory of magnetism of Brillouin (1927). Langevin's theory is a slightly modified version of Brillouin's general description.

From equation 7.35, the Langevin expression for sinusoidal field intensity of $\underline{H} = H\sin\omega t$, therefore, is

$$L(a)=\frac{\Theta H}{16KT}\left(\frac{10}{3}\sin\omega t+\frac{1}{9}\sin 3\omega t+\frac{2}{9}\sin 5\omega t+...\right) \qquad 7.36$$

where H is the amplitude of the field intensity. The specimen is magnetized weakly for paramagnetic and highly for ferromagnetic, and the resulting field of the specimen contains odd harmonics. The harmonics effect in paramagnetic materials is very small and negligible because of their weak magnetic properties (very low magnetic

permeability and very small positive magnetic susceptibility). However, for ferromagnetic with high magnetic permeability and susceptibility the magnitude of the harmonics can be large resulting in distortion of the applied field.

The Langevin theory can only be considered as a partial explanation of the harmonic phenomena not least because the even harmonics, although small in magnitude compared to the odd harmonics, are not accounted for. Other factors which should be considered and may influence harmonic distortion are the strength of the applied field, the remanence magnetization in the ferromagnetic materials, saturation, eddy currents and the frequency of the field.

To avoid the distortion, the AD549 op-amps along with the other electronics of the flowmeter were housed in an aluminium box away from the applied magnetic field (refer to figure 7.2). A twisted pair of coaxial cables, with copper conductors and copper mesh shielding were used to connect the electrodes to the op-amps.

7.10 Concluding remarks on the design

(1) - Perspex was chosen as the flow conduit of the meter because both BP180 and the perspex pipe have a clear bright appearance, and it was possible to observe air bubbles in the flow. Since the flowmeter was a single phase (*i.e.* it was designed for liquid only), the flow rig had to be free from air bubbles during experiments.

(2) - The large electrodes average not only the flow generated potential across more of the flow but also the flow related charge noise. The flow potential on large electrodes is smaller in magnitude than point electrodes for a given flowrate, but it is more stable (further analysis on this will be given in the next chapter). The large capacitive electrodes average the random charge noise and compared to

point electrodes the charge noise magnitude is smaller.

(3) - Whenever possible, twisted pairs of wires were used to minimize the net area traversed by the applied magnetic field in order to reduce additional quadrature and coupling effects.

(4) - Even though the electrostatic shield was grounded, a small extraneous capacitance, in the region of 1 to 2 pF, between the coils and the electrodes was still expected. In order to avoid changes in the distance between the coils and the electrodes because of the vibration of the flexible shield (resulting from the very high voltage on the coils) the shield was tightly wrapped on the supporting perspex pipe with a strong double-sided adhesive tape. A change in the distance, which means a change in the magnitude of the extraneous capacitance, may introduce a second harmonic at the output of the flowmeter.

To illustrate this let the coils and the electrodes of the flowmeter be represented by the two electrodes of a capacitor (see figure 7.29). The electrostatic force on the shield can be found from the electrostatic equation

$$\underline{F} = \frac{1}{2} q \underline{E} \qquad 7.37$$

where q is the charge, E is the electric field. Now $q = Cu$, where C and u are the capacitance and potential difference between the coils and the electrodes of the meter at a distance $x + \Delta x$ (Δx represents vibration distance). Since $C = \frac{\varepsilon_o A}{x + \Delta x}$ for an area A of the electrodes and dielectric permittivity of air ε_o,

$q = \varepsilon_o A \underline{E}$ where $\underline{E} = \frac{u}{x + \Delta x}$. Substituting for q in equation 7.37,

$$\underline{F} = \frac{1}{2}\varepsilon_o A \underline{E}^2 \qquad 7.38$$

For a sinusoidal electric field of $\underline{E} = E\ sin(\omega t)$, the electrostatic force takes the form $\underline{F}=\frac{\varepsilon_o A E^2}{4}(1-\sin(2\omega t+\frac{\Pi}{2}))$, the 2ω being the second harmonic.

The force that could be exerted on the shield for a vibration distance Δx of 0.1 mm was estimated to be around 0.5 Newton for the flowmeter assembly described in this chapter.

(5) - Since the frequency of the current in the coils was relatively high for an electromagnet, identifying the size of the skin-effect was important. The common method of approximating the skin-effect of a coil is to determine the critical frequency at which the skin-effect is appreciable. For low frequency coils of wire diameter d, this critical frequency occurs when $\frac{d}{\delta_s}=2$, where δ_s (depth of penetration) is the depth below the surface of the wire at which the current density falls to about 37 % of its surface value . For a copper wire , the simplified expression (Welsby, 1950) for the critical frequency (f_c in Hz) is

$$f_c=(2^2)(\frac{6.6}{d})^2 \qquad 7.39$$

where d is in cm.

The critical frequency for the coils (wire diameter = 0.8 mm) of the meter was found to be 27 kHz; which is 18 times the working frequency of 1.5 kHz, hence,

the skin-effect was negligible.

(6) - The theoretical phase relationship between the coil voltage (u_L), coil current (i_L), quadrature voltage (u_q), magnetic field (B), and flow signal (u_g) is shown in figure 7.30. u_L and u_q are 90° out of phase from i_L, B and u_g.

8.0 PREDICTING THE SENSITIVITY OF THE FLOWMETER

8.1 Introduction

The sensitivity or the magnitude of the flow signal of an electromagnetic flowmeter for unit flow velocity cannot be accurately predicted because of such factors as eddy currents, random noise and magnetic field distribution. In addition, an exact analysis of the geometrical configuration of the flowmeter, which in most cases involves a three dimensional representation and complex mathematical expressions, is required. Therefore, flowmeters are individually calibrated adding extra cost to the manufacturing process. However, with the help of simplified but realistic assumptions it is possible to estimate the sensitivity of an electromagnetic flowmeter.

8.2 Estimation of the sensitivity of the flowmeter

Figure 8.1 shows the cross-sectional view of the electromagnetic flowmeter configuration described in the previous chapter. In the analysis of the design to estimate the sensitivity of the flowmeter, the following assumptions are made:

(1) - The flow conduit has interior radius a, exterior radius b and the walls are sufficiently smooth so as not to disturb the flow.

(2) - The alternating magnetic field $\boldsymbol{B}$ is uniform both in magnitude and direction across the whole length (axial direction) of the electrodes. Any components of the magnetic field other than in the y-direction are ignored.

(3) - The flow profile is symmetrical with respect to the axis of the pipe. The flowrate is a function of r, *i.e.* $v = v(r)$ and the flowrate at the pipe wall is zero, *i.e.* $v(a) = 0$.

(4) - The electrical properties of both the pipe wall and the liquid are homogeneous with dielectric permittivity of the pipe wall ε_1, of the liquid ε_2, conductivity of the pipe wall σ_1 and of the liquid σ_2.

(5) - The electrodes are on the outside surface of pipe wall each (together with shields) covering half the circumference.

The potential u_e in the pipe wall is given by

$$u_e = u_{II} + u_{III}$$

where we define potentials u_{II} and u_{III} in region 1 (the pipe wall) as follows.

(I) - u_{II} is the voltage (with no flow) at any point in the pipe wall for a general context voltage of $\pm u$ on the electrodes ($-u$ on the left hand side electrode and u on the right hand side electrode, see figure 8.2). This is assuming the detection and the driven-shield electrodes are at the same potential, *i.e.* the follower amplifier gain is 1.

(II) - u_{III} is the voltage at any point in the pipe wall as a result of the flow induced potential of the meter where the two electrodes are at zero potential (see figure 8.3).

We similarly define potentials u_{2I} and u_{2II} in region 2 (the liquid).

When the two electrodes of the flowmeter are at $\pm u$ potential (case I), the charge density in both the liquid and the pipe wall is zero. Therefore, the potential distribution in both the pipe wall (u_{II}) and the liquid (u_{2I}) can be found from the homogenous equations:

$$\nabla^2 u_{II} = 0 , \quad \text{for} \quad a < r < b \qquad 8.1$$

$$\nabla^2 u_{2I} = 0 , \quad \text{for} \quad 0 < r < a \qquad 8.2$$

The boundary conditions are

$$u_{1I}(a,\theta) = u_{2I}(a,\theta) \tag{8.3}$$

$$\varepsilon_1 \frac{\partial u_{1I}(a,\theta)}{\partial r} = \varepsilon_2 \frac{\partial u_{2I}(a,\theta)}{\partial r} \tag{8.4}$$

$$u_{1I}(b,\theta) = \pm u \tag{8.5}$$

$$u_{2I}(0,\theta) = 0 \tag{8.6}$$

where $\omega\varepsilon_o\varepsilon_1 \gg \sigma_1$ for the insulating pipe wall and $\omega\varepsilon_o\varepsilon_2 \gg \sigma_2$ for a dielectric liquid.

The solution to equations 8.1 and 8.2 are

$$u_{1I} = \sum_{n=1,3,5,}^{\infty} \left(\frac{4\sin(n\frac{\pi}{2})}{n\pi} \left(\frac{r}{b}\right)^n \left(\frac{(1+\frac{\varepsilon_1}{\varepsilon_2}) - (\frac{a}{r})^{2n}(1-\frac{\varepsilon_1}{\varepsilon_2})}{(1+\frac{\varepsilon_1}{\varepsilon_2}) - (\frac{a}{b})^{2n}(1-\frac{\varepsilon_1}{\varepsilon_2})} \right) \cos n\theta \right) u \tag{8.7}$$

$$u_{2I} = \sum_{n=1,3,5,}^{\infty} \left(\left(\frac{r}{b}\right)^n \left(\frac{8\varepsilon_1 \sin(n\frac{\pi}{2})}{\varepsilon_2 n\pi \left((1+\frac{\varepsilon_1}{\varepsilon_2}) - (\frac{a}{b})^{2n}(1-\frac{\varepsilon_1}{\varepsilon_2}) \right)} \right) \cos n\theta \right) u \tag{8.8}$$

When the two electrodes of the meter are at zero potential (case II), the charge density in the pipe wall is zero. The charge density in the liquid, on the other hand, is dependent on the flow generated potential of the flowmeter as described by the general

electromagnetic potential equation of Cushing (1958). The potential distribution in the pipe wall u_{1II} and in the liquid u_{2II}, therefore, can be determined from the equations

$$\nabla^2 u_{1II} = 0 , \qquad \text{for } a < r < b \tag{8.9}$$

$$\nabla^2 u_{2II} = ZB\frac{dv(r)}{dt}\cos\theta , \qquad \text{for } 0 < r < a \tag{8.10}$$

where B is the magnetic field and $Z = 1 - \varepsilon^{-1}$ is the simplified expression for the attenuation factor of electromagnetic flowmeter of equations 3.2 to 3.4 of chapter 3 (because of the assumption $\omega\varepsilon_0\varepsilon_2 \gg \sigma_2$).

The boundary conditions are

$$u_{1II}(a,\theta) = u_{2II}(a,\theta) \tag{8.11}$$

$$\varepsilon_1\frac{\partial u_{1II}(a,\theta)}{\partial r} = \varepsilon_2\frac{\partial u_{2II}(a,\theta)}{\partial r} \tag{8.12}$$

$$u_{1II}(b,\theta) = 0 \tag{8.13}$$

$$u_{2II}(0,\theta) = 0 \tag{8.14}$$

The solution to equations 8.9 and 8.10 are

$$u_{1II}=\frac{FZB}{\pi r}\left(\left(1-\left(\frac{r}{b}\right)^2\right)\left(\frac{1}{\left(1+\frac{\varepsilon_1}{\varepsilon_2}\right)-\left(\frac{a}{b}\right)^2\left(1-\frac{\varepsilon_1}{\varepsilon_2}\right)}\right)\right)\cos\theta \qquad 8.15$$

$$u_{2II}=\frac{FZB}{\pi r}\left(\frac{\pi}{F}\int_0^r (rv(r)\,dr)+\frac{1}{2}\left(\frac{r}{a}\right)^2\left(\frac{\left(1-\frac{\varepsilon_1}{\varepsilon_2}\right)-\left(\frac{a}{b}\right)^2\left(1+\frac{\varepsilon_1}{\varepsilon_2}\right)}{\left(1+\frac{\varepsilon_1}{\varepsilon_2}\right)-\left(\frac{a}{b}\right)^2\left(1-\frac{\varepsilon_1}{\varepsilon_2}\right)}\right)\right)\cos\theta$$

8.16

where F is the volumetric flowrate of liquid.

u_e , therefore, is the sum of the expressions in equation 8.7 and equation 8.15. The flowmeter can be considered as a voltage generator. To determine its open circuit terminal voltage, the total charge across the detection electrodes (terminals) must be maintained at zero; *i.e.* no current is drawn by the associated detection electronics. The total charge (Q) on the right detection electrode, from Gauss' law, is given by

$$\int_{-\alpha}^{\alpha}\varepsilon_o\varepsilon_1\left(\frac{\partial u_e(b,\theta)}{\partial r}\right)d\theta=Q \qquad 8.17$$

where α is the semi-angle subtended by the detection electrode (refer to figure 8.1).

The open circuit electrode voltage u_g of the flowmeter is found by setting

$$\int_{-\alpha}^{\alpha}\left(\frac{\partial u_e(b,\theta)}{\partial r}\right)d\theta=0 \qquad 8.18$$

Substitution of equations 8.7 and 8.15 in to 8.18 yields:

$$u_g = \frac{FZB}{2bk} \left(\frac{\sin\alpha}{(1+\frac{\varepsilon_1}{\varepsilon_2}) - (\frac{a}{b})^2 (1-\frac{\varepsilon_1}{\varepsilon_2})} \right) \qquad 8.19$$

where

$$k = \sum_{n=1,3,5,}^{\infty} \frac{1}{n} \left(\frac{(1+\frac{\varepsilon_1}{\varepsilon_2}) + (\frac{a}{b})^{2n} (1-\frac{\varepsilon_1}{\varepsilon_2})}{(1+\frac{\varepsilon_1}{\varepsilon_2}) - (\frac{a}{b})^{2n} (1-\frac{\varepsilon_1}{\varepsilon_2})} \right) \sin(n\frac{\pi}{2}) \sin(n\alpha) \qquad 8.20$$

For 0.1% accuracy in u_g , 1000 terms are required for the summation in k.

Figure 8.4 shows u_g for different values of the subtending angle α at a nominal flowrate of 2 metre/second (4 litre/second) of BP180 (the magnitude of the other terms in equation 8.19 are given in table 8.1). u_g decreases as α increases indicating the limitation of large area electrodes in collecting the maximum possible flow generated potential out of the system. At $\alpha = 90°$ the two electrodes join and as a result the flow signal is shorted, *i.e.* $u_g = 0$.

The other factors which determine the size of the flow signal are the physical and electrical properties of the flow conduit walls. u_g is small for conduit pipe walls of

high dielectric permittivity (see figure 8.5). This may be expected because high dielectric permittivity pipe walls short some of the flow signal to ground. u_g also decreases with the increase in the thickness of the walls of the flow conduit as it is shown in figure 8.6. In the case of thin flow conduit walls where $a \gg (a - b)$, the physical size is not as critical as the dielectric permittivity or conductivity of the walls.

Because of symmetry (u_g for $-\frac{\pi}{2}<\theta<\frac{\pi}{2}$ and $-u_g$ for $\frac{\pi}{2}<\theta<\frac{3\pi}{2}$) the combined flow signal of the two electrodes is $2u_g$. For the nominal flow rate of 2 metre/second of BP180 the flow signal of the meter ($2u_g$) was estimated to be 0.31mv.

The expression in equation 8.19 applies only for dielectric liquids. For moderately conducting liquids $\frac{\varepsilon_1}{\varepsilon_2}$ is replaced by $\frac{j\omega\varepsilon_o\varepsilon_1}{\sigma_2}$, since $\sigma_2 \gg \omega\varepsilon_o\varepsilon_2$. In the generalized expression for equation 8.19 which includes the complex conductivity of both the pipe wall and the liquid, $\frac{\varepsilon_1}{\varepsilon_2}$ is replaced by $\frac{\sigma_1+j\omega\varepsilon_o\varepsilon_1}{\sigma_2+j\omega\varepsilon_o\varepsilon_2}$; where $j = \sqrt{-1}$.

8.3 Estimation of the internal impedance of the flowmeter

Following the same analysis as Cushing (1965) the internal impedance of the flowmeter, as a voltage source, can be determined from the admittance:

$$\mathbf{Y}_o = \frac{i_s}{u_g} \qquad 8.21$$

where i_s is the short circuit current. From Ohm's law equation of $i = (J + \frac{dD}{dt}) A$,

where J is the conduction current density, D is the displacement current density and A is the surface area of the detection electrode, the total current i_s entering the detection electrode (with the shielding electrode grounded) under short circuit condition (*i.e.* $u_{II}\,|_{r=b} = 0$) is

$$i_s = -(\sigma_1 + j\omega\varepsilon_o\varepsilon_1)\, 2lb \int_{-\alpha}^{\alpha} \left(\frac{\partial u_{1II}(b,\theta)}{\partial r}\right) d\theta \qquad 8.22$$

where l is the axial length of the detection electrode from the centre. Substituting equation 8.15 in to equation 8.22 and performing the indicated operations in equation 8.21:

$$\mathbf{Y}_o = \frac{1}{R_o} + j\omega C_o \qquad 8.23$$

where R_o is the internal resistance

$$R_o = \frac{\pi}{\sigma_1 8 (2l) k} \qquad 8.24$$

and C_o is the internal capacitance (in parallel with R_o)

$$C_o = \frac{8\,(2l)\,\varepsilon_o \varepsilon_1 k}{\pi} \qquad 8.25$$

Since $\omega \varepsilon_o \varepsilon_l \gg \sigma_l$, the flow signal path is through C_o (i.e. a.c. coupled).

8.4 End-effects

In the analysis to estimate the flow signal of the meter it was assumed that the applied uniform magnetic field was constant across the axial length of the electrodes and the edges of the magnetic field were reasonably remote. In practice, however, the magnetic field falls off gradually as the distance from the centre increases (refer to figure 7.22). In addition the electrodes are not infinitely long and when fitted in the flow rig some of the flow signal of the meter may be shorted at the ends. To have a realistic estimation of the flow signal, these factors commonly known as end-effects, must be taken into consideration.

For simplicity, the analysis for end-effects is carried out without the walls of the perspex conduit, see figure 8.7. If the voltage u_l is the two-dimensional distribution of the flow induced potential of the flowmeter in the liquid for a general context voltage of $\pm u$ on the whole electrode areas (*i.e.* u for $-\frac{\pi}{2} < \theta < \frac{\pi}{2}$ and $-u$ for $\frac{\pi}{2} < \theta < \frac{3\pi}{2}$), then

$$\nabla^2 u_l = ZB \frac{dv(r)}{dr} \cos\theta \,, \quad \text{for } |z| < L \text{ and } r < a \qquad 8.26$$

where L is the length of the driven-shield electrode from the centre and $\frac{\partial u_1}{\partial z}=0$ at

the edges of the electrodes (*i.e.* $z = \pm L$). The solution to u_1 is the sum of u_{2I} and u_{2II} (equations 8.8 and 8.16) in which a is substituted for b. From equations 8.8 and 8.16, assuming a flat profile and retaining only the term $n = 1$ in the Fourier series in θ,

$$u_1 = \frac{4}{\pi a}(r\cos\theta)\,u \qquad 8.27$$

We take $u_1 = 0$ outside the region $|z| < L$ and $r < a$, and define another potential, "end-effect potential" u_2 that must be added to u_1 . u_2 extends over all space and must satisfy

$$\nabla^2 u_2 = 0 \qquad 8.28$$

everywhere as there are no sources outside the region where u_1 is defined (*i.e.* $B\frac{dv(r)}{dr}=0$ outside because the magnetic field is considered to have fallen to zero

). The fall-off of u_2 on $r = a$ and $z > L$ is assumed to be $u_2=\pm e^{\frac{L-z}{a}}$ (+ referring to $-\frac{\pi}{2}<\theta<\frac{\pi}{2}$ and - to $\frac{\pi}{2}<\theta<\frac{3\pi}{2}$) and the boundary conditions (for one side of

one of the electrodes) are

$$\frac{\partial u_2(a,\theta,L_+)}{\partial z} = \frac{\partial u_2(a,\theta,L_-)}{\partial r} \quad , \quad \text{at} \quad z = L \tag{8.29}$$

$$u_2(a,\theta,L_+) - u_2(a,\theta,L_-) = u_1(a,\theta,L_-) \quad , \quad \text{at} \quad z = L \tag{8.30}$$

where L_+ and L_- are approaches from the right and left to $z = L$ respectively (see figure 8.8). The general potential u_2 (with $cos\theta$ dependence) from the Fourier-Bessel expansion (Smythe, 1950) for $z < L$ is

$$u_2 = \left(\frac{4mJ_2(j_{1,1})}{\pi (J'_1(j_{1,1}))^2}\right) \left(J_1\left(j_{1,1}\frac{r}{a}\right)\right) \left(\cos\theta e^{-j_{1,1}\frac{L-z}{a}}\right) u \tag{8.31}$$

where

$$m = \frac{j_{1,1} - 1}{j_{1,1}(1-(j_{1,1})^2)} \tag{8.32}$$

and J_1 and J_2 are Bessel functions of the first and second order respectively, J'_1 is the derivative of J_1 and $j_{1,1}$ is the first positive zero of J_1 . Since the fall-off of u_2 was approximated on $r = a$ for z - L increasing, the first term (*i.e.* $n = 1$ in the Fourier series in θ) is adequate for estimation of u_2. Higher terms decay more rapidly on approaching the central electrode. Equation 8.31 is for one end of one of the electrodes. Because of symmetry the end-effect for both edges of the electrodes (*i.e* $z = -L$ and $z = L$) can be found by replacing u_2 by $2u_2$ in analysis to follow.

The end-effect adjusted potential at one of the electrodes of the meter therefore is the sum of u_1 and $2u_2$. The end-effect adjusted open circuit terminal voltage of the meter is determined by insisting that the total charge (Q) on the detection electrodes is zero. Therefore,

$$\int_{-l}^{l}\int_{-\alpha}^{\alpha}\left(\frac{\partial(u_1+2u_2)\,(a,\theta,z)}{\partial r}\right)d\theta dz=Q=0 \qquad 8.33$$

where l is the axial length of the detection electrode from the centre. Substituting equations 8.8, 8.16 and 8.31 in to 8.33 and performing the indicated operations results in

$$u_s=\frac{FZBl}{4a^2}\left(\frac{1}{\frac{l}{a}+\frac{2mJ_2(j_{1,1})}{J'_1(j_{1,1})}\left(e^{-j_{1,1}\frac{L-l}{a}}-e^{-j_{1,1}\frac{L}{a}}\right)}\right) \qquad 8.34$$

Comparison of equations 8.19 and 8.34 shows that u_s should be about 10% less than u_g (*i.e.* the end-effects reduce the flow signal by 10 %) in the experimental flowmeter. According to the analysis offered by Shercliff (1962) for an electromagnetic flowmeter with point electrodes and the same magnetic field length the end-effects would reduce the flow potential by 5 %. It means that large electrodes suffer from a relatively high degree of end-effects compared to point electrodes for an identical distribution in the applied magnetic field. This may be expected as the two edges of the axial length of large electrodes are closer to the edges of the gradually falling magnetic field than point electrodes would be.

8.5 Equivalent circuit of the flowmeter

The equivalent circuit of the flowmeter as a voltage generator together with the follower amplifiers are shown in figure 8.9. It consists of:

(i) The flow signal u_g quantified in equation 8.19 and the internal resistance R_o and capacitance C_o quantified in equations 8.24 and 8.25 respectively.

(ii) Residual capacitance C_a between the detection electrode and ground. Although driven-shield electrodes are designed to minimize the capacitance to ground, a small residual capacitance may always be difficult to avoid.

(iii) The capacitance C_e between the detection electrode and the driven-shield electrode.

From the analyses of the equivalent circuit, the output voltage u_o at the follower amplifier of each electrode is related to u_g as follows:

$$u_o = \left(\frac{G_o C_o}{G_o(C_o+C_a) + j\omega(C_o+C_a+C_e)}\right) u_g \qquad 8.35$$

where G_o is the open-loop gain of the operational amplifier (AD549). In theory, once the sizes of the detection and driven-shield electrodes are fixed the only design parameter is G_o. However the open loop gain of most operational amplifiers, at least those with high input impedance, is commonly around 10^6.

The bandwidth of the system is given by

$$\omega_{BW}=\frac{G_o(C_o+C_a)}{C_o+C_a+C_e} \qquad 8.36$$

The ± 3db or half power points can be determined by setting $\left|\frac{u_o}{u_g}\right| = \frac{1}{\sqrt{2}}$. It is also possible to work out the gain of the system, *i.e.* $\left|\frac{u_o}{u_g}\right|$ at 1.5 kHz.

Approximating the value of C_e to 1.5 pF, obtaining R_o and C_o from equations 8.24 and 8.25 and taking the measured value of C_e (= 870 pico farad), the bandwidth of the equivalent circuit was estimated to be 4.6 kHz with the +3 db point at 80 Hz and -3 db point at 4.7 kHz. The gain at 1.5 kHz was found to be 0.8 which compares well with the simulation result of 0.76 (section 7.5 of chapter 7).

9.0 EXPERIMENTAL RESULTS

9.1 Purpose and scope of the experiments

The main objective of the experimental effort has been to see whether the flow of dielectric liquids could be measured by the principle of magnetic induction and to verify equation 8.34 of the last chapter.

The experimental work carried out consisted of three parts. First, the flowrate of BP dielectric 180 was measured using the electromagnetic flowmeter described in chapter 7. Second, the meter was used to measure the flowrate of tap water. The third and final experiment was to monitor the effect of a relaxation tank on the magnitude and distribution of charges generated by the flow of BP180.

The flow rig described in chapter 5 was used to experiment both on the measurement of the flowrate of BP180 and the magnitude of charges. An existing flow circuit in the department was used in the experiment to measure the flowrate of tap water.

9.2 Experimental procedures and results

9.2.1 Measuring the flow rate of BP180

Having tested the correct functioning of the electronics, electromagnet and the electrostatic shield, the electromagnetic flowmeter was inserted at the test section of the flow rig (see figure 9.1(a) and (b)). Before the experiment began, the rotary turbine reference flowmeter (KDG MOBREY M2/2000/250 type) had to be calibrated for

BP180. Although it was already calibrated for water, because of the difference in viscosity between water and BP180 recalibration was necessary. A clamp-on ultrasonic flowmeter attached on the outside of the pipe at the long straight section of the flow rig (upstream of the test section), was used to recalibrate the reference flowmeter up to the maximum flowrate of the flow circuit.

The electromagnet of the meter was powered-on at zero flow condition. The voltage derived from the reference coil *emf* was adjusted in phase and magnitude (to equal that of the resulting quadrature voltage) and mixed with the electrode signal to reduce the quadrature voltage to near zero. The *emf* in the reference coil was also used as a reference signal *via* a T-junction to the lock-in amplifier. Since the lock-in amplifier had a single phase output (Brook-deal ORTEC-9401 type), the flow signal was read directly from its output (*i.e.* what was left of the quadrature signal was rejected and only the flow signal was displayed at the output).

After the above described zeroing procedure, the flow generated signal of the meter was observed at various flowrates as indicated in figure 9.2. The flow signal was linear for flowrates above 1.25 metres/second. For flowrates under 1.25 metres/second, on the other hand, the flow signal was non-linear. This is illustrated more clearly in the graph of the meter factor (see figure 9.3). The cause of this non-linearity was found to be the vibration of the impeller of the pump at low flows. The line pressure did not directly influence the reading of the flow signal.

9.2.2 Measuring the flowrate of tap-water

The experiment on measuring the flowrate of water was performed on an existing multipurpose departmental flow rig. A simplified schematic diagram of the flow circuit is shown in figure 9.4. It was made from 2 inch plastic pipe. The reference flowmeter (KDG MOBREY M2/2000/250 type) was already calibrated and in use. Brass plates were included at the upstream and downstream flanges of the test section for grounding

purposes. The flowmeter was fitted at the test section (see figure 9.5 (a) and (b)). Before the test run was made, with stationary water in the flow loop, the quadrature voltage was reduced to zero as in the above section by adjusting the voltage derived from the reference coil for synchronous annulment.

The flow signal of the meter recorded at the output of the lock-in amplifier at various flowrates is shown in figure 9.6. The flow signal was linear for all flowrates. As in the case of BP180, it was checked that the line pressure had no effect on the readings. The flow signal of the meter was 1.96 times that obtained for BP180. This was very close to the expected figure of 2 since the flowmeter attenuation factor $Z = \frac{1}{2}$ for BP180 and $Z = 1$ for water (refer to equation 3.3).

9.2.3 Effect of the relaxation tank

The relaxation tank in the flow rig of figure 5.1, with cone shaped entrance and exit for smooth flow transition and to avoid excess charges slows the flowrate by $\frac{1}{20}^{th}$. For a nominal flowrate of 2 m/s, for instance, the residence time of BP180 in the relaxation tank is about 0.36 second; which is higher than its relaxation time of 0.3 second. Therefore, some excess charges generated by the pump are expected to relax to ground. The purpose of this experiment was to asses the effect of these excess charges on the charge distribution noise of the meter.

The relaxation tank in the flow loop was replaced by a straight 2 inch mild steel pipe. The electromagnet of the flowmeter was disconnected, and the output of the flowmeter was connected to a digital oscilloscope (ONO SOKKI CF-930 type); *i.e.* the output of the instrumentation amplifier of figure 7.7 (with the reference input grounded) was fed to the oscilloscope as there was no need for the lock-in amplifier.

The averaged charge distribution noise spectra recorded at the output of the meter for flowrates of 1 m/s and 3 m/s are shown in figure 9.7 (a) and (b) respectively. These charge distribution noise spectra were on average about 2 dB higher in magnitude across the whole bandwidth than those obtained with the relaxation tank in the flow rig (refer to figure 7.5 (a) and (b)). The main difference, however, was in the instantaneous (unaveraged) spectra of the noise at all frequencies over the bandwidth. The unaveraged spectra varied slowly (for each flowrate) from one instant to another when the relaxation tank was in the flow rig, whereas, without the relaxation tank the instantaneous values from one instant to the next varied wildly. Although it was difficult to prove accurately, repeated experiment and continuous observation indicated that the cause of this exaggerated fluctuation in the instantaneous magnitude of the charges was the intermittent contact between the BP180 and the impeller of the pump (*i.e.* without the relaxation tank to allow time for some of the charges to relax to ground, the instantaneous values were high for parts of the liquid which came in contact with the impeller and small for those that did not).

9.3 Discussion

Since the research has been into developing an electromagnetic flowmeter for dielectric liquids, the discussion here is mainly on the result of the experiment in measuring the flowrate of BP180.

The minimum quadrature voltage, even after adjusting the signal wires for the smallest possible projection area, was measured to be 100 mv. This was about 200 times the maximum flow signal of the meter. Unlike low frequency (commonly between 50 to 200 Hz) electromagnetic flowmeters designed for moderately conducting liquids in which the quadrature voltage can be minimized to the flow signal level or at least to a multiple of a single digit, the 1.5 kHz magnetic field combined with the small flow signal (half that of moderately conducting liquids) generated by dielectric liquids made it difficult to reduce the quadrature voltage to the signal level.

Capacitive coupling, in-phase or otherwise, was not a problem when reading the flow signal. As described earlier, the reading of the meter was set to zero at zero flow condition. The chart recording of the zero stability of the meter is shown in figure 9.8. The zero drift was around 2.5 % per hour of the full scale voltage (the maximum flow signal) of the meter. Considering the size of the current (2 Amp) on the coils, it was a satisfactory stability. The drift was found to be 1 % per hour for half the working current 1 Amp, which is a reduction in the drift of more than a half. This trend continued for further reduction in the current. Mechanical vibration of the flow rig as a result of the pump action may also have contributed to a slight drift in the zero line.

Although difficult to quantify, some of the non-linearity of the flowmeter output at low flowrates might have been avoided if the control valve had not been situated at the far end downstream of the flowmeter where it caused high pressure in the test section. This effect (which may be more severe than was anticipated when designing the flow loop) was unavoidable since placing the control valve upstream of the test section would have resulted in more excess charge owing to friction.

The experimental result confirms that in general the expression for the flow signal in equation 8.34 (hence 8.19) holds for all flowrates. The values obtained for the flow related signal from equation 8.34 are up to 4 % higher than those of the experiment. The 4 % discrepancy is reasonably good considering that equation 8.34 is basically a two dimensional result with the magnitude of the magnetic field assumed to be constant throughout the meter.

The magnetic field was found to fall by up to 1 % of the working magnitude (= 104 Gauss) during the experiment. This is mainly due to the rise in temperature of the coils which causes their combined impedance to increase. The increase in the impedance reduces the current in the coils (and hence the applied magnetic field) for the same applied voltage across the resonant circuit.

The response time of the meter, *i.e.* the time it took for the meter to respond to a change in the flowrate, was 10 seconds (measured using a stop-watch: SEIKO 200/A

type). However at the lower flowrates where the output of the flowmeter was not linear, the response time was 1 to 2 seconds longer; *i.e.* for flowrates under 1.5 metre/second the response time was between 10 to 12 seconds (closer to 10 seconds for large changes in the flowrate and near 12 seconds for small changes).

10.0 CONCLUSIONS AND RECOMMENDATIONS FOR FUTURE WORK

10.1 Conclusions

(1) The results of the experiment prove that measuring the flowrate of dielectric liquids based on Faraday's law of induction is possible.

(2) The formula derived to estimate the flow signal of a capacitive signal pick-off type electromagnetic flowmeter when used on dielectric liquids applies for all flowrates. By inference it is reasonable to assume that the generalized form of the equation for both moderately conducting and dielectric liquids, which can be obtained by adjusting the expression in 8.34 as suggested in section 8.2, also holds.

(3) The response time of the flowmeter is very promising, and the zero stability is satisfactory for the size of the current in the coils. A more refined design with fewer discrete electronic devices, use of small non-standard coaxial cables and application of digital signal processing techniques might enable the current in the coils to be reduced at least down to 100 mA; which should result in a vastly improved zero stability.

(4) The choice of the frequency of operation of an electromagnetic flowmeter suitable for dielectric liquids is heavily dependent on the charge noise. This charge noise has a low frequency spectrum. As the charge noise determines the signal to noise ratio at the front-end of the meter, appropriate choice of the operational frequency is important.

(5) Since the operating frequency of an electromagnetic flowmeter suitable for dielectric liquids is higher than that for moderately conducting liquids, the

design of the eddy current free electrostatic shield is critical in the functioning of the meter.

10.2 Recommendations for future work

(1) An eddy current free electrostatic shield with improved attenuation capability of capacitive coupling voltage needs to be designed and tested. The design can take the form shown in figure 10.1 and manufactured either on a flexible printed circuit board or formed into the walls of the coil supporting pipe. It is estimated that this type of shielding could offer an attenuation of over 100db (refer to section 7.8.1 and 7.8.2).

(2) A solution to the problem of high quadrature voltage and one that may also improve the zero stability of the meter is driving the coils with a current wave form containing a period of constant magnetic field where the transformer signal is zero. To achieve this end and still maintain the high operational frequency required to avoid the charge noise, one cannot use the conventional methods of square, triangular and trapezoidal wave forms used in the past mainly due to their frequency limitation and the high voltage that can be developed across the coils. The ideal wave form would be a sinusoidal with a flat top. Theoretical as well as practical work is needed to find if such a wave form is possible to generate.

(3) Perhaps the most important work that has to be done is in the area of design of a suitable magnetic shield for the meter. Conventional ferromagnetic materials such as iron and mumetal can not be used due to eddy currents and harmonic distortion. Two possible approaches can be followed in order to come up with a solution: to use ferrites or to adopt a similar design to that of the eddy current free electrostatic shield.

The eddy current can be minimized by the use of ferrites which normally have a resistivity of at least a million times that of a ferromagnetic. It is also possible to envisage that if a shield made of a ferrite can be placed at a reasonable distance from the coils depending on the strength of the applied magnetic field of the meter, the harmonic distortion generated as a result of the non-linear magnetization curve of ferrites can be kept to a tolerable level.

If thin insulated mumetal wires are formed in a similar fashion as in the eddy current free electrostatic shield but with no connection at either ends, the eddy current can easily be reduced to near zero. To avoid saturation two or more of this shields may be used together. If the shield is formed into a box (either by wrapping it around a non-conducting material or by meshing it into a physically strong plastic) and placed at a reasonable distance from the coils the harmonic distortion can be minimized.

REFERENCES

Abedian B. Sonin A. — Theory for electric charging in turbulent pipe flow J. Fluid mech., 1982, 120, pp 199-217.

Al-Rabeh R. — PhD thesis ,1981, Imperial college, London, pp 168-232.

Al-Rabeh R. Baker R.C Hemp J. — Induction flow-measurement for poorly conducting fluids Proc. R. Soc. London ,1978, A.361, pp 93-107.

Astely E.R. — Magnetic Flowmeter Output Potentials, March 1952, General Electric Report R52GL52.

Barnes D.C. — Design and Testing of Electromagnetic Flowmeter for use with Dielectric Fluids, February 28, 1991, Schlumberger internal report.

Bevir M.K. — PhD thesis, April 1969, Warwick University.

Bonfig k.w. Hoffman F. Reinhold I. Feuerstein M. — A new method of magnetic-inductive flow metering, proceedings of international conference on fluid flow in the mid 1970's, N.E.L., April 1975.

Brillouin L. — Les moments de rotation el le magnétime dans la mécanique onduclatoire, Journal de pfysique, 8, (6), 1927, pp 74 - 81.

Codazzi D. Mioque J.Y. — Electromagnetic Flowmeter with Capacitive Pick-off, RD86/325, 1986 Schlumberger internal report.

Corson D.
Lorrain P. Introduction to electromagnetic fields and waves, Freeman and Company, San Francisco, 1962, pp 181 - 182.

Coustols E. Proceedings of the 4th European Drag reduction Meeting, Lausanne, 1990.

Cullity B. D. Introduction to magnetic materials, Addison - Wesley publishing company, Reading (Mass.), 1972, pp 92 - 96.

Cox T.J.
Wyatt D.G. An electromagnetic flowmeter with insulated electrodes of large area, J. Phys. E: Sci. Ins., 17, 1984, pp 488-503.

Cushing V. Induction flowmeter, Review of scientific instruments, 1958, No. 29, pp 692 - 696.

Cushing V. Erratum: Induction flowmeter, Rev. of Sci. Ins., 1961, 32, p 225.

Cushing V. Electromagnetic flowmeter, Review of scientific instruments, 1965, No. 36, pp 1142 - 1148.

Cushing V. Patent No. 3,274,831, U.S. patent office, September 22, 1966.

Cushing V. Patent No. 3, 329, 020, U.S. patent office, July 4, 1967.

Cushing V. Electromagnetic flowmeter, Review of scientific instruments, 1971, No. 12, pp 240 - 251.

Engl W.L. Der induktive durchflubmesser mit inhomogenem magnetfeld, Archiv für Electrotechnik, 53Bd, 6Heft, 1970, pp 344-359.

Engl W.L. Der induktive durchflubmesser mit inhomogenem magnetfeld, Archiv für Electrotechnik, 1972, 54, pp 269-277.

Faraday M. Experimental researches in electricity, Phil. Trans. Roy. Soc. (London), vol. 15, 1832, p 175.

Gallagher T.J. Simple Dielectric Liquids: mobility, conduction and breakdown, 1975, Oxford University Press.

Griffiths D. J. Introduction to electrodynamics, Prentice - Hall publishing Company, Englewood cliffs (N.J.), 1981.

Halsey D. M. A survey of industrial usage of flowmeters, Measurement and control, Vol. 19, No. 5, June 1986, pp 52 - 55.

Head P. V. Electromagnetic flowmeter primary elements, Trans. ASME paper No. 58 A, p 126.

Hemp J.
Spendel K.D.
Lochhead A.C. Static charge flowmeter studies, C.I.T., report, TR18/310/70, April 1987.

Higham E. H. Private communications 1985, but see measurement and instrumentation for control edited by M. G. Mylroi and G. Calvert, IEE control engineering series No. 26, Peter Peregrinus 1984.

Hentschel R. PhD Thesis, 1973, Technical University of Hannover, Germany.

Jones H.M. A practical introduction to electronic circuits, second edition, Cambridge University press, 1985, p 45.

Kolin A. An alternating field induction flowmeter of high sensitivity, Rev. Scint. Instumnt., 1945, 16, 109.

Klinkenberg A.
Van der Minne J.L.
Electrostatics in the petroleum Industry, Elsevier, Amsterdam, 1958

McComb W. D.
The physics of fluid turbulance, Clarendon Press, Oxford, 1990, pp 130 - 141.

McComb W. D.
Rabie L. H.
A I Che. Journal., 1982, No. 28, p 547.

Nakano K.
Tanaka Y.
Electrostatic flowsensor, Flow measurement and instrumentation, July 1990, Vol. 1, pp 191-200.

Nussbaum A.
Electromagnetic theory for engineers and scientist, Prentice - Hall Inc., Englewood cliffs (N.J.), 1965, pp 294 - 296.

Panofsky H. K.
Phillips M.
Classical electricity and magnetism, Addison - Wesley publishing Company, Cambridge (Mass.), 1955, p 206.

Schmoock R.
Capacitance-type electrode assemblies for electromagnetic flowmeter, patent No. 4,631,969, U.S. patent office, December 30, 1986.

Shercliff J.A.
The Theory of Electromagnetic Flow Measurement, 1962, Cambridge University Press.

Smythe W.
Static and dynamic electricity, second edition, 1950, McGraw-Hill book company, New York, pp 170 - 190.

Stoll R.
The analysis of eddy currents, Clarendon Press, Oxford 1974.

Terman F. — Radio engineer's handbook, first edition, McGraw - Hill, New York, 1943, pp 61 - 62.

Walmsley H. Woodford G. — The generation of electric currents by the laminar flow of dielectric liquids, Journal of physics D, No. 14, 1981, p 1767.

Welsby V. — The theory and design of inductance coils, Macdonald, London, 1950, pp 65 - 70.

Williams E.J. — The induction of e.m.f.s in a moving fluid by a magnetic field and its application to an investigation of the flow of liquids, Proc. Phys. Soc., London, 1930, 42, 466.

Wilmshurst T. H. — Signal recovery from noise in electronic instrumentation, Hilger, Bristol, 1985.

Wilson H.A. — Phil. Trans. A, London, 1904, vol. 204, pp 121-137.

Wyatt D. — Cardiovascular flowdynamics and measurements, University park press, Oxford, 1977, pp 89 - 149.

Yanof H. Slaz P. Rosen A. — Improvements in trapezoidal-wave electromagnetic flowmeter, Journal of Appl. Physiol., 1963, No. 18, pp 230 - 232.

Zakariah Z. — M. Sc. thesis U.M.I.S.T., March 1981.

Zosimov A. — Journal of fluid mechanics, Soviet research, Vol. 8, No.3, May - June 1979, pp 123 - 128.

Abbreviations

The following abbreviations for the names of meter and liquid types are used for tables 2.1 to 2.4, figures 2.1 to 2.5 and appendix A.

For flowmeter type:

DP = Differential Pressure.

PD = Positive displacement.

T/R = Turbine or Rotary inferential.

FO = Fluidic Oscillator.

UL = Ultrasonic.

MS = Mass.

EM = Electromagnetic.

For liquids types:

P/PP = Petroleum or Petroleum Products.

LPG = Liquid Petroleum Gases or cryogenics.

OIL = Vegetable or animal oil.

W/WW = Water or Waste Water.

	DP	PD	T/R	FO	UL	MS	EM	OTHER	TOTAL
1-50	3	10	7	0	0	2	4	0	15
50-500	8	8	9	2	2	3	1	0	14
>500	10	9	10	1	7	3	10	2	13
Total	21	27	26	3	9	8	15	2	42

Table 2.1 Number of users in each group.

	DP	PD	T/R	FO	UL	MS	EM	OTHER	TOTAL
1-50	7	117	101	0	0	17	6	0	248
50-500	1055	1039	450	11	200	13	20	0	2788
>500	10775	283700	85700	5	2153	17	12013	26	394389
Total	11837	284856	86251	16	2353	47	12039	26	397425

Table 2.2 Number of each type of flowmeter in each group.

Example

There are 3 small users out of 15 who have 7 differential pressure flowmeters from a total of 248 meters for this group.

There are 21 users out of 42 owning 11837 differential pressure flowmeters from a total sum of 397425 meters.

	P/PP	LPG	OIL	W/WW	MILK	OTHER	TOTAL
1-50	86	140	3	0	4	15	248
50-500	1400	1068	0	320	0	0	2788
> 500	8959	3957	0	381473	0	0	394389
TOTAL	10445	5165	3	381793	4	15	397425

Table 2.3 Number of flowmeters for each type of liquid in each group of users.

	DP	PD	T/R	FO	UL	MS	EM	OTHER	TOTAL
P/PP	5701	4015	667	6	3	27	0	26	10445
LPG	2310	2455	380	0	0	20	0	0	5165
OIL	0	3	0	0	0	0	0	0	3
W/WW	3825	278375	85200	10	2350	0	12033	0	381793
MILK	0	2	2	0	0	0	0	0	4
OTHER	1	6	2	0	0	0	6	0	15
TOTAL	11837	284856	86251	16	2353	47	12039	26	397425

Table 2.4 Numbers of each type of flowmeter for each type of liquid.

B (rms)	104 Gauss
f	1.5 kHz
a	22 mm
b	25 mm
ε_1 (wall)	3.5 (measured)
ε_2 (BP180)	2.0
σ_1 (wall)	$\approx 10^{-14}$ S/m
σ_2 (BP180)	5.7×10^{-11} S/m
α	$\frac{\pi}{3}$
Detection electrode axial length (**2l**)	72 mm
Driven-shield axial length (**2L**)	100 mm

Table 8.1 A summary of the magnitude of the frequency and the magnetic field strength, and the electrical and physical properties of the flowmeter.

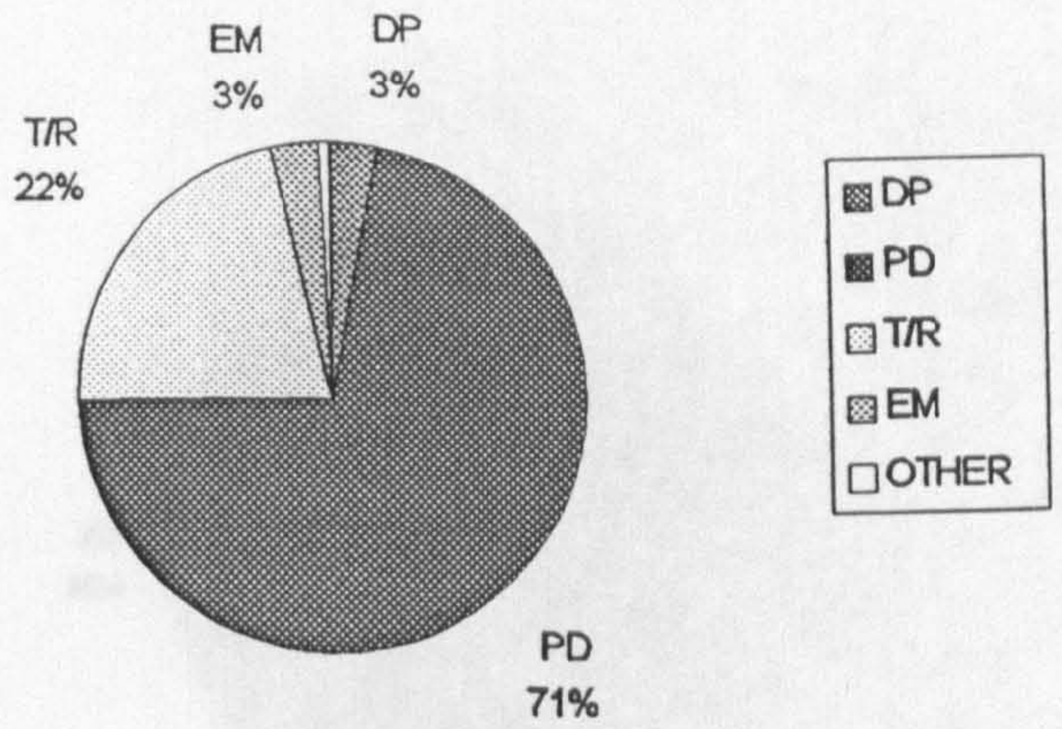

Figure 2.1: Percentage of each type of flowmeter in use.

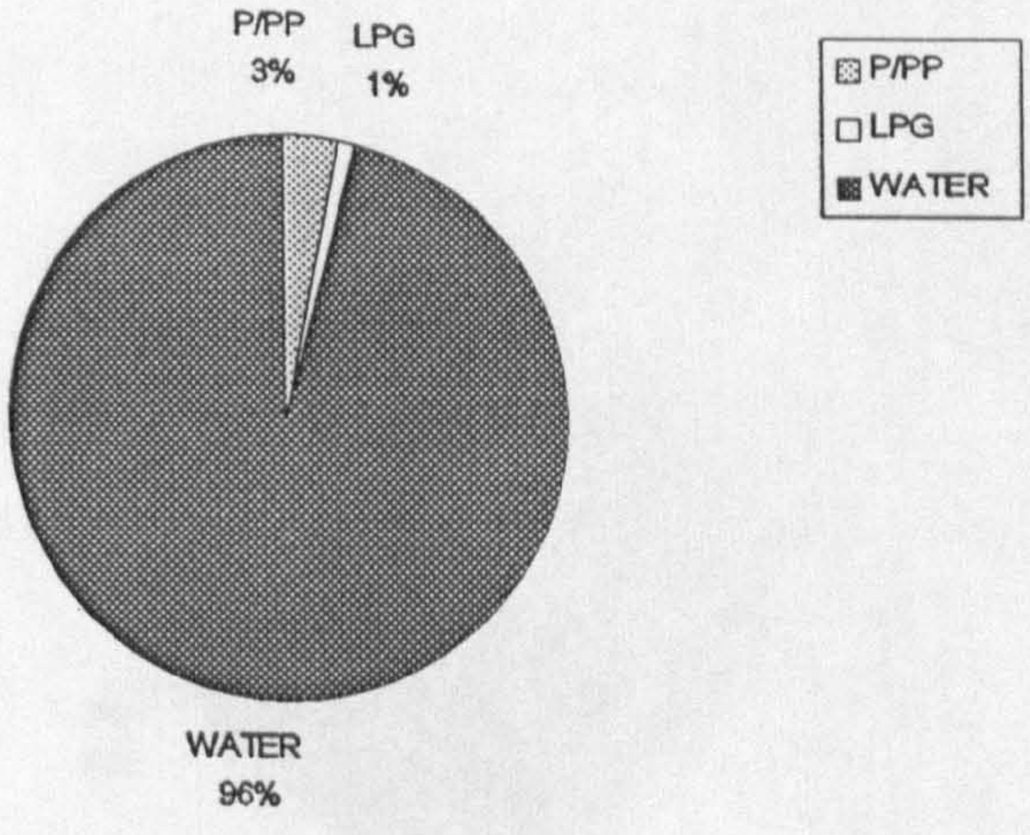

Figure 2.2 Percentage of number of flowmeters for each type of liquid.

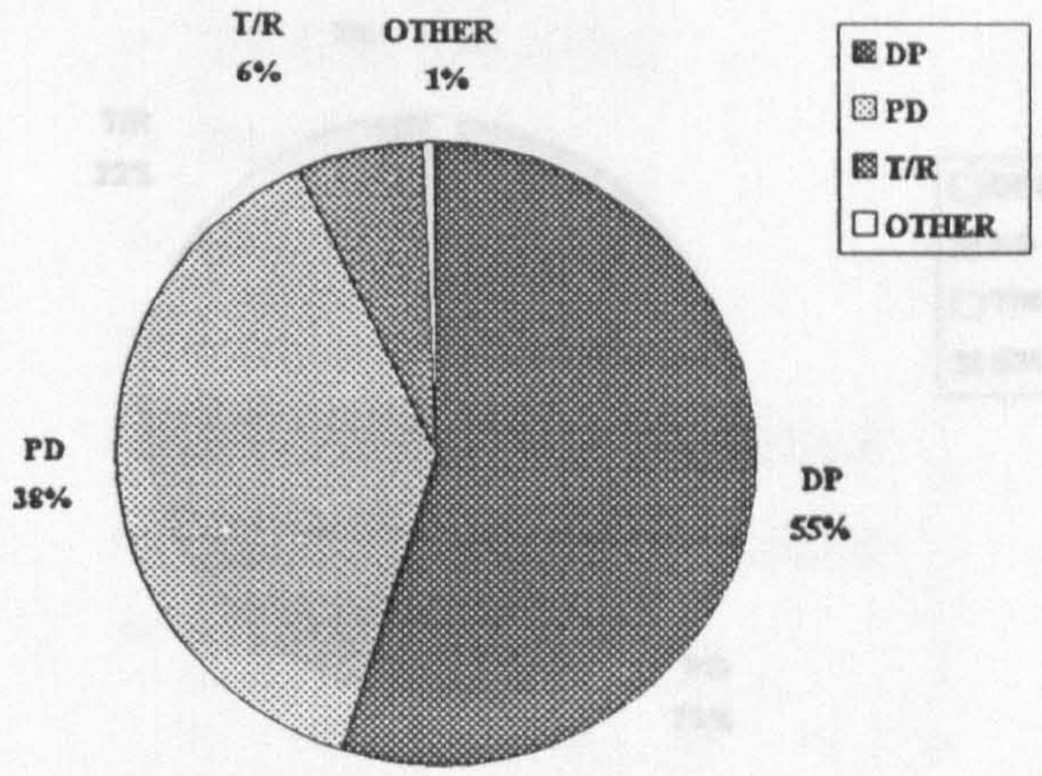

Figure 2.3 (a): Percentage of flowmeter types in use to measure petroleum or petroleum products.

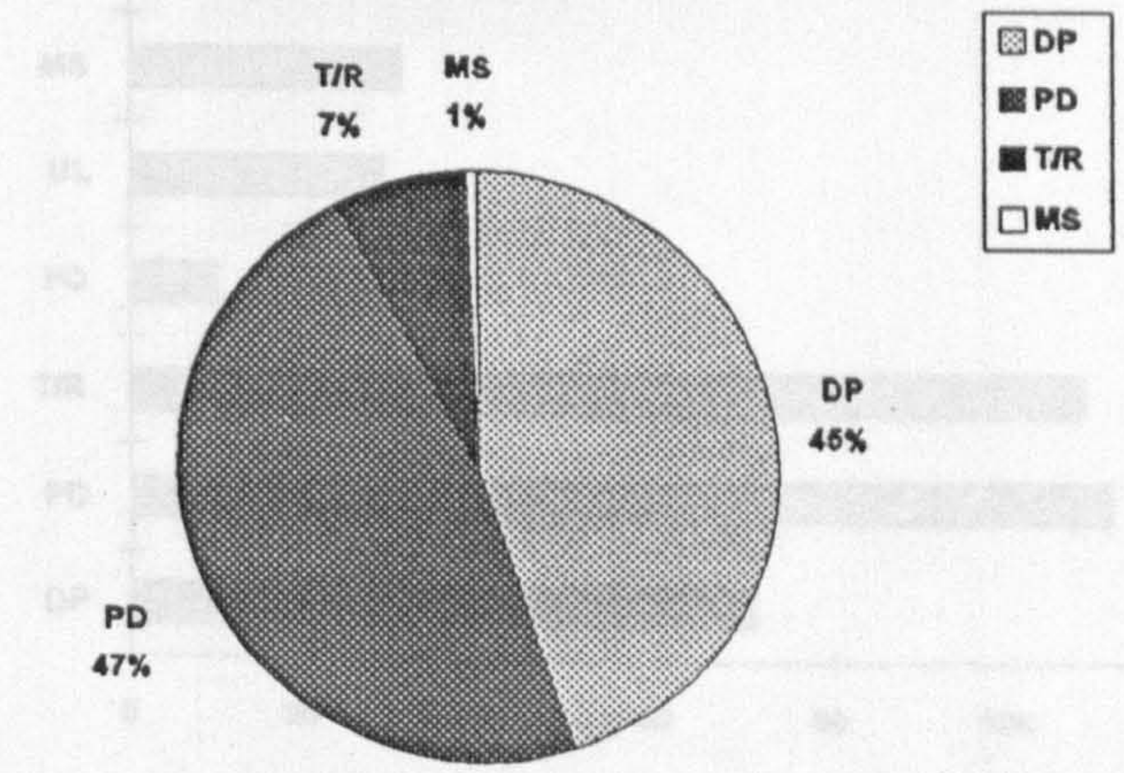

Figure 2.3 (b): Percentage of types of flowmeter in use for liquidified peteroleum gases or cryogenics.

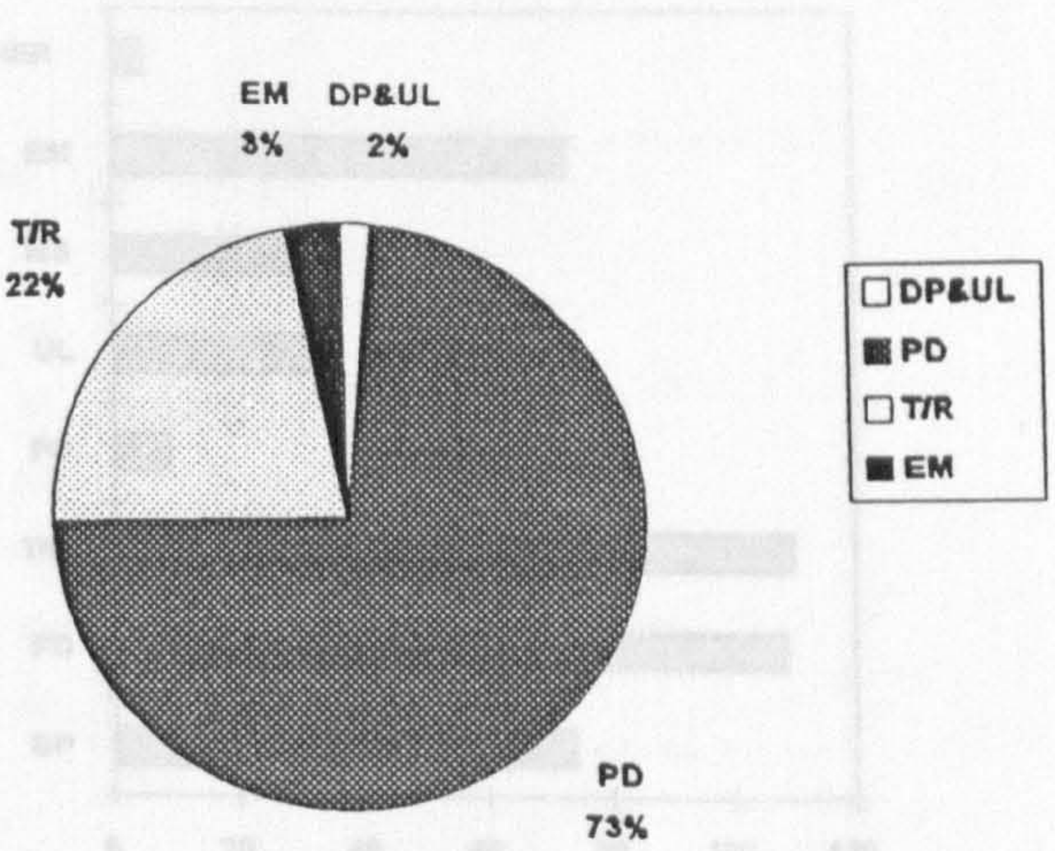

Figure 2.3 (c): Percentage of flowmeter types in use for water and waste water.

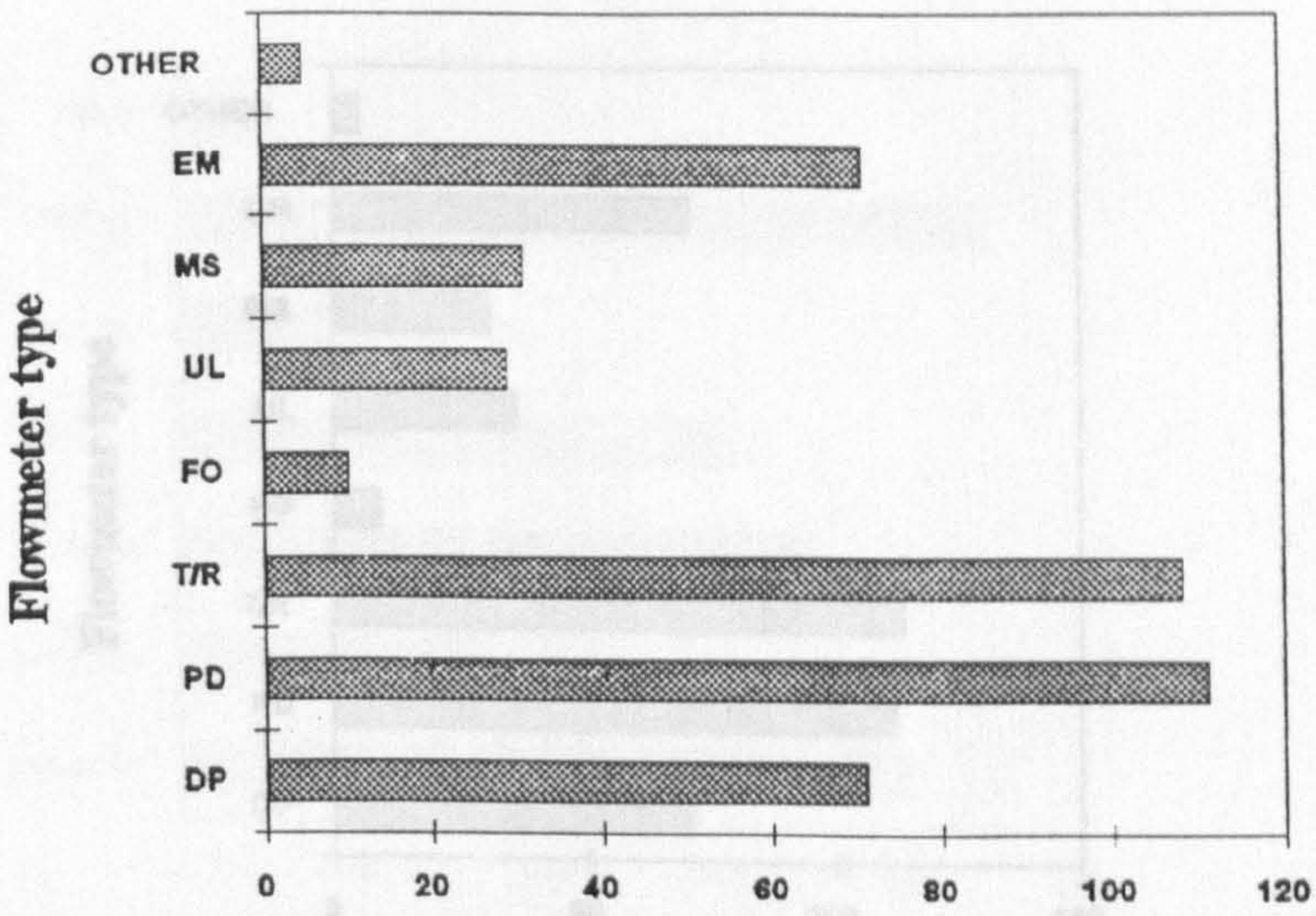

Figure 2.4 (a): Estimation of users on the ACCURACY of their flowmeter.

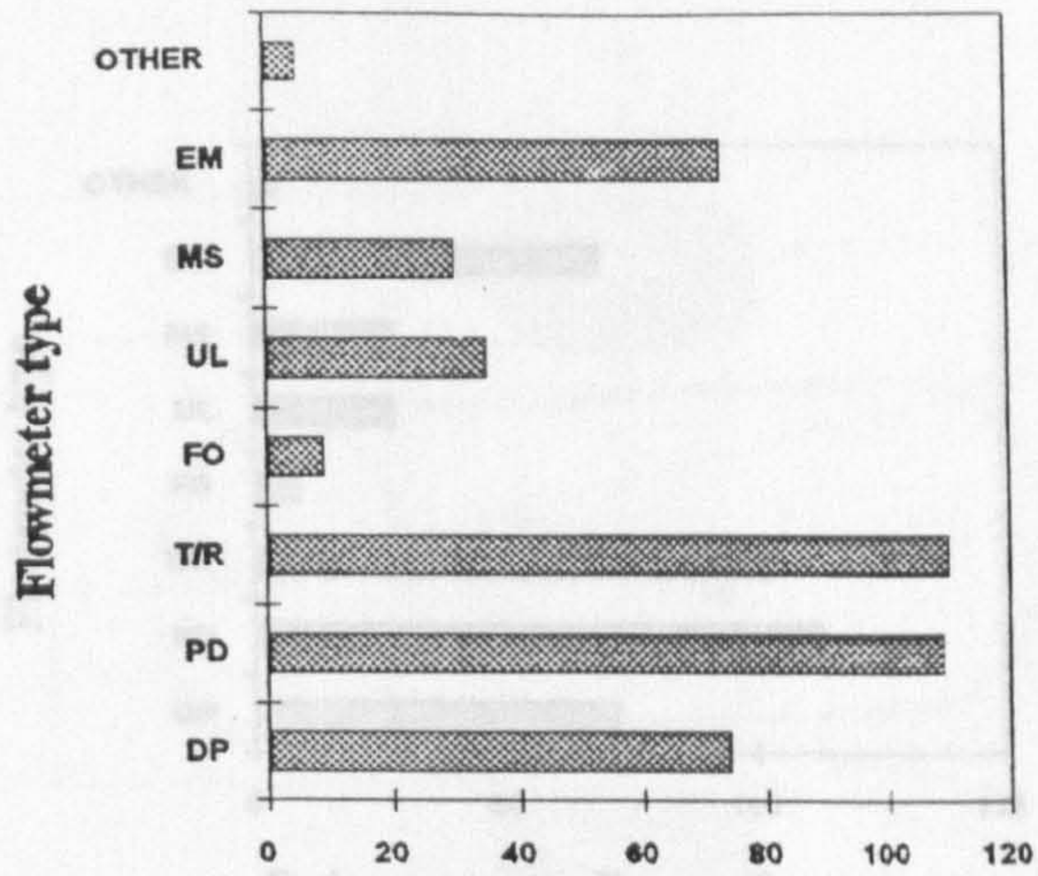

Figure 2.4 (b): Estimation of users on the RELIABILITY of their flowmeter

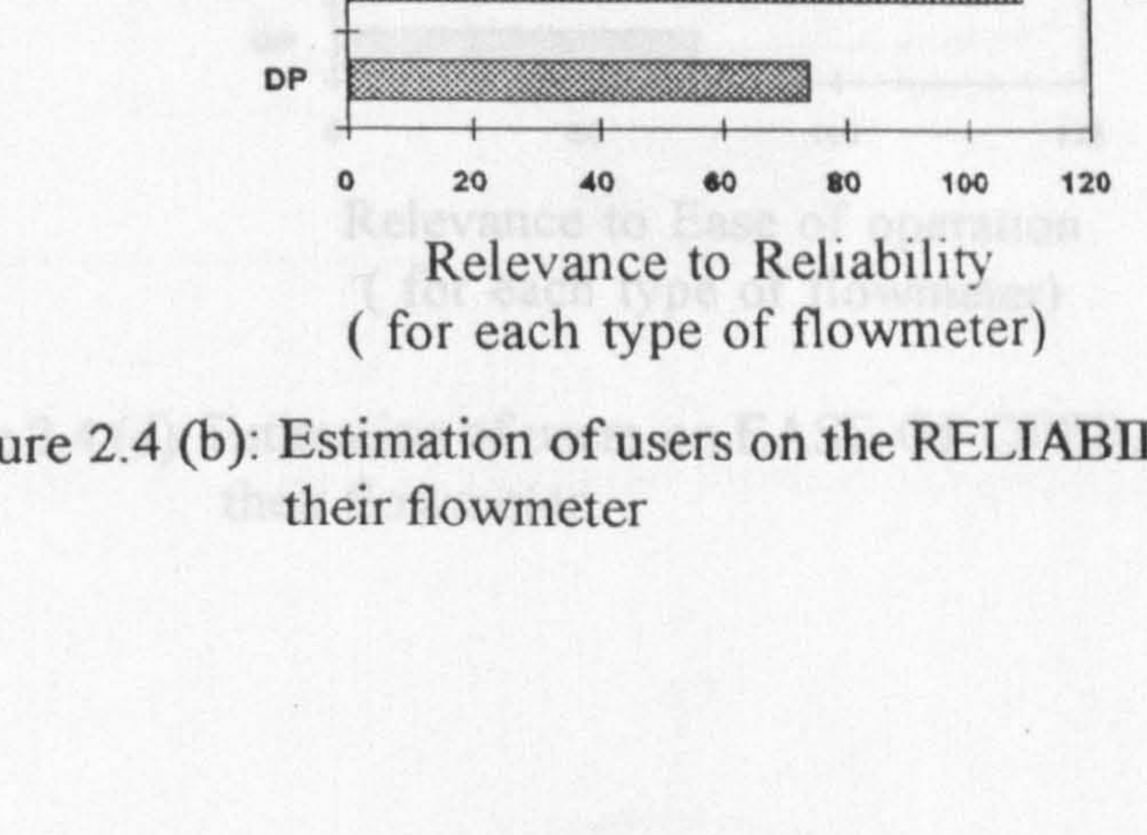

Figure 2.4 (c): Estimation of users CONFIDENCE in their flowmeter

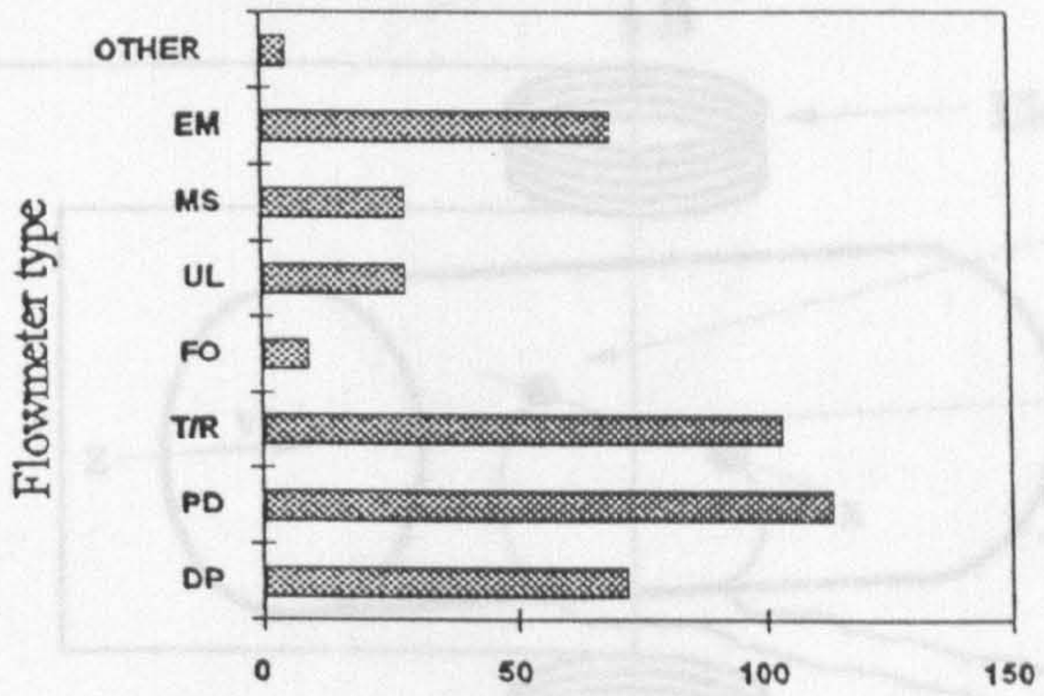

Figure 2.4 (d): Estimation of users on EASE OF OPERATION of their flowmeter.

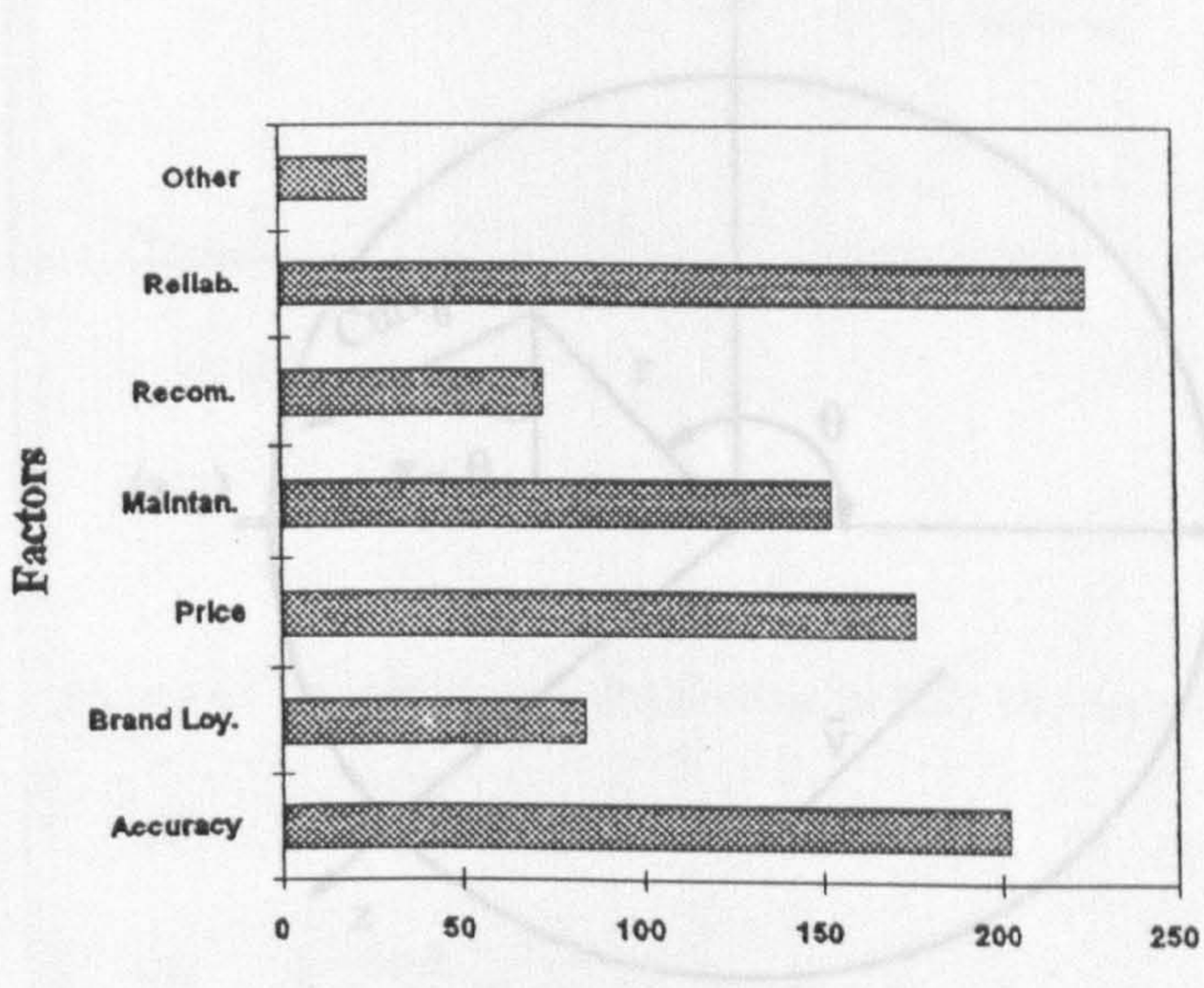

Figure 2.5 Relevance of factors affecting decisions of users when purchasing a new flowmeter.

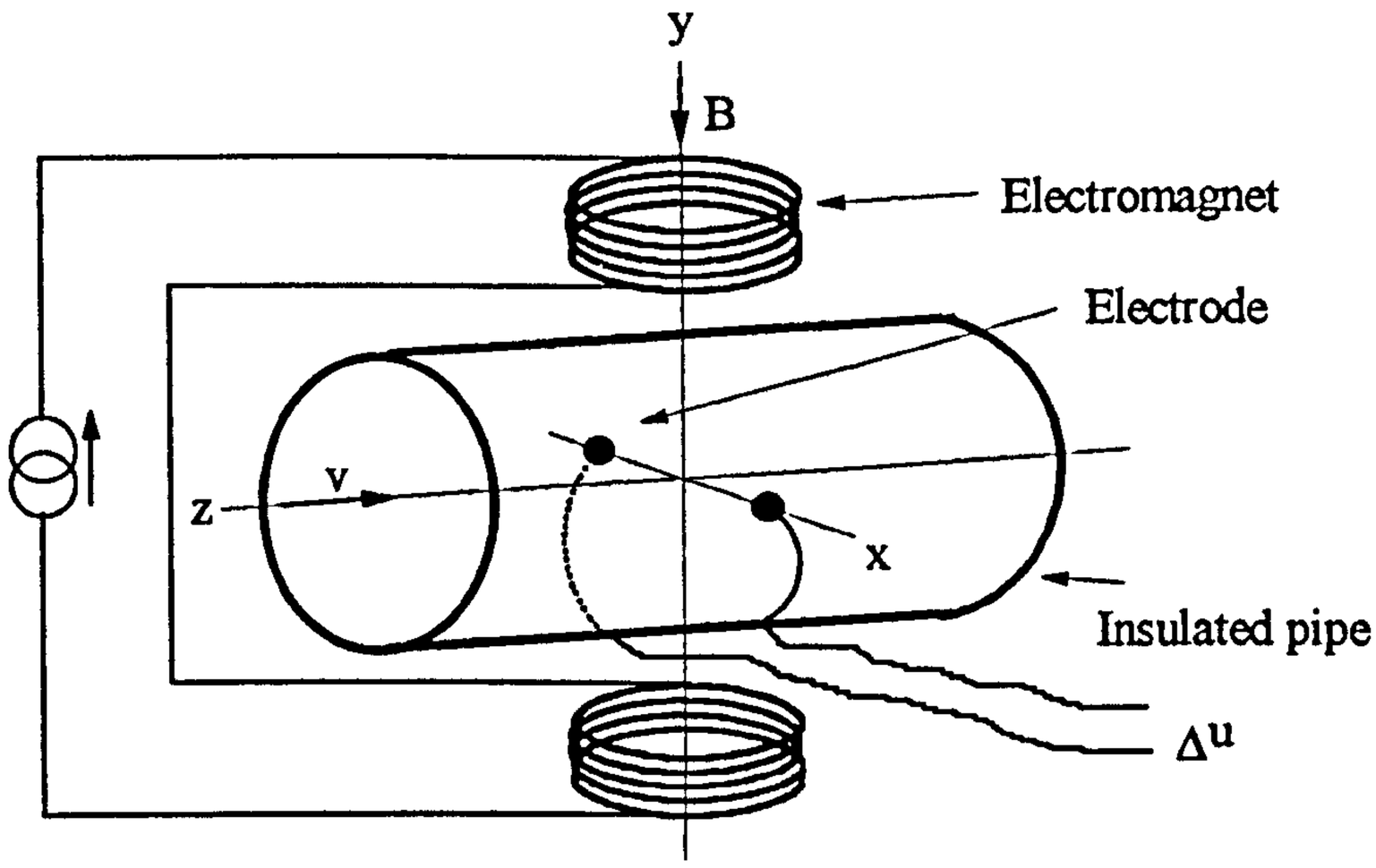

Figure 3.1 : Basic arrangement for an electromagnetic flowmeter.

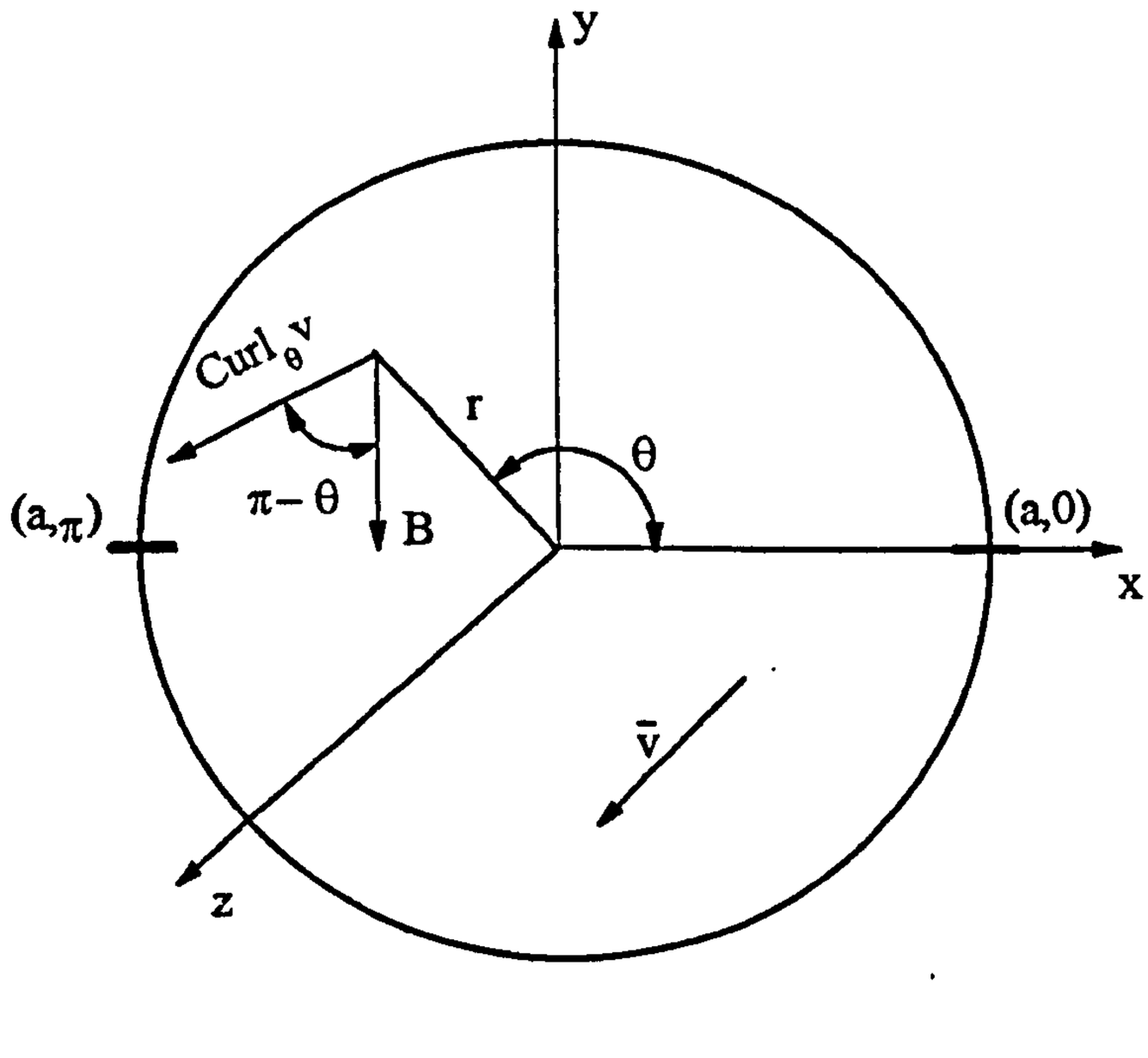

Figure 3.2 : Coordinate system for analysis of flow in a circular pipe.

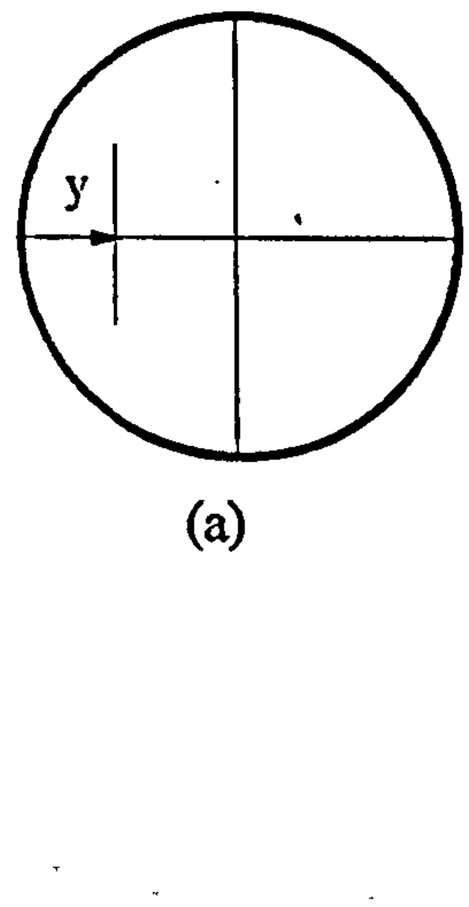

Figure 4.1 : Mean charge distribution in fully developed flow

(a) Distance from pipe wall (y)

(b) $\lambda^2 << \delta^2$

(c) $\lambda^2 > \delta^2$

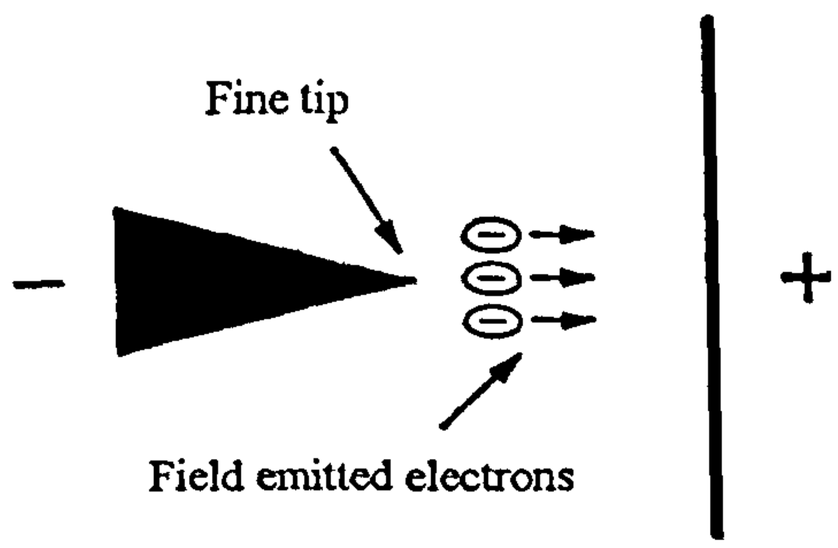

Figure 4.2 : Field emission or ionisation

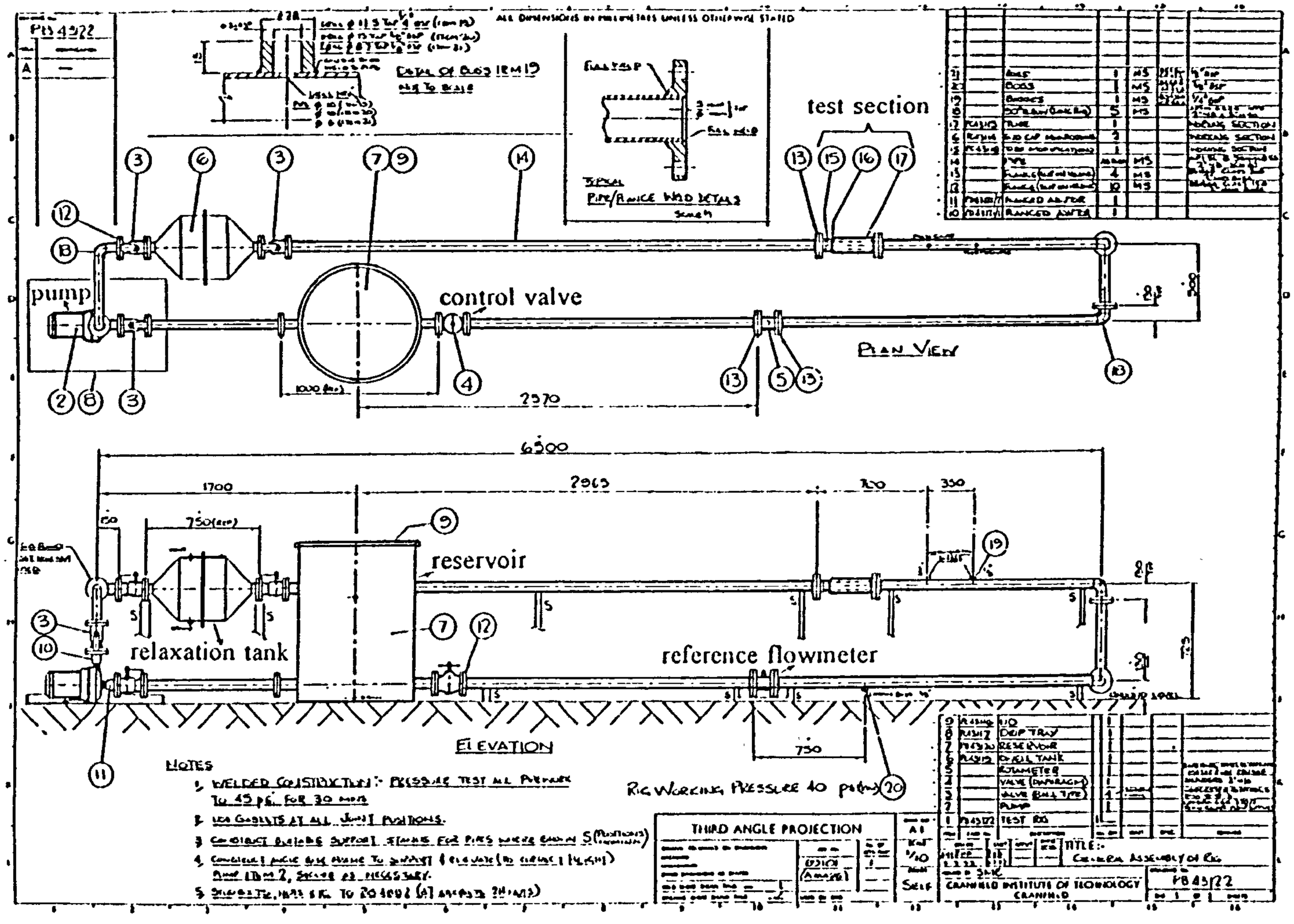

Figure 5.1: Design diagram of the flow circuit for BP 180 oil

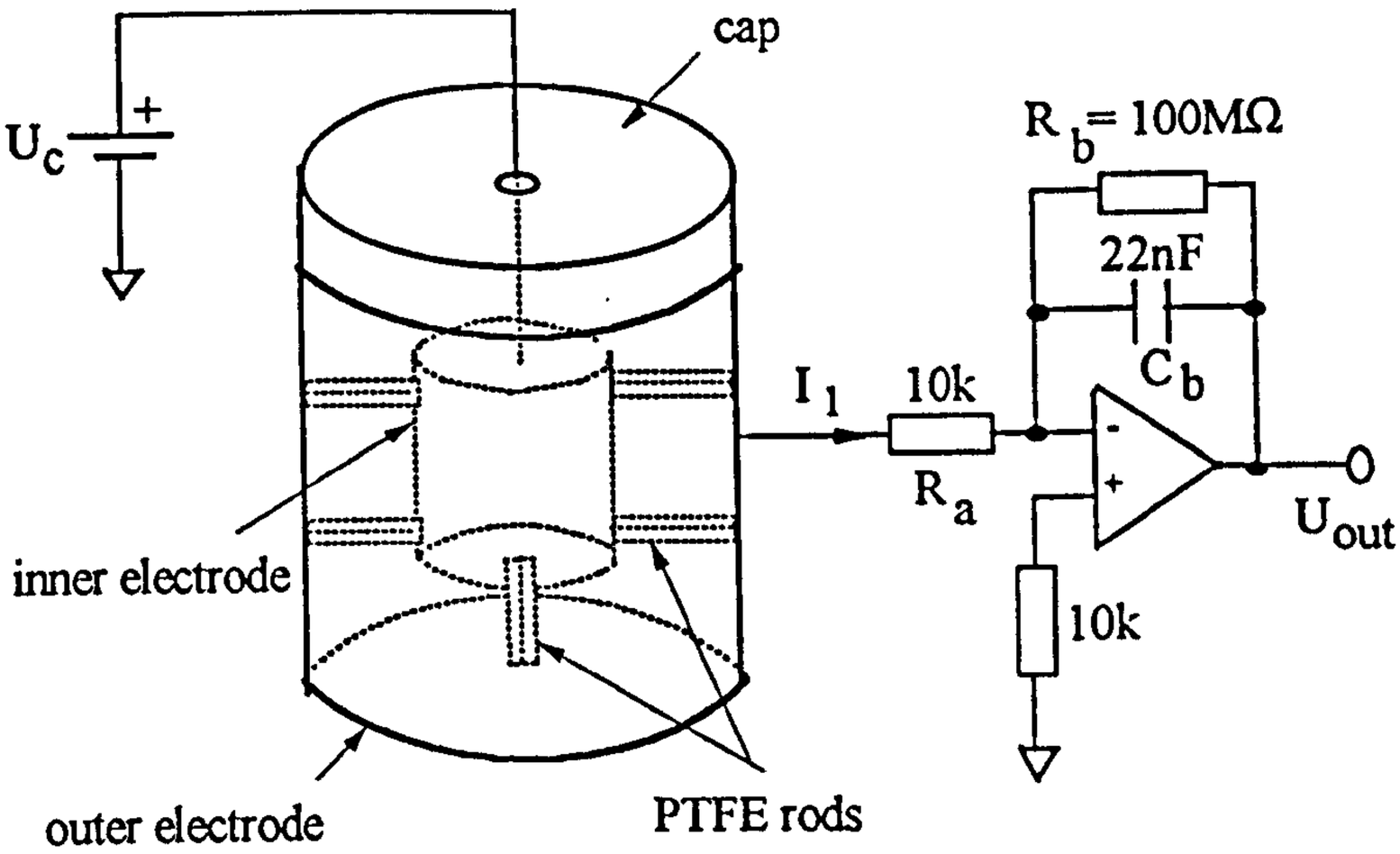

(a) Configuration of the device.

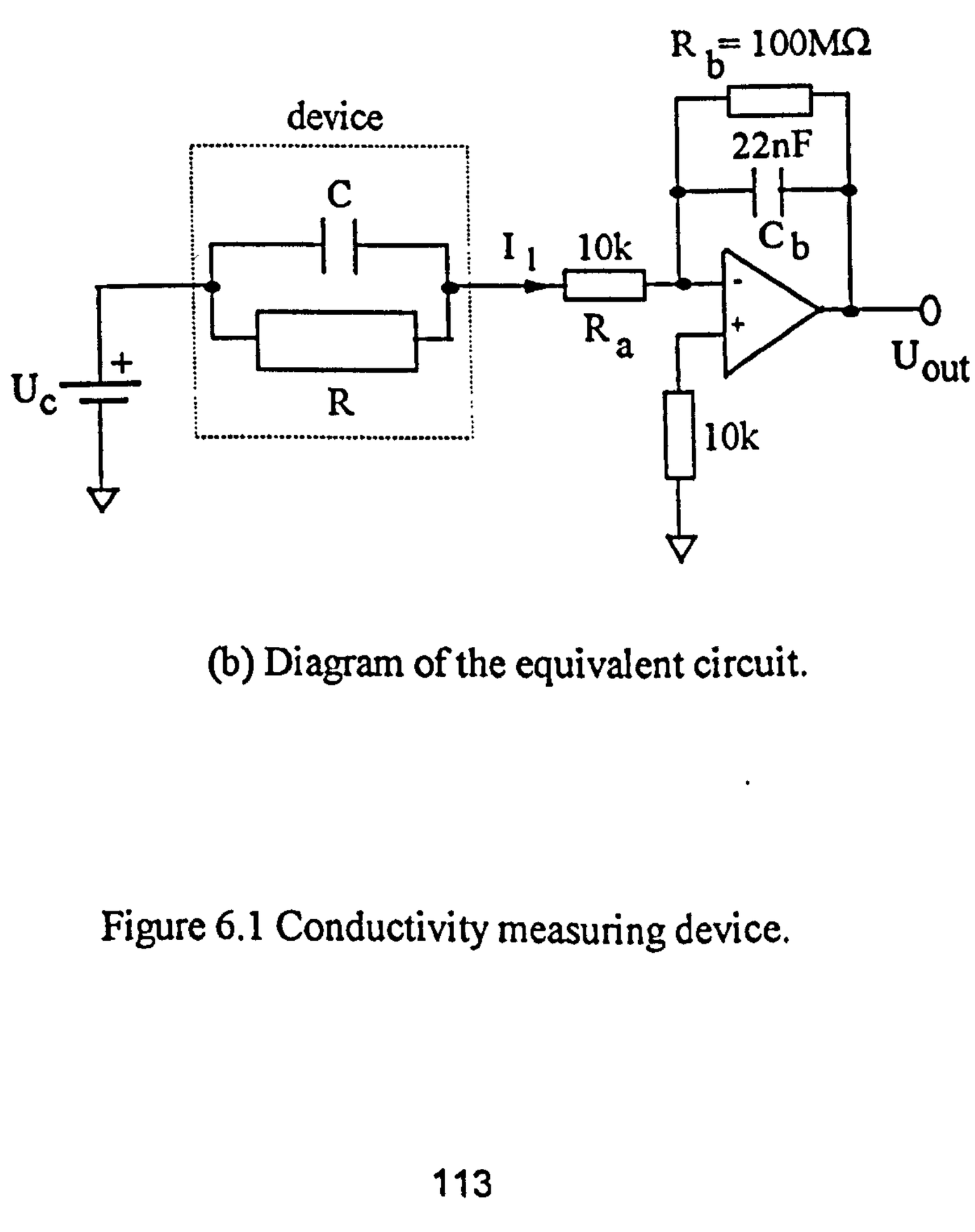

(b) Diagram of the equivalent circuit.

Figure 6.1 Conductivity measuring device.

Figure 6.2: The conductivity measuring cell.

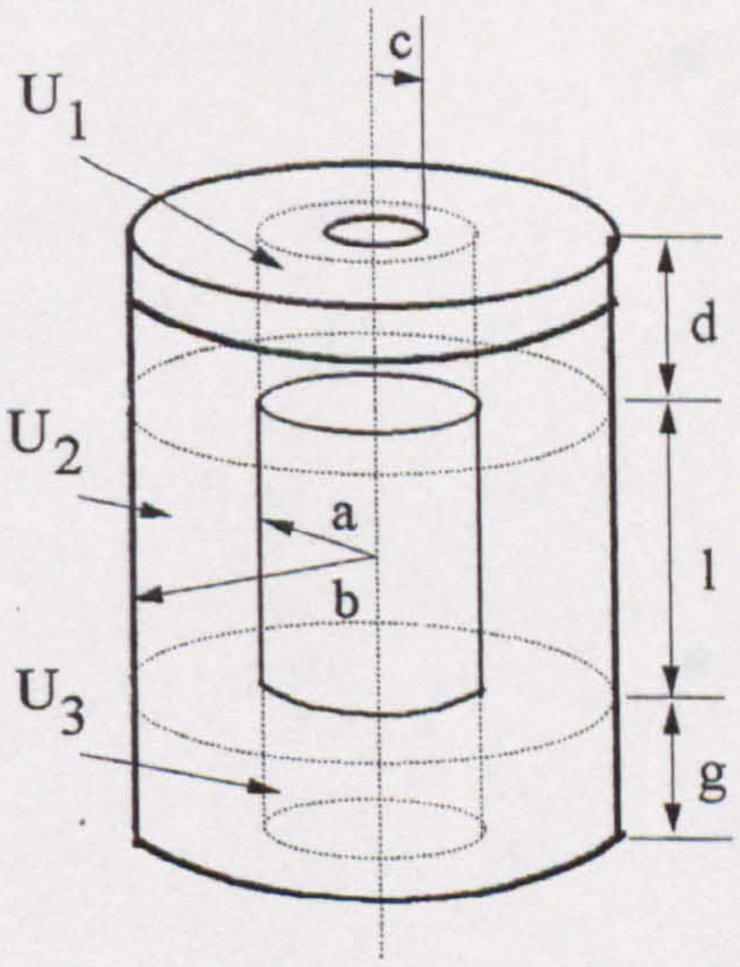

Figure 6.3: Physical dimensions of the conductivity measuring cell.

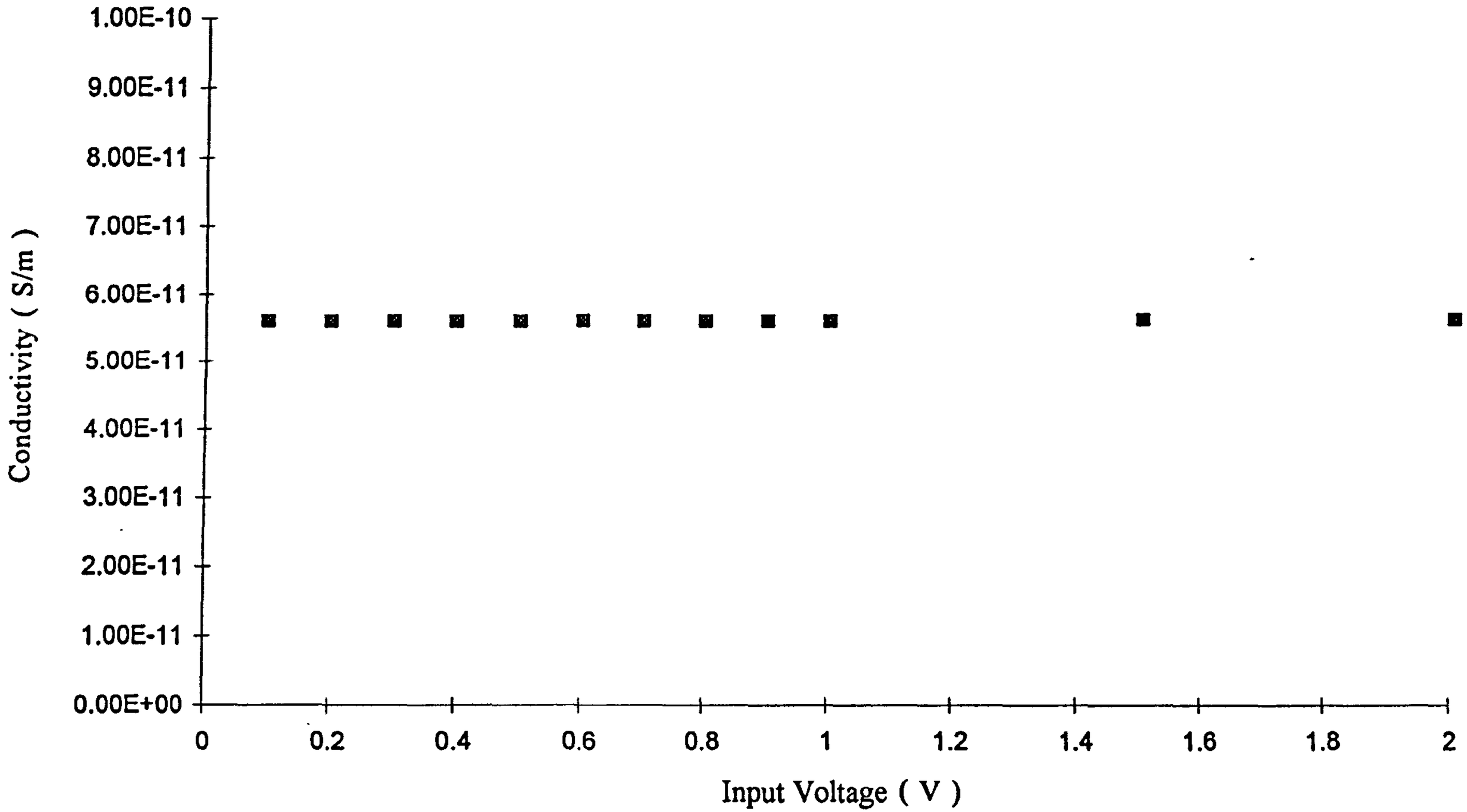

Figure 6.4: The conductivity of BP Dielectric 180 measured using the device.

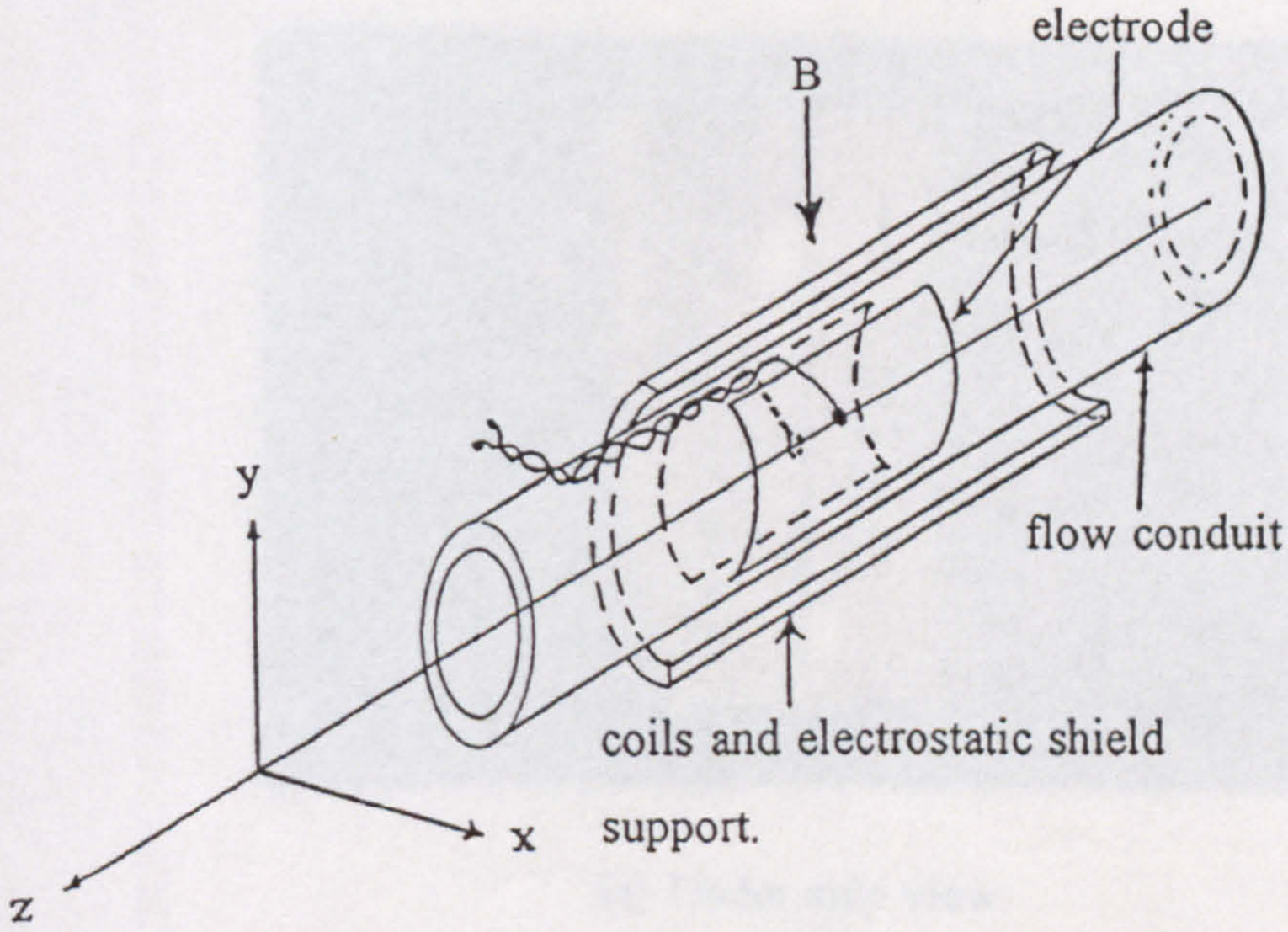

Figure 7.1: Schematic diagram of the flowmeter configuration.

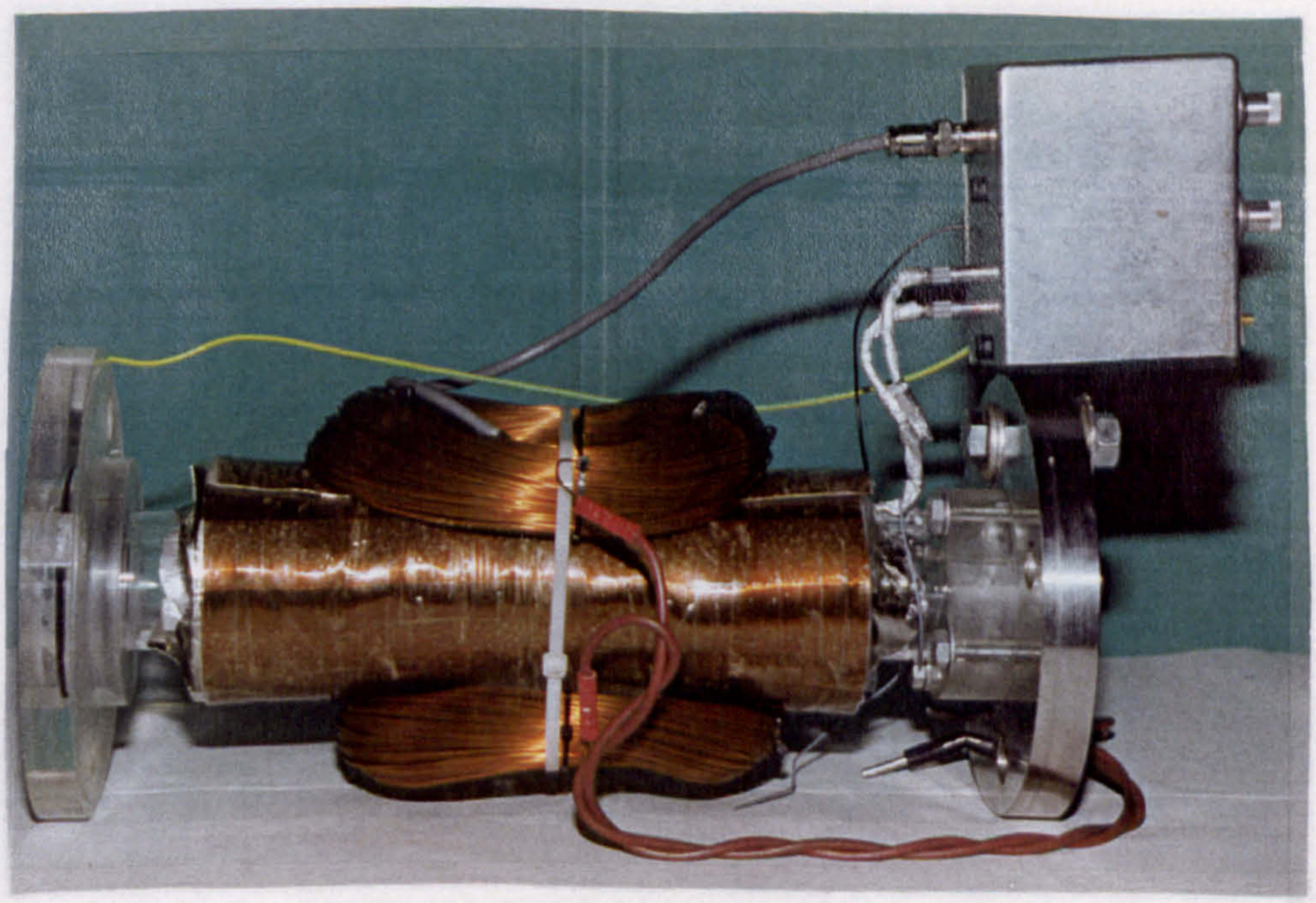

Figure 7.2: The experimental electromagnetic flowmeter designed to be used with dielectric liquids.

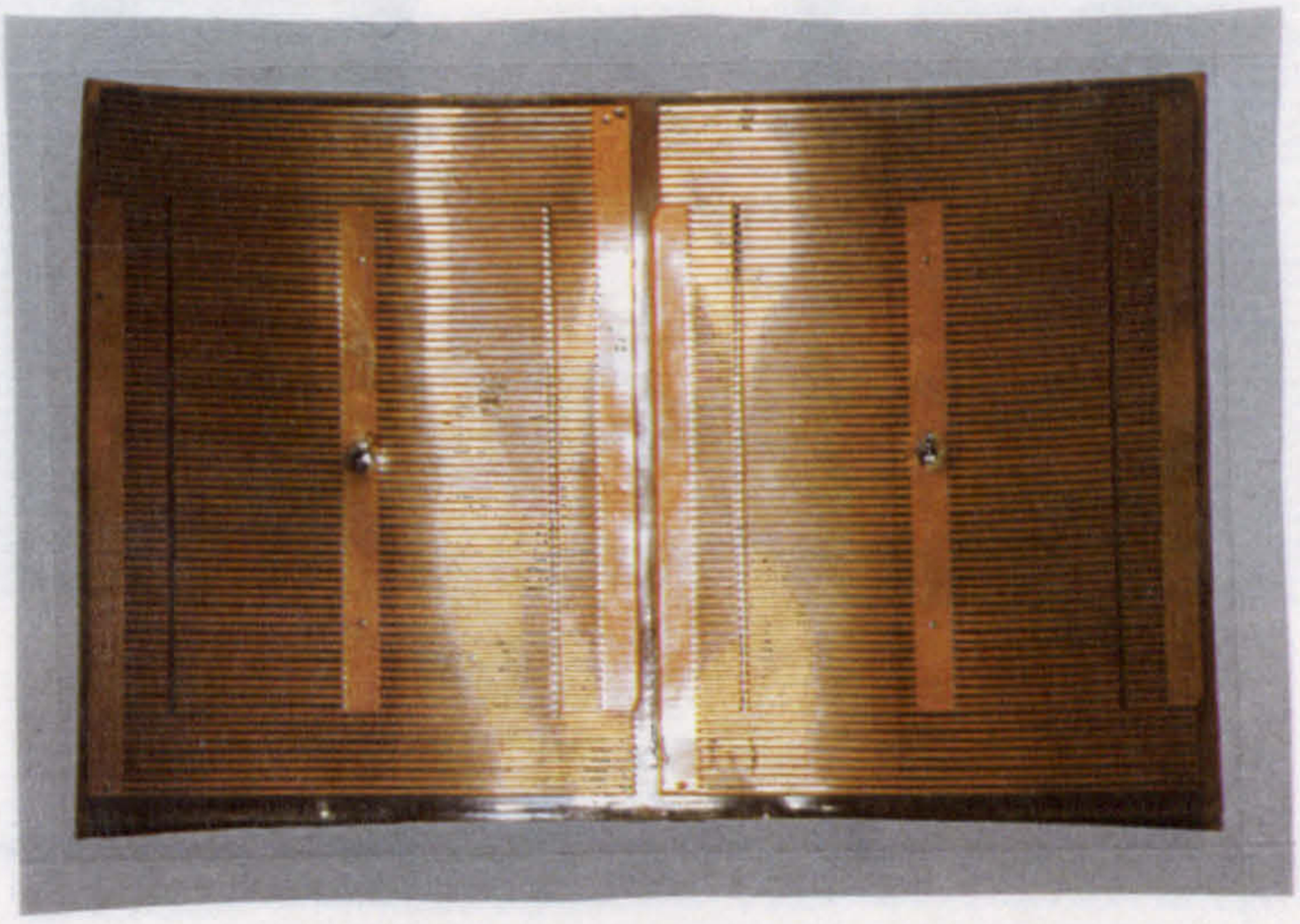

(a) Under side view

(b) Top side view

Figure 7.3 Electrodes of the electromagnetic flowmeter.

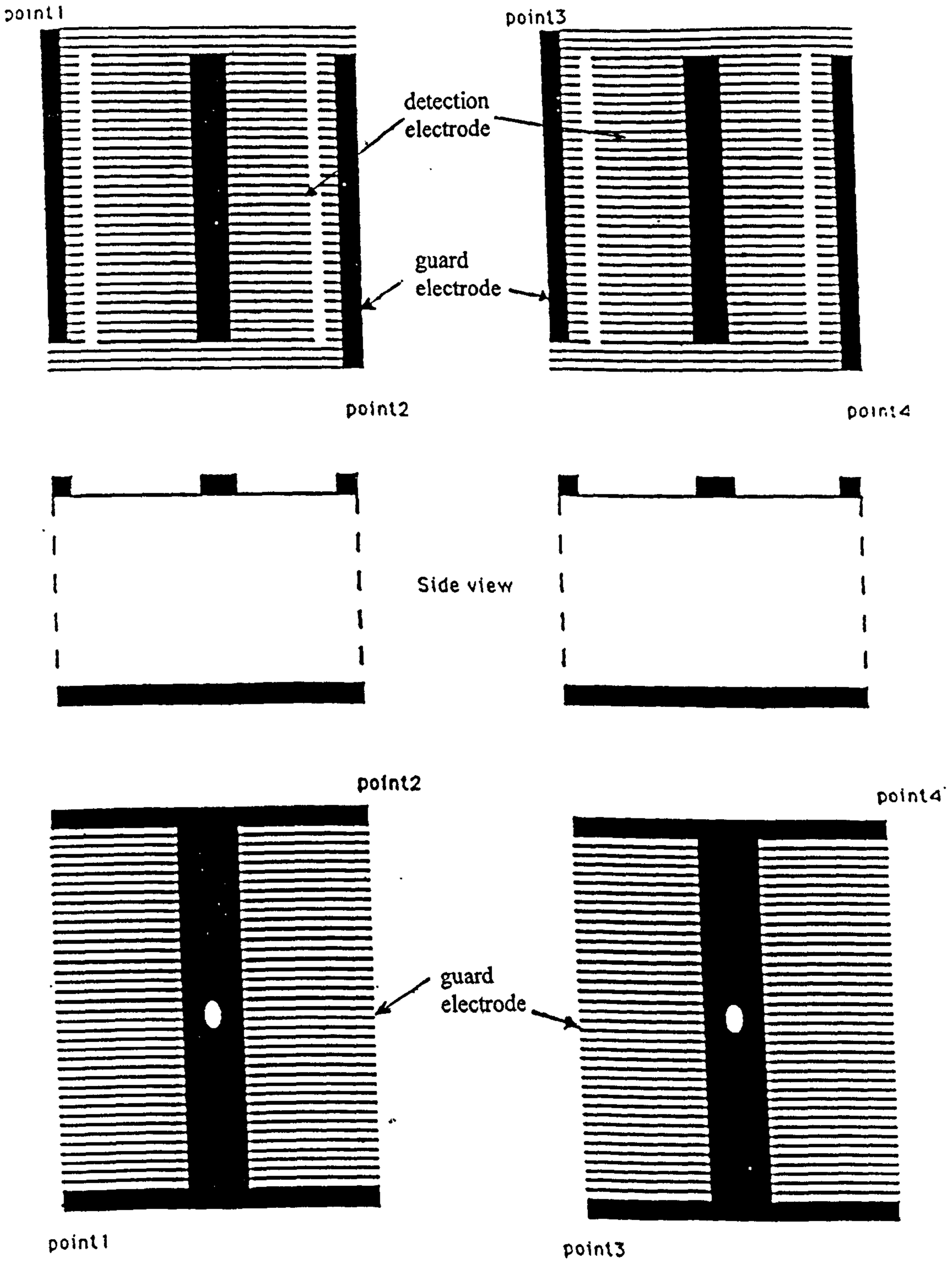

Figure 7.4: Schematic of the electrode design.

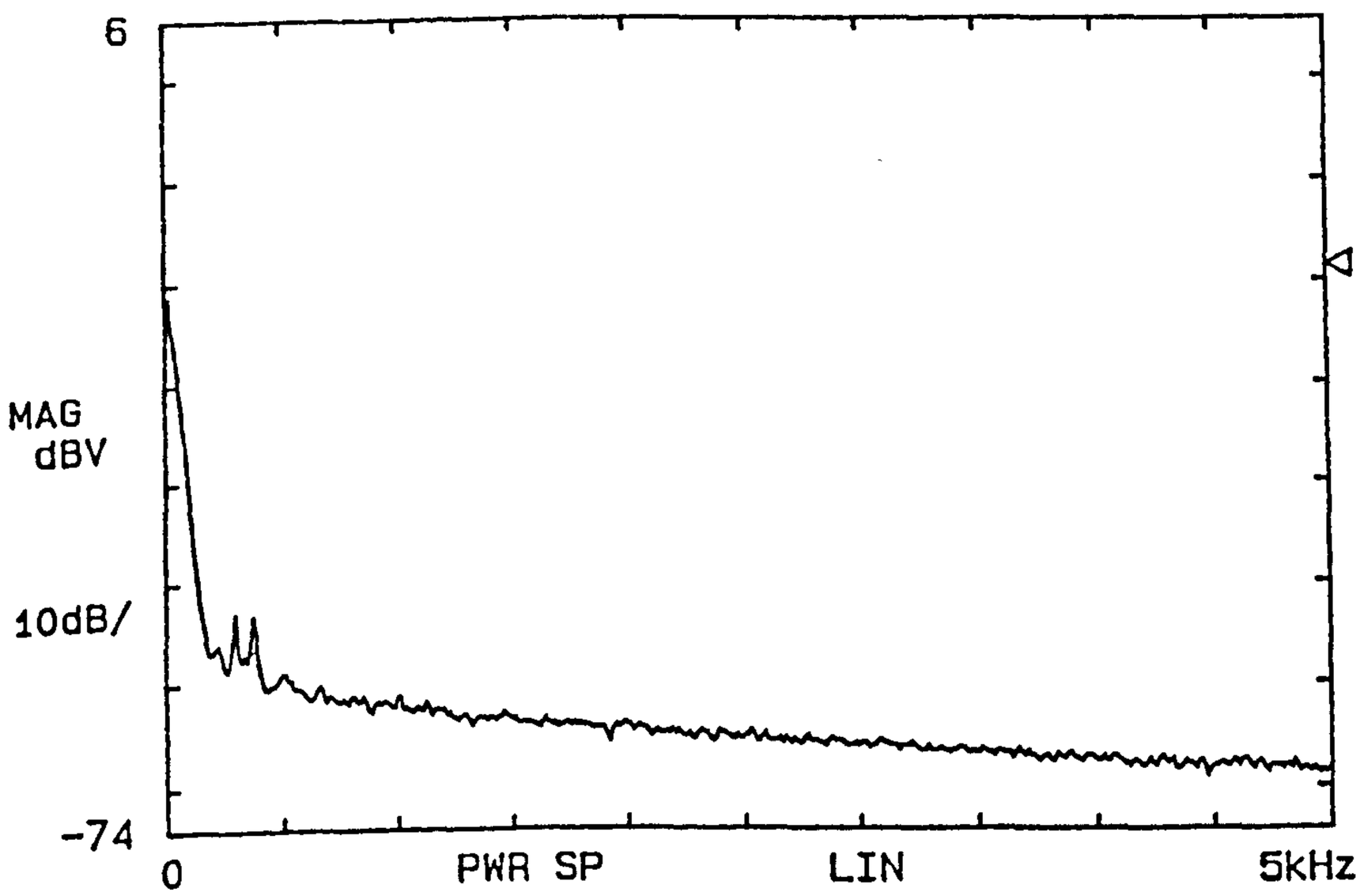

Figure 7.5 (a): Frequency spectrum of the charge noise at a flow velocity of 1 m/s.

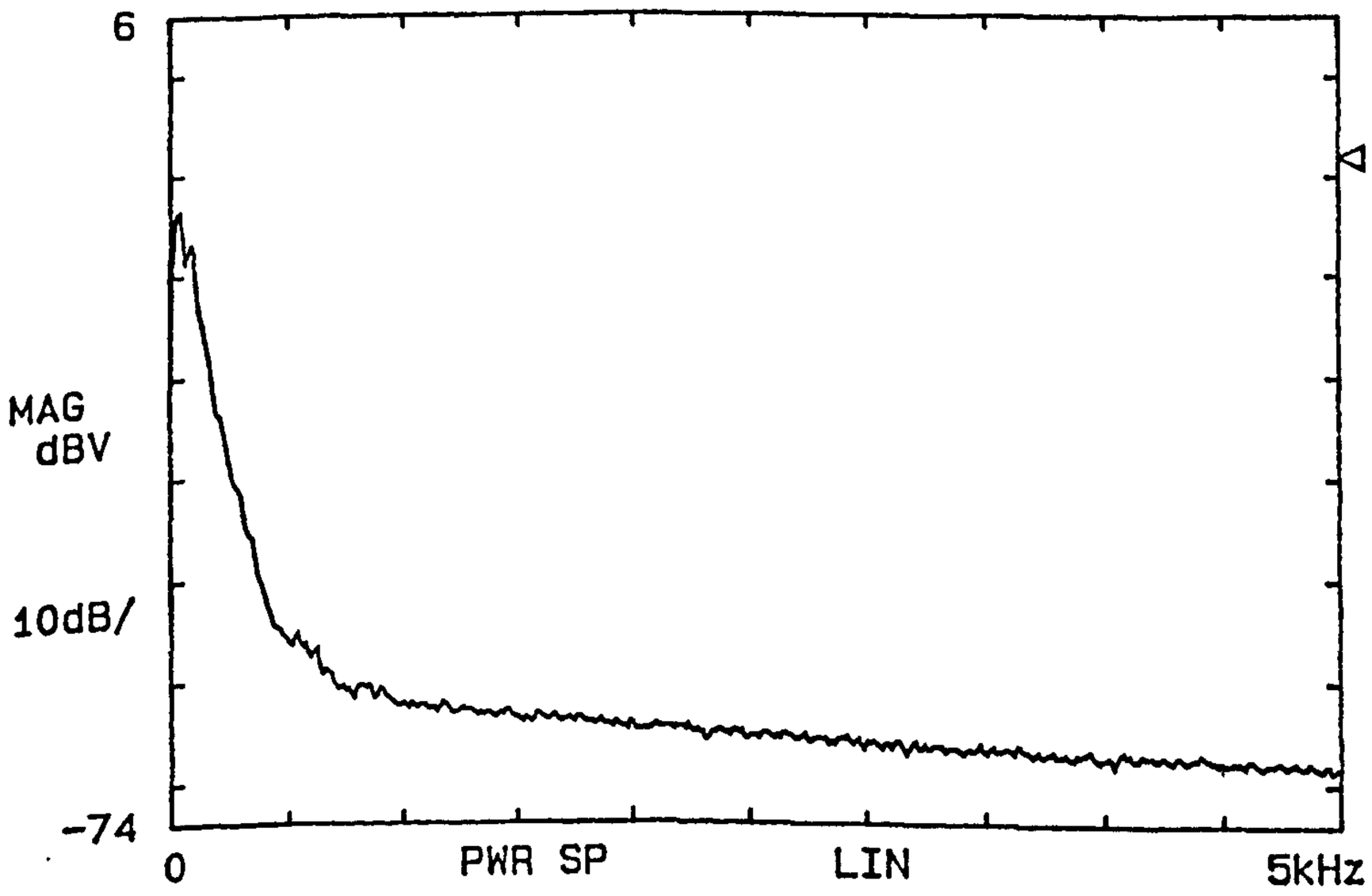

Figure 7.5 (b): Frequency spectrum of the charge noise at a flow velocity of 3 m/s.

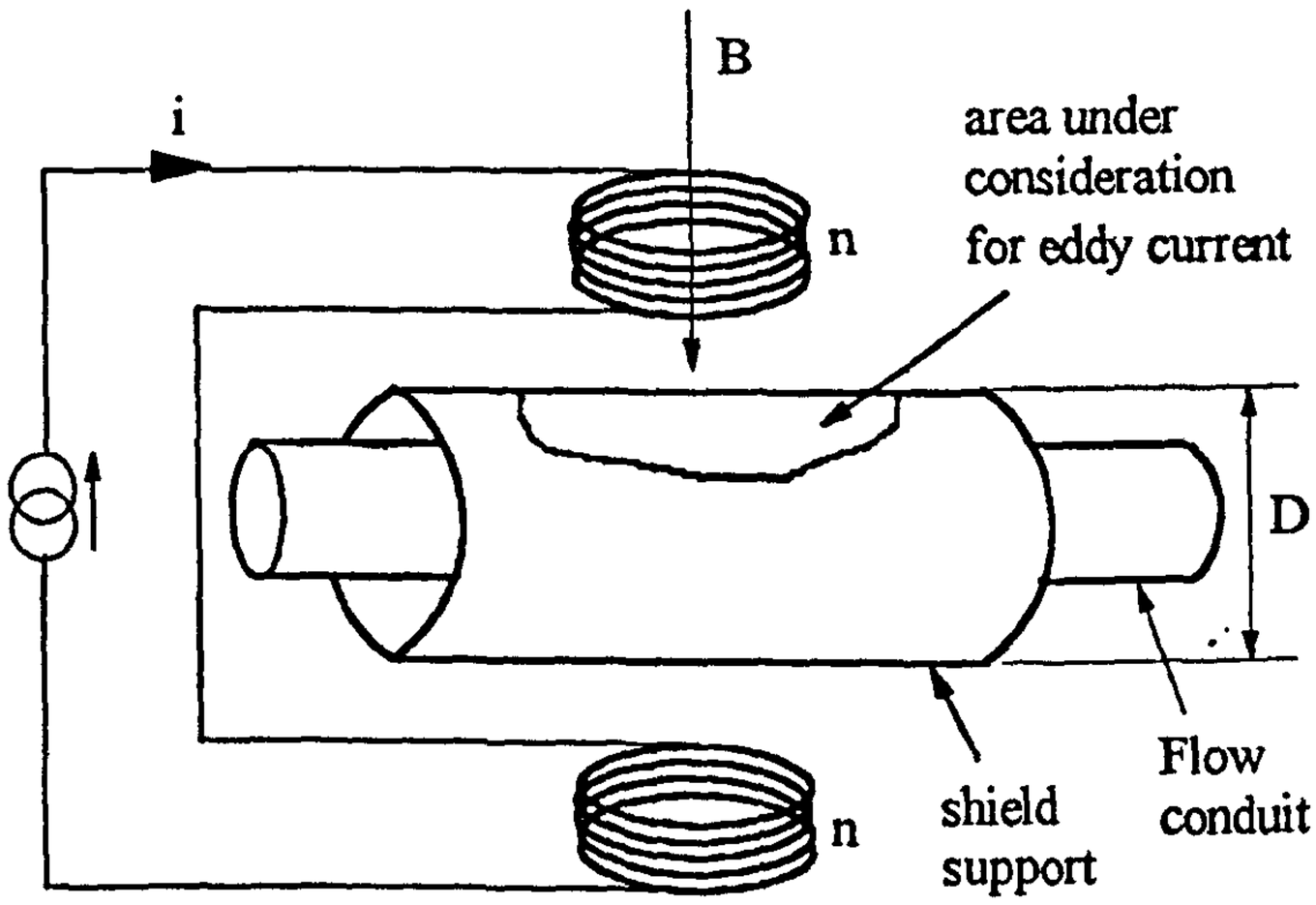

(a) Magnetic circuit

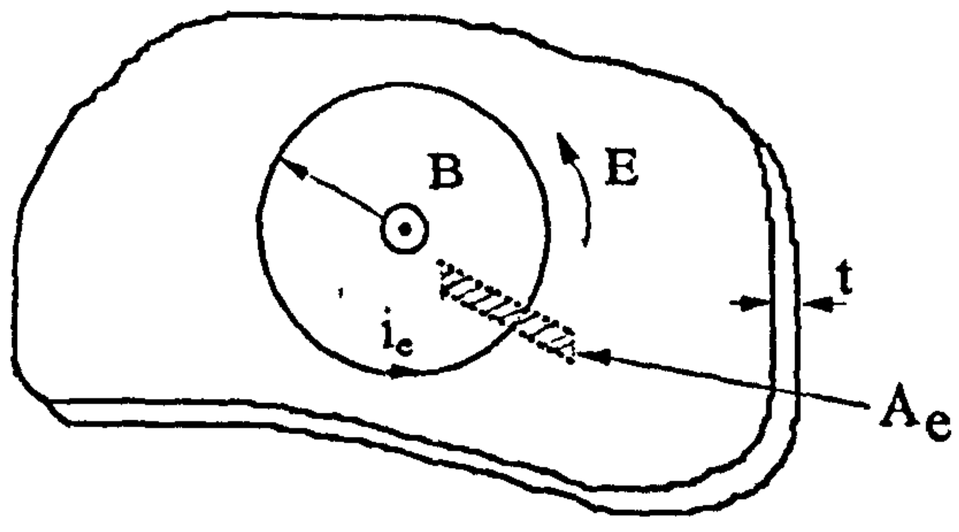

(b) Area under consideration for eddy current

Figure 7.6 : Schematic of the flowmeter magnetic circuit and direction of the associated eddy current.

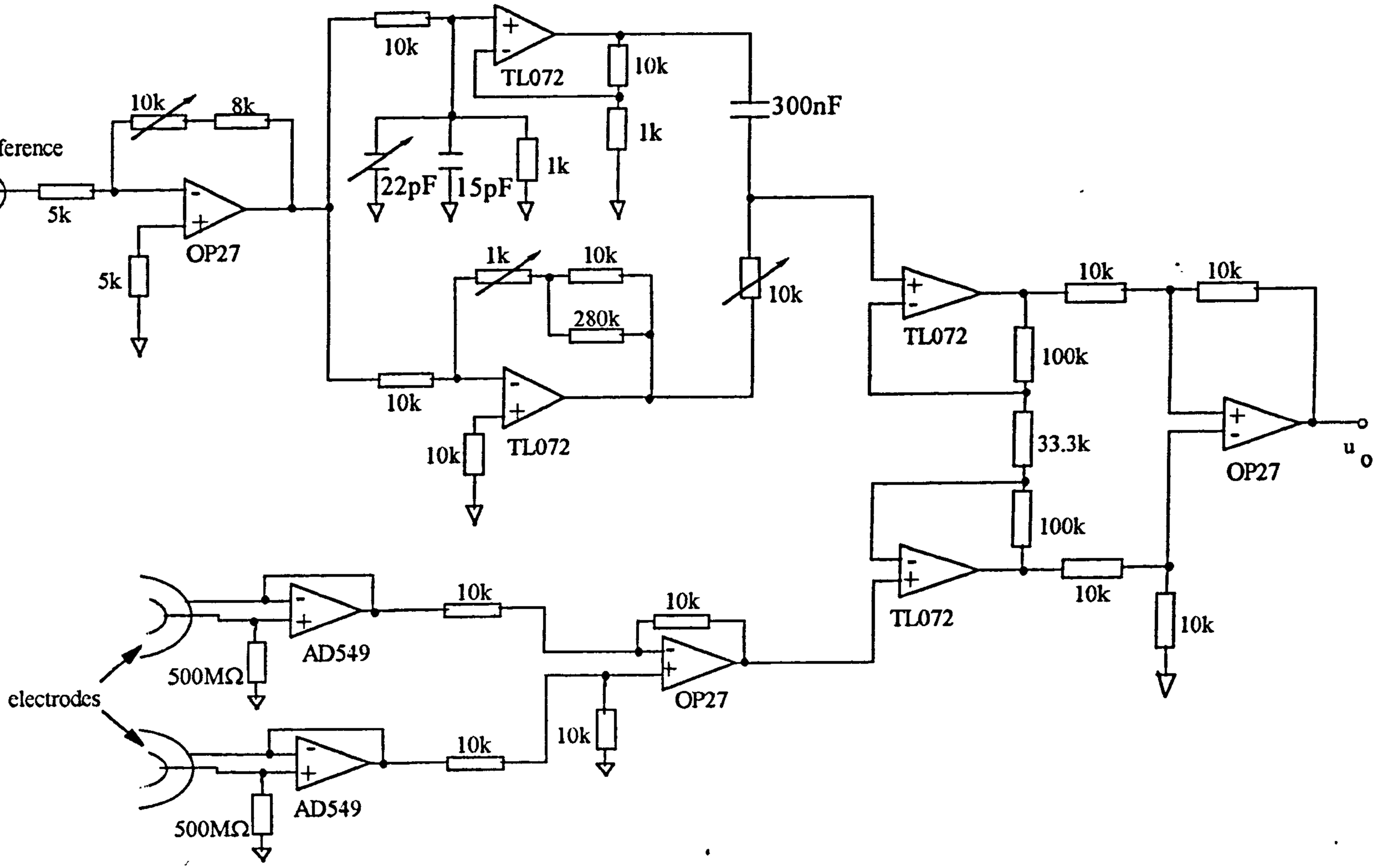

Figure 7.7: The circuit diagram of the electronics used in the flowmeter.

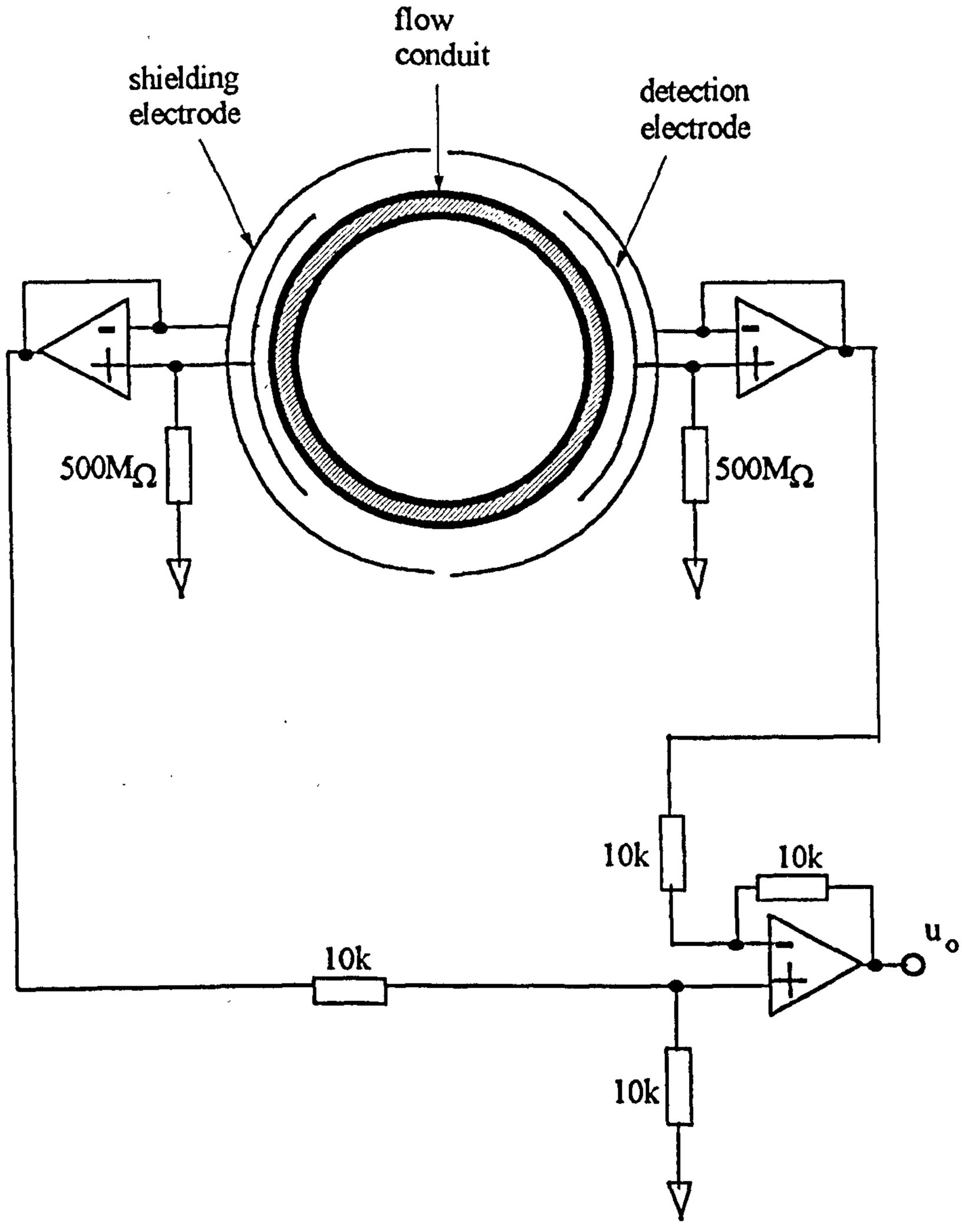

Figure 7.8 : Schematic of the connection of the detection electronics.

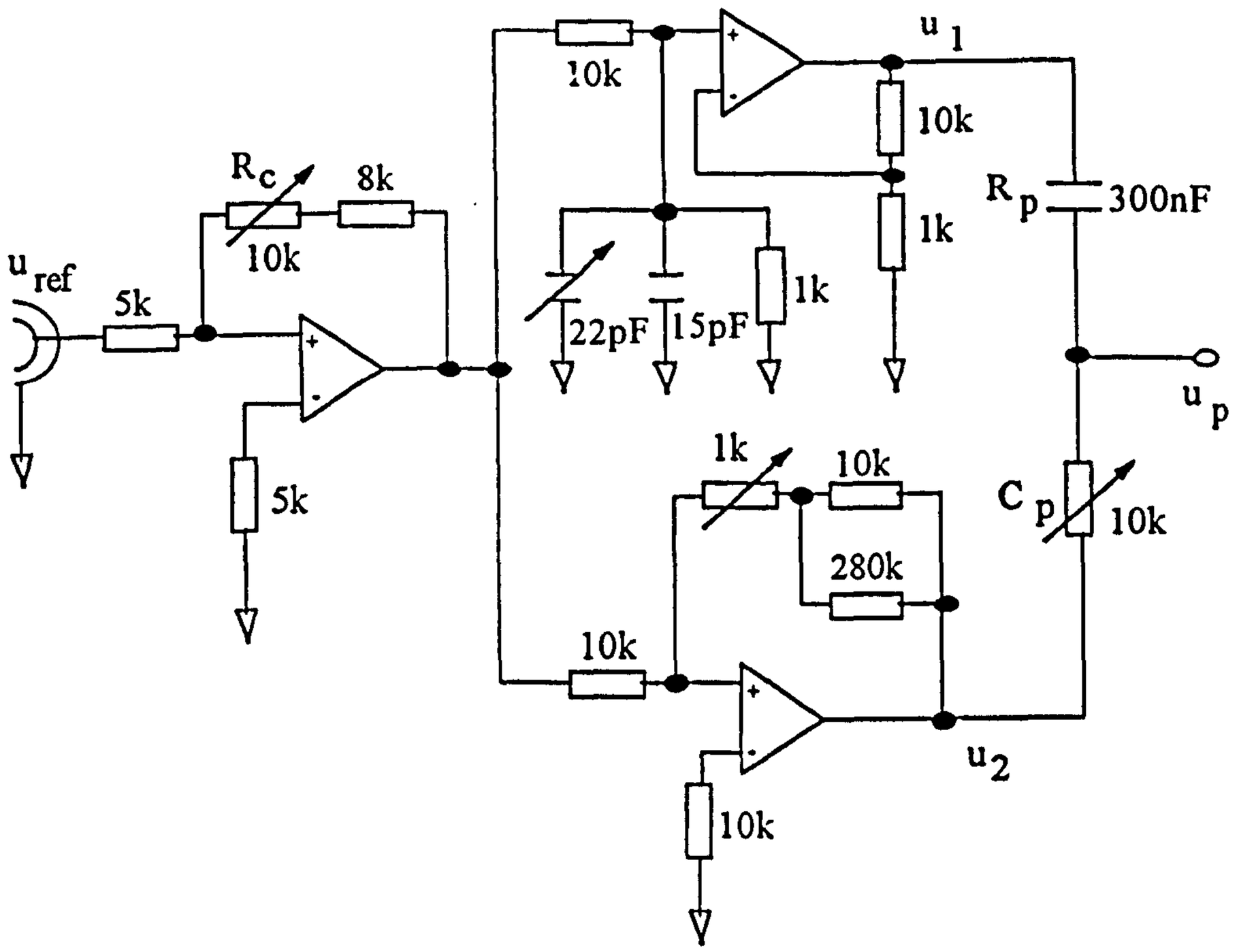

Figure 7.9: Amplitude and phase control circuit for the reference voltage.

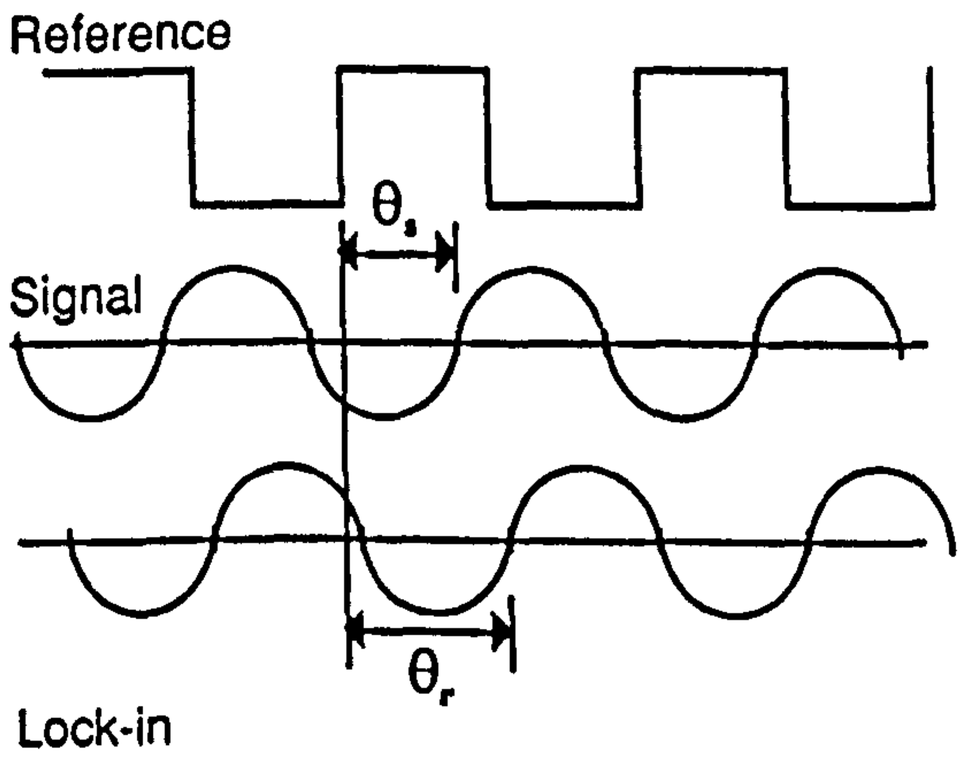

Figure 7.10: Phase-locking in a lock-in amplifier.

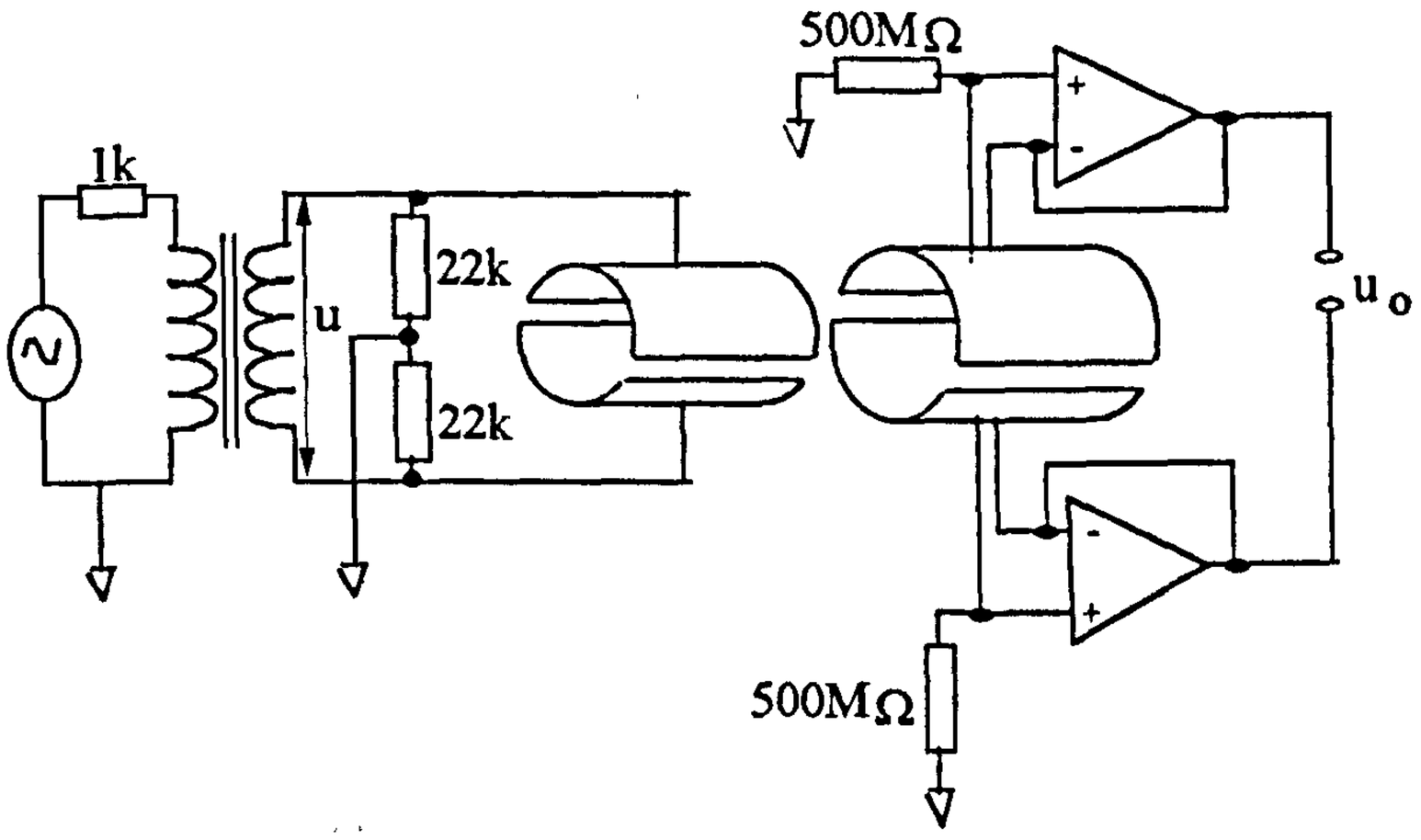

Figure 7.11: Configuration for simulation to test the detection electronics.

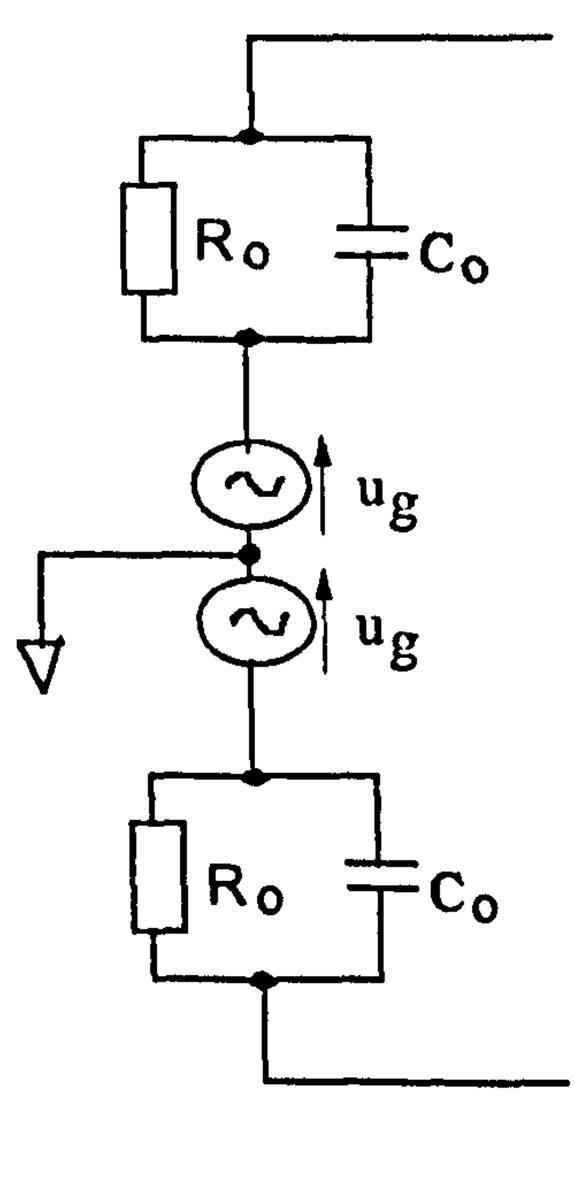

Figure 7.12: Equivalent circuit of the meter as a voltage source.

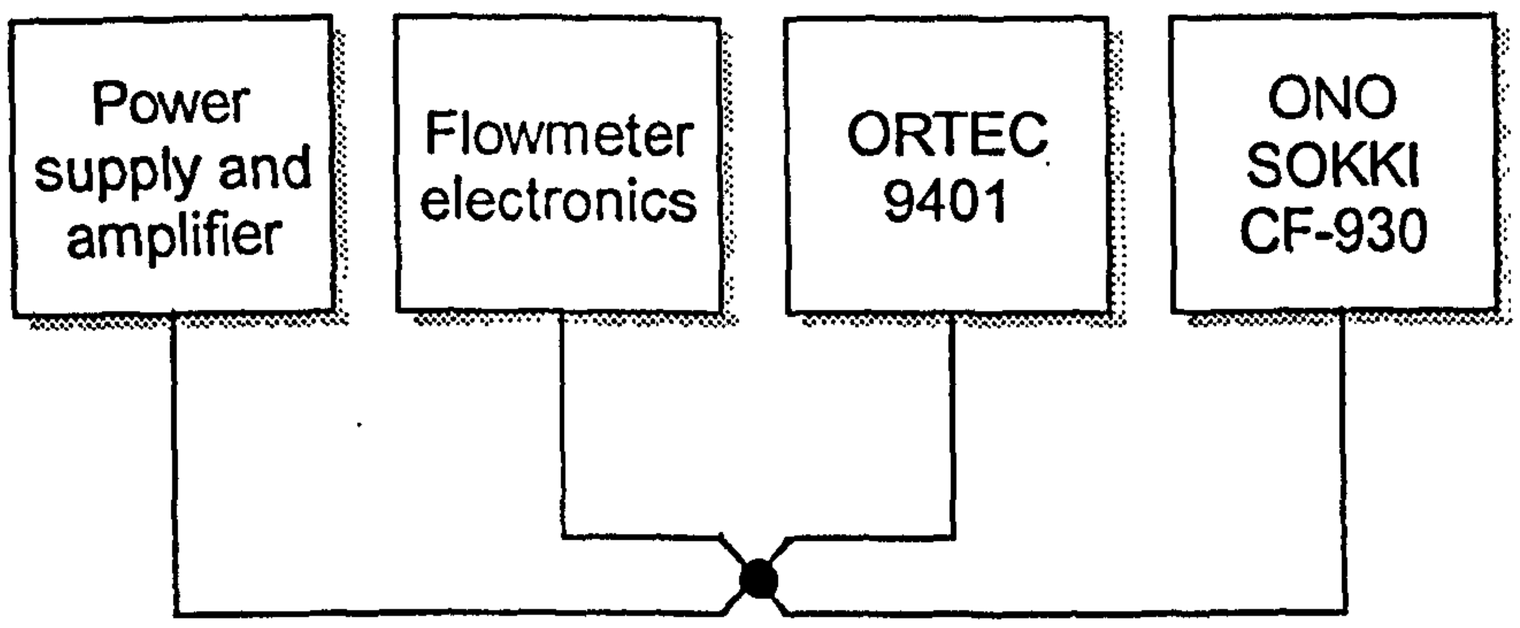

Figure 7.13 : Star-type earth connection.

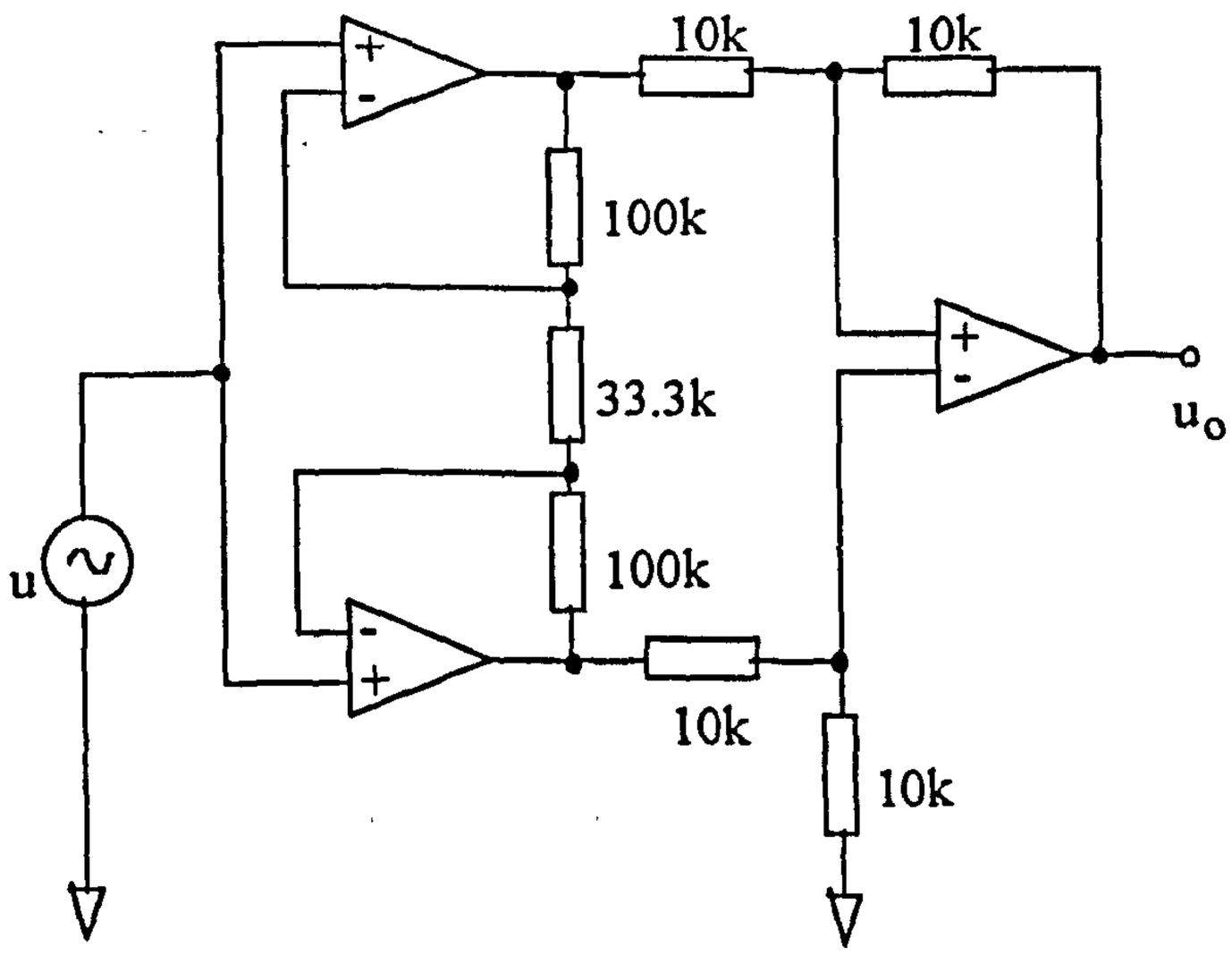

Figure 7.14: Configuration for measuring the CMRR of the instrumentation amplifier.

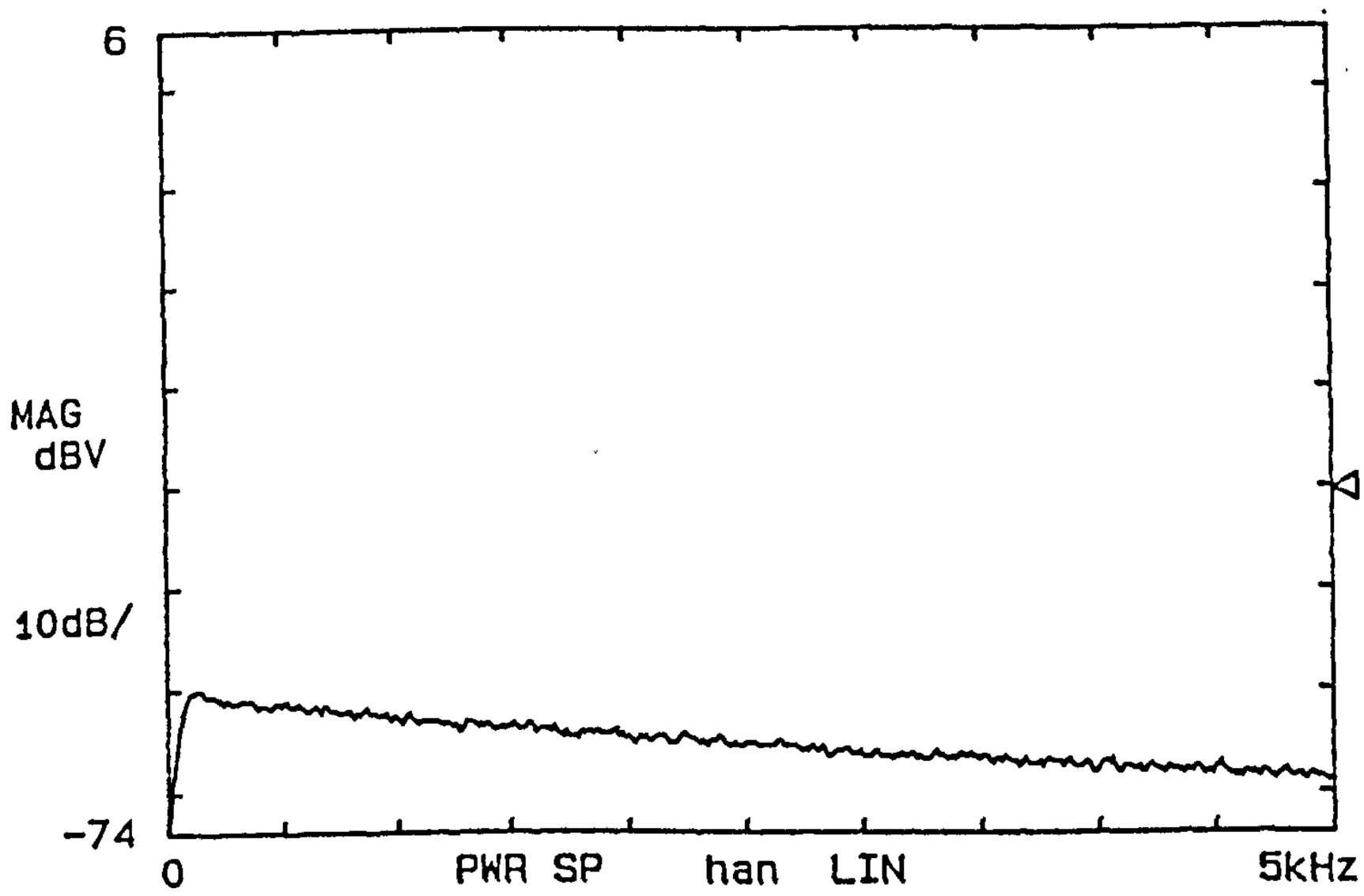

Figure 7.15 Frequency spectrum of the random noise of the meter at zero flowrate.

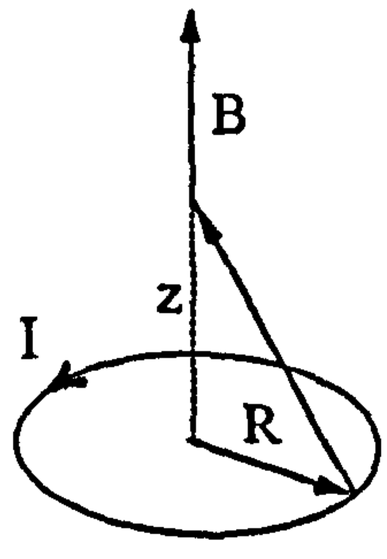

Figure 7.16: Configuration for estimation of the magnetic field at the centre of a circular coil

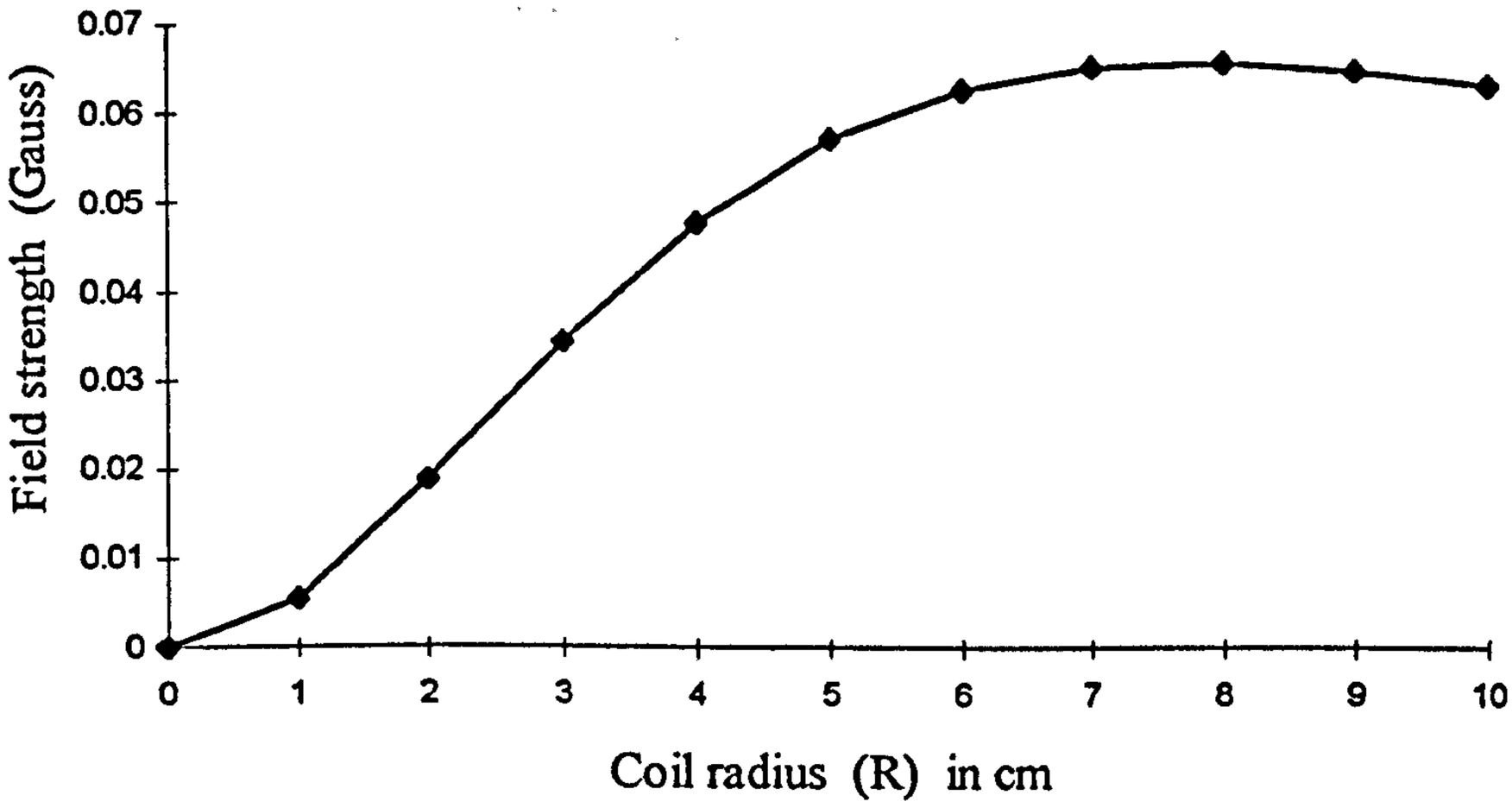

Figure 7.17 (a): Loop radius verses magnetic field distribution for 2 A current at a vertical distance (z) of 5.5 cm from the centre.

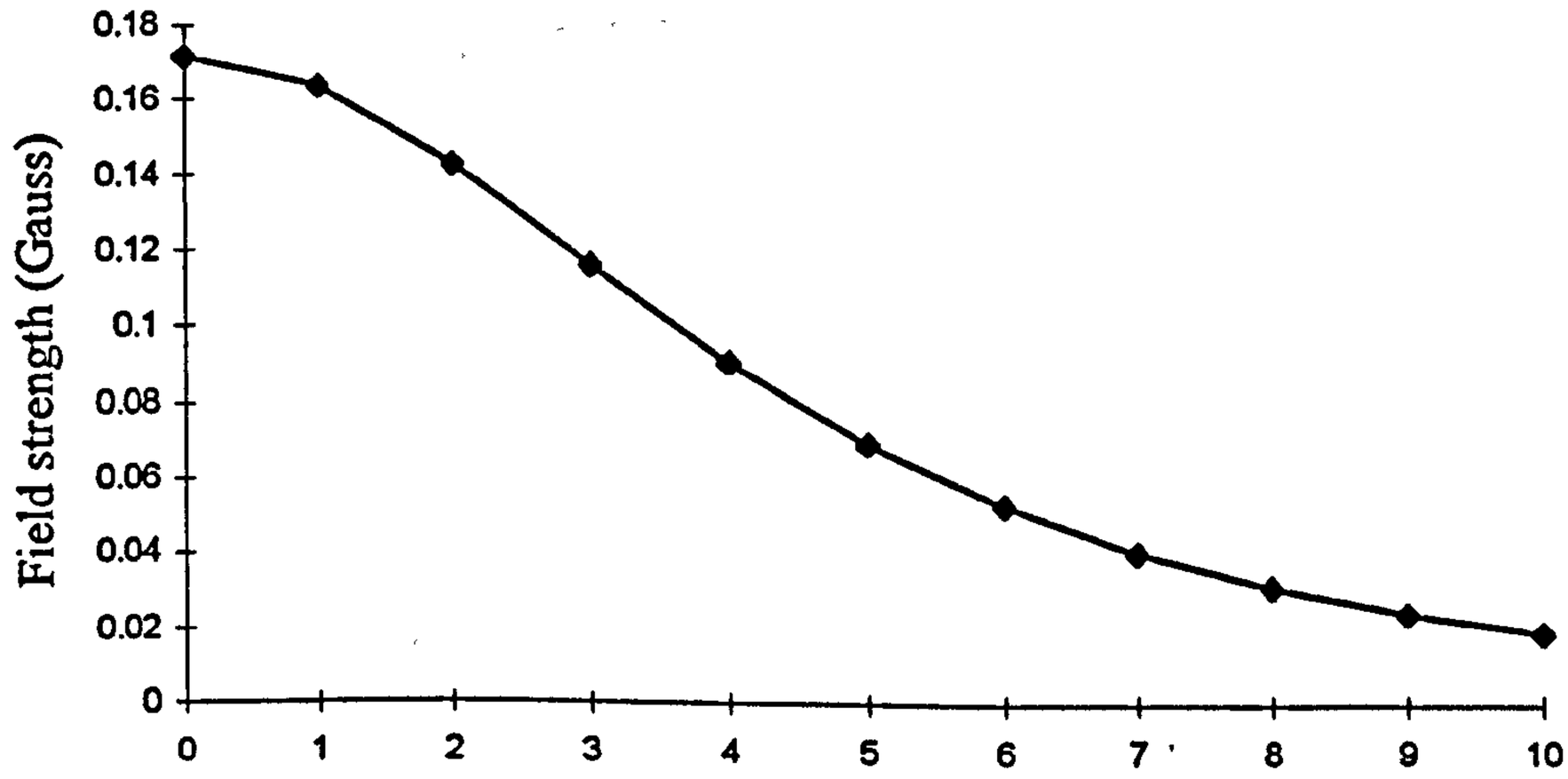

Figure 7.17 (b): Vertical distribution of the magnetic field for 2 A current and loop radius (R) of 5.5 cm.

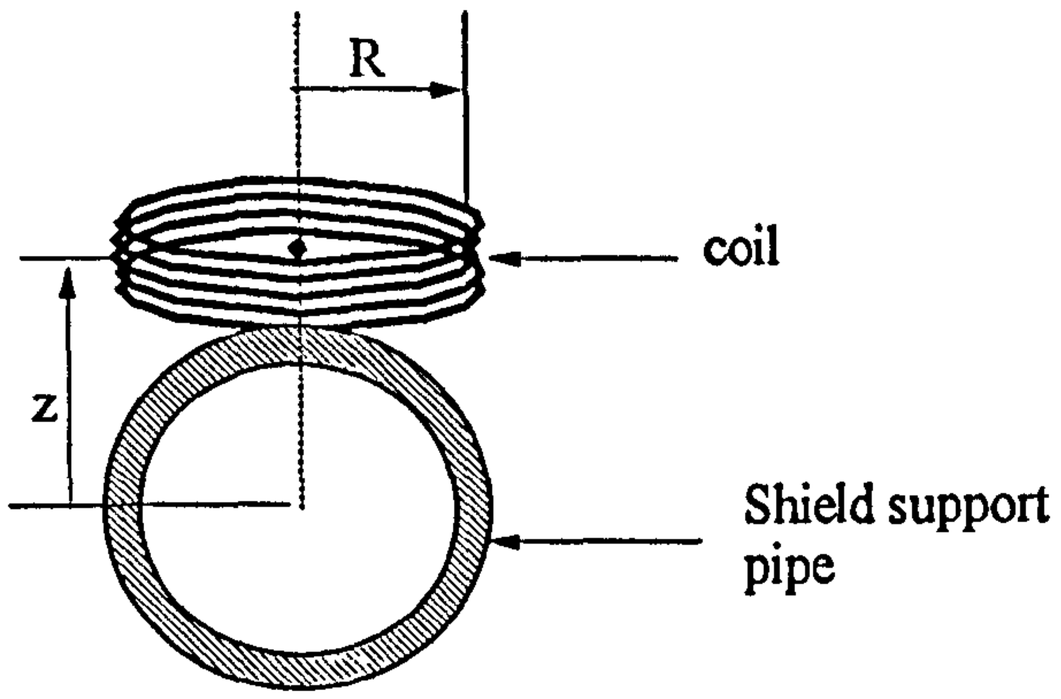

Figure 7.18 : Configuration for estimation of the magnetic field strength at the centre of the meter.

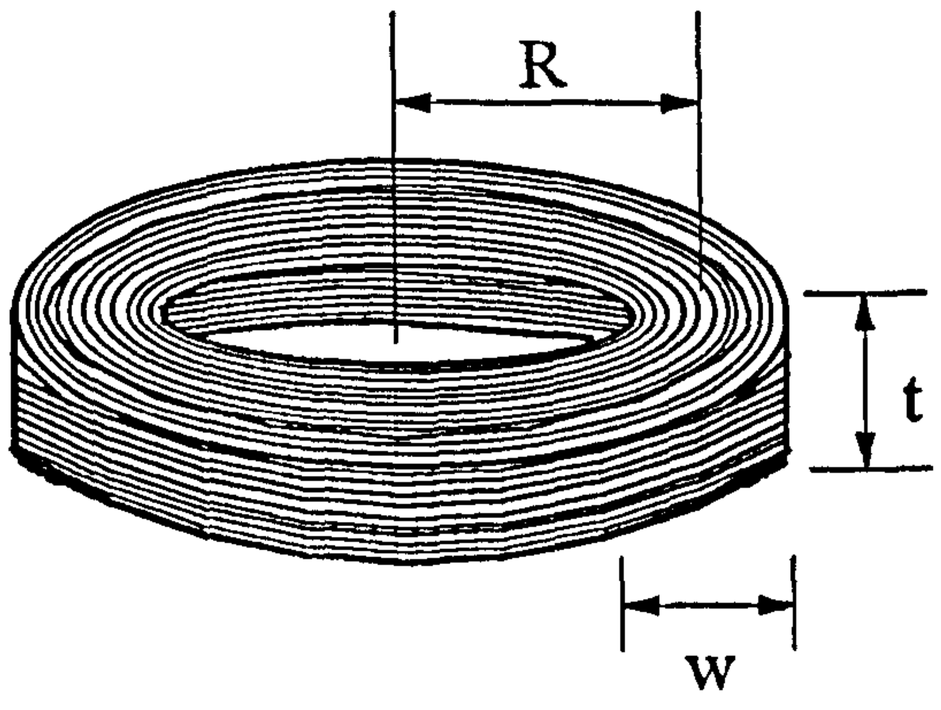

Figure 7.19: Dimensions for a circular coil.

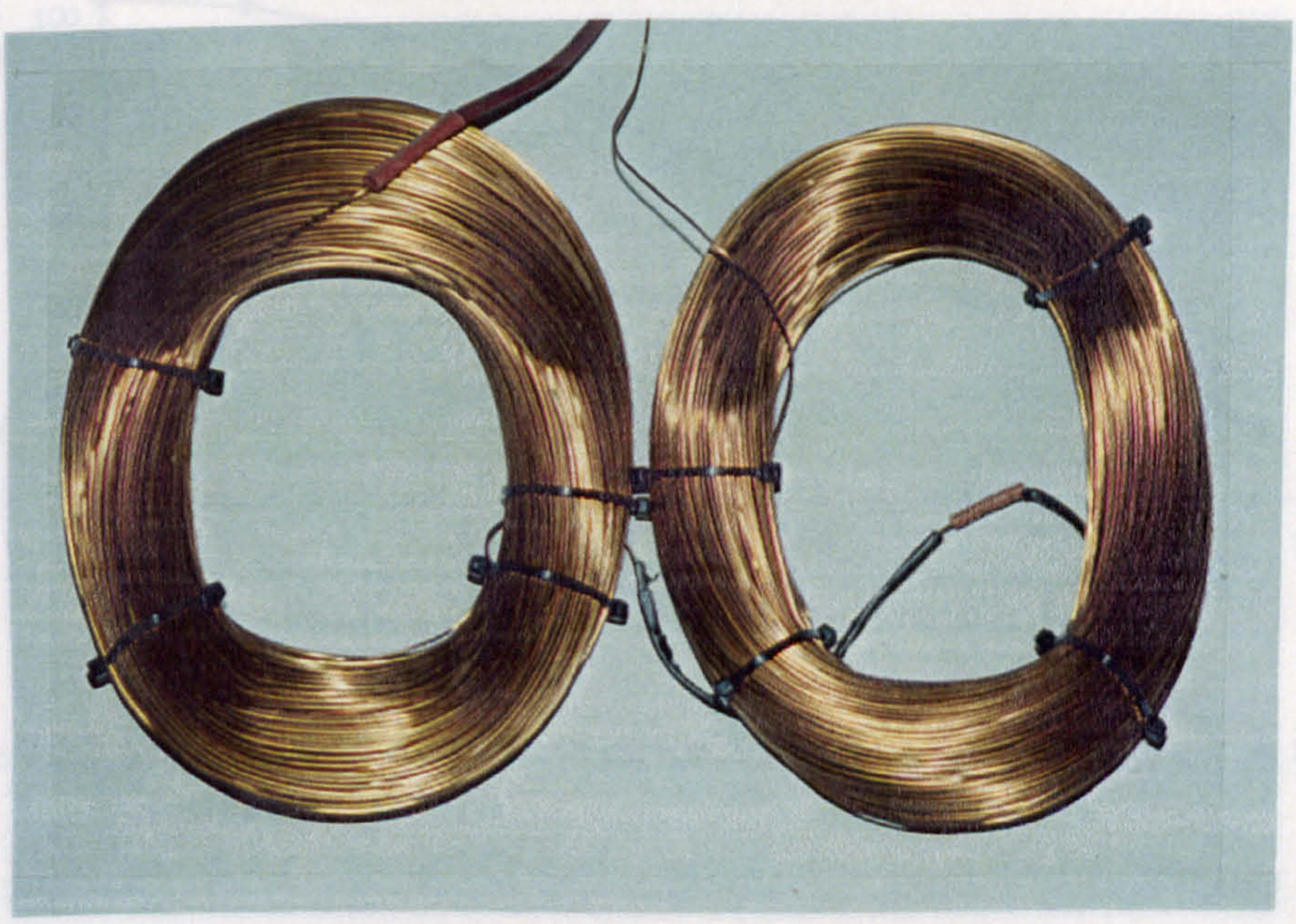

Figure 7.20: Coils of the electromagnetic flowmeter.

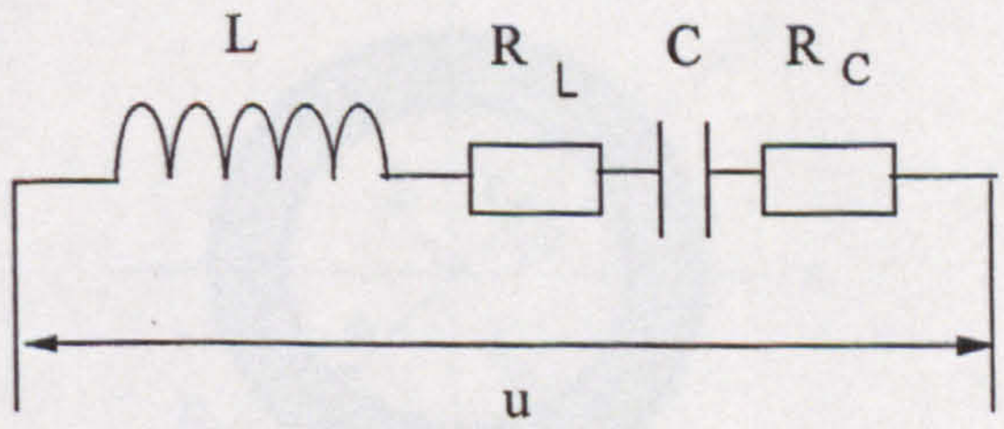

Figure 7.21: Equivalent circuit for the electromagnet.

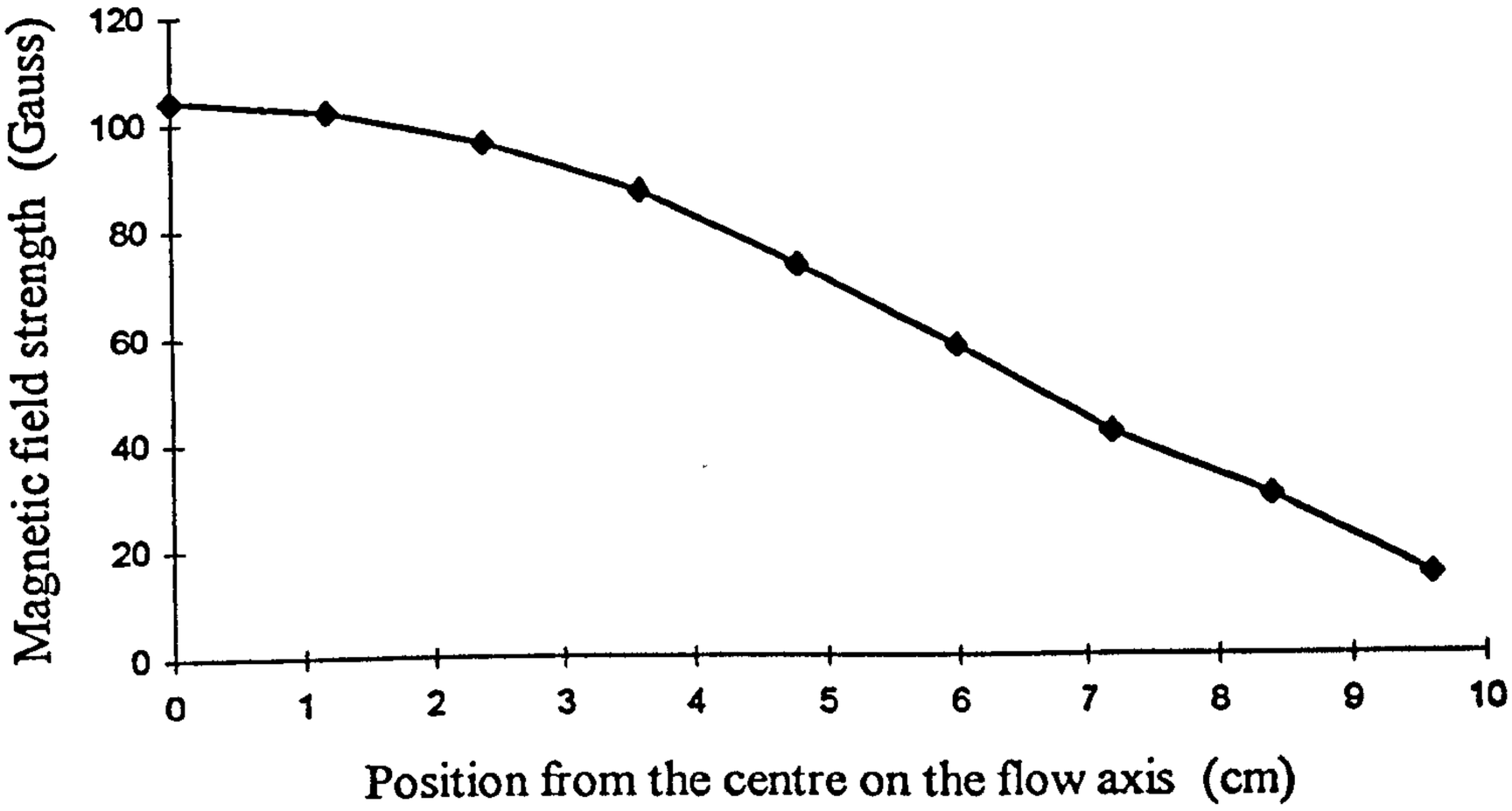

Figure 7.22: Magnetic field distribution on the flow axis of the meter for 2 A (rms) current.

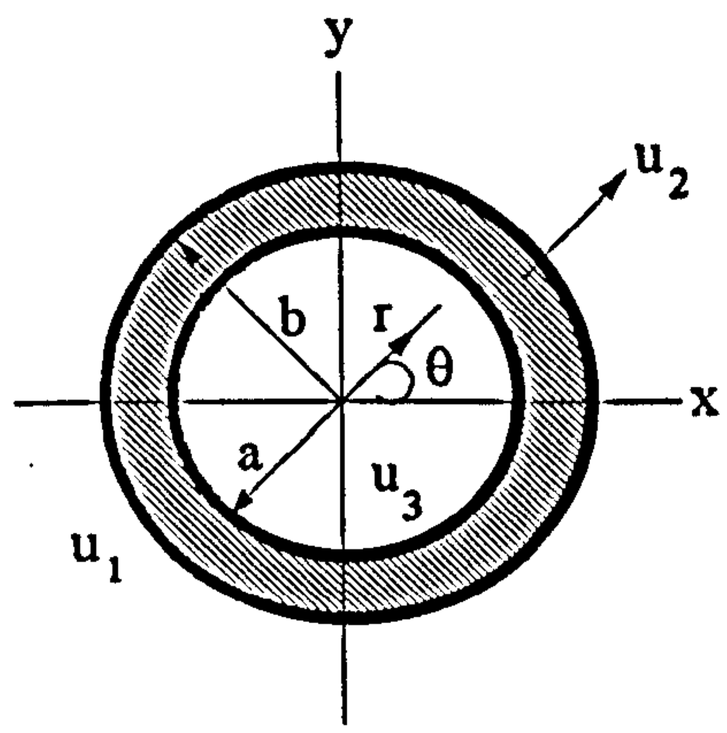

7.23: Shielding of electric field by a hollow cylinder.

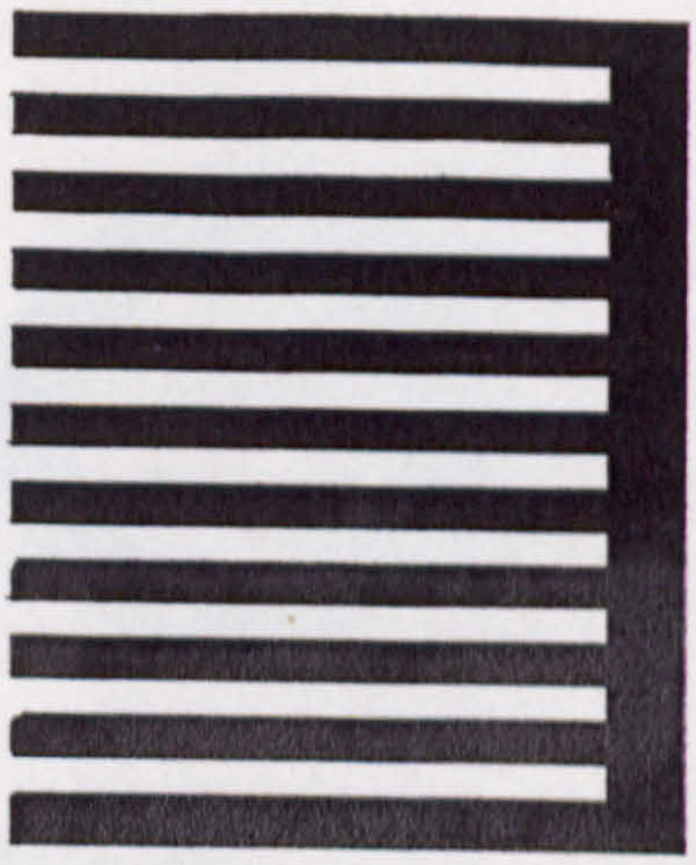

Figure 7.24: Schematic of the design of eddy current free shield.

Figure 7.25: The eddy current free electrostatic shield of the meter.

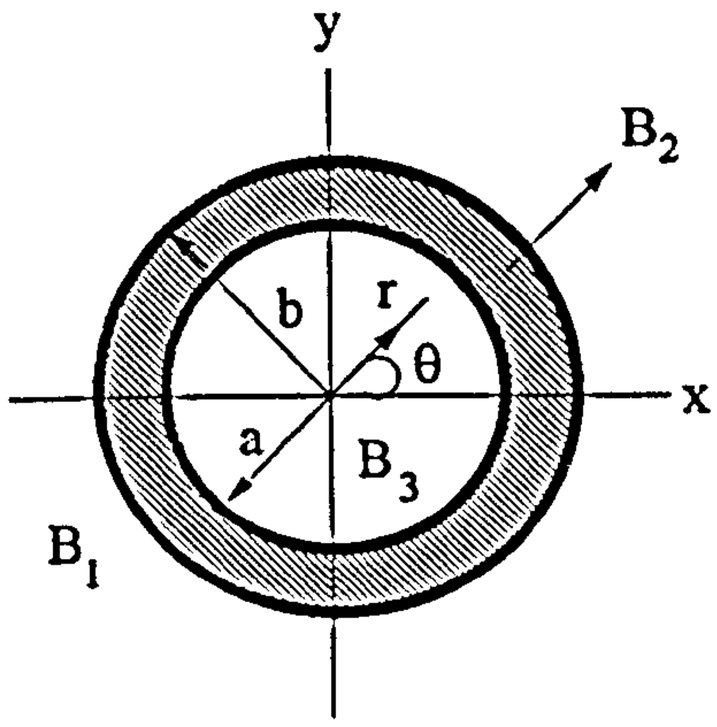

7.26: Shielding of magnetic field by a hollow cylinder.

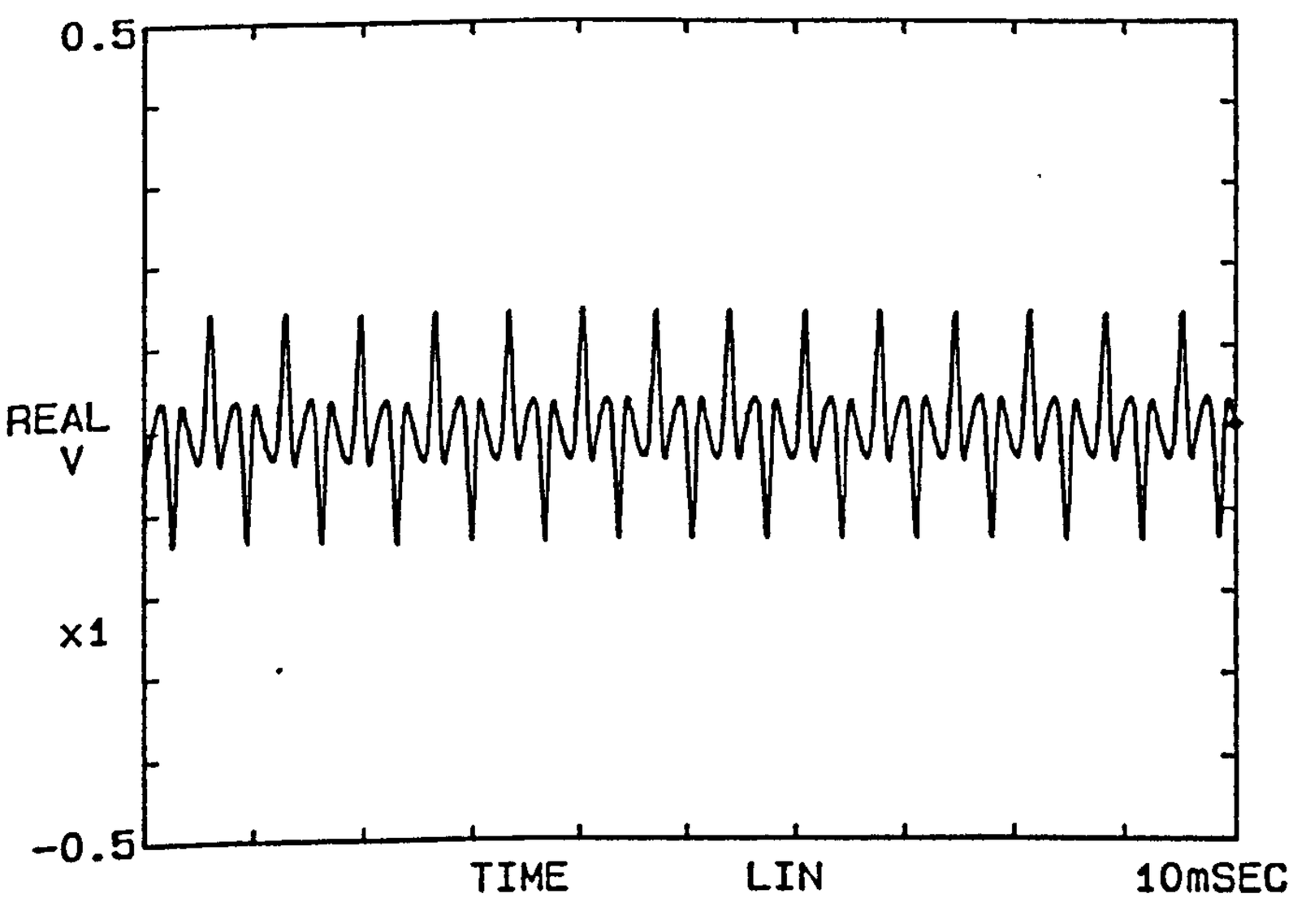

Figure 7.27 (a) Time domain graph of the distorted magnetic field as detected with a search coil.

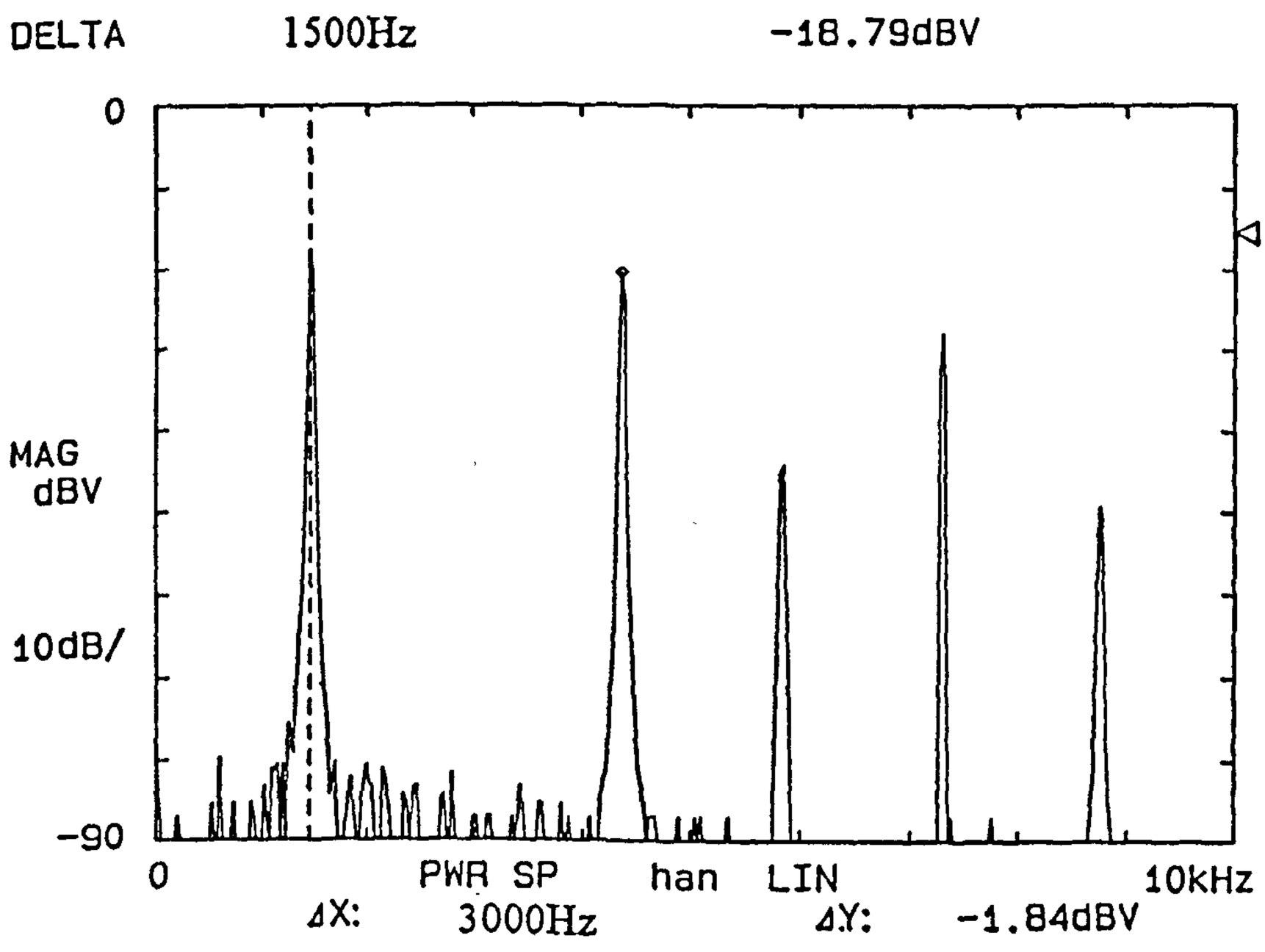

Figure 7.27 (b): Frequency spectrum of the distorted magnetic field.

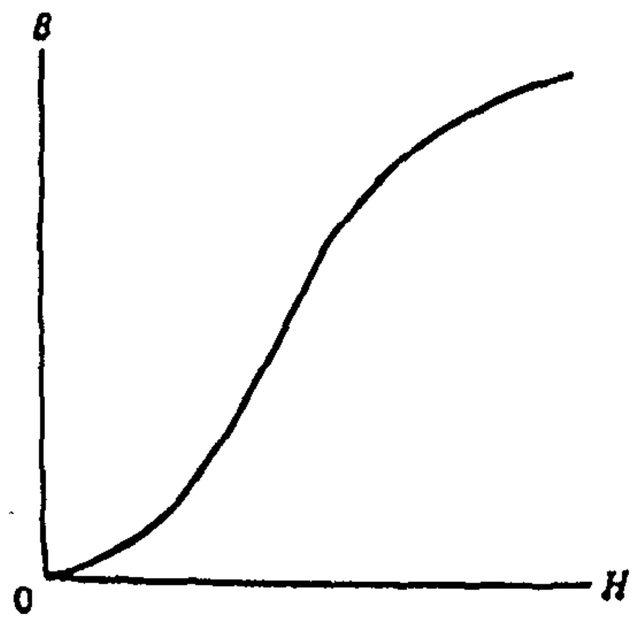

Figure 7.28: **B** versus **H** curve of a ferromagnetic.

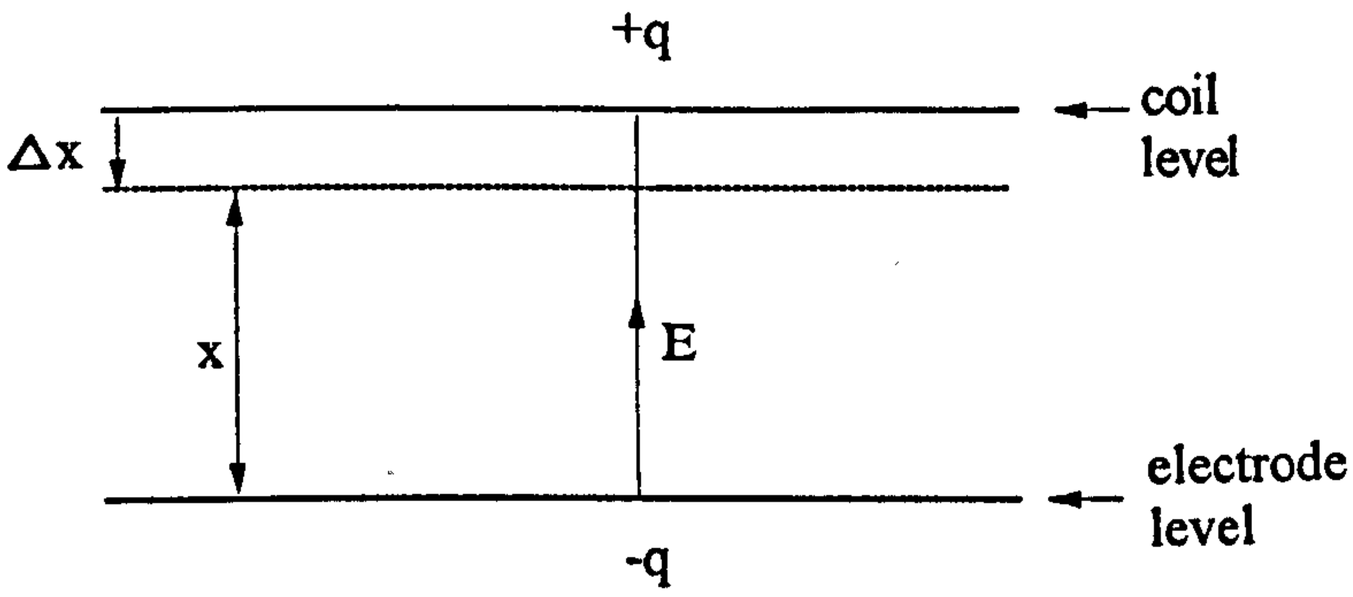

Figure 7.29 :Equivalent representation for analysis of the electrostatic force on an electrostatic shield.

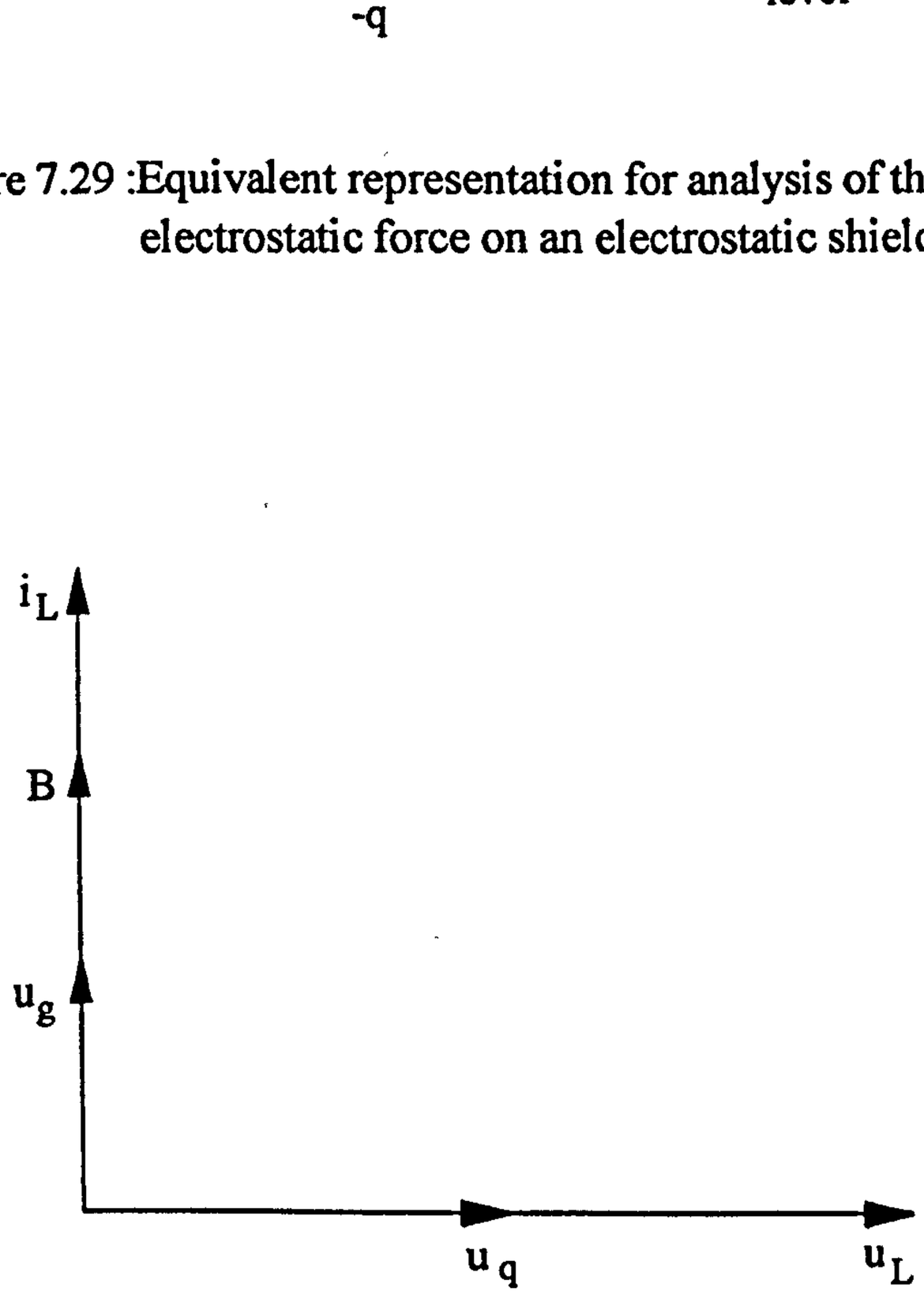

Figure 7.30: Phase relation of the primary elements of the flowmeter.

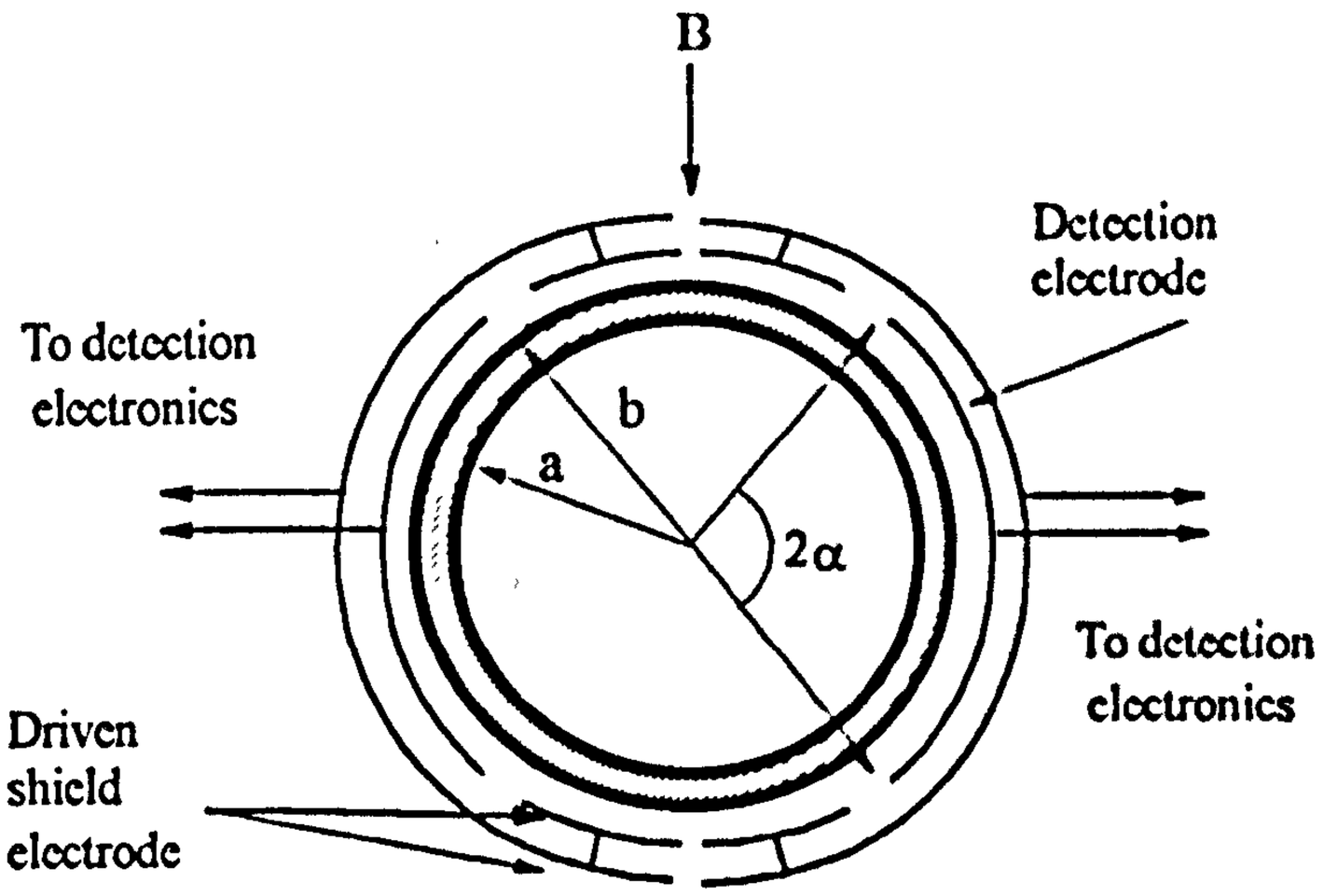

Figure 8.1 : Cross sectional view of the electromagnetic flowmeter configuration

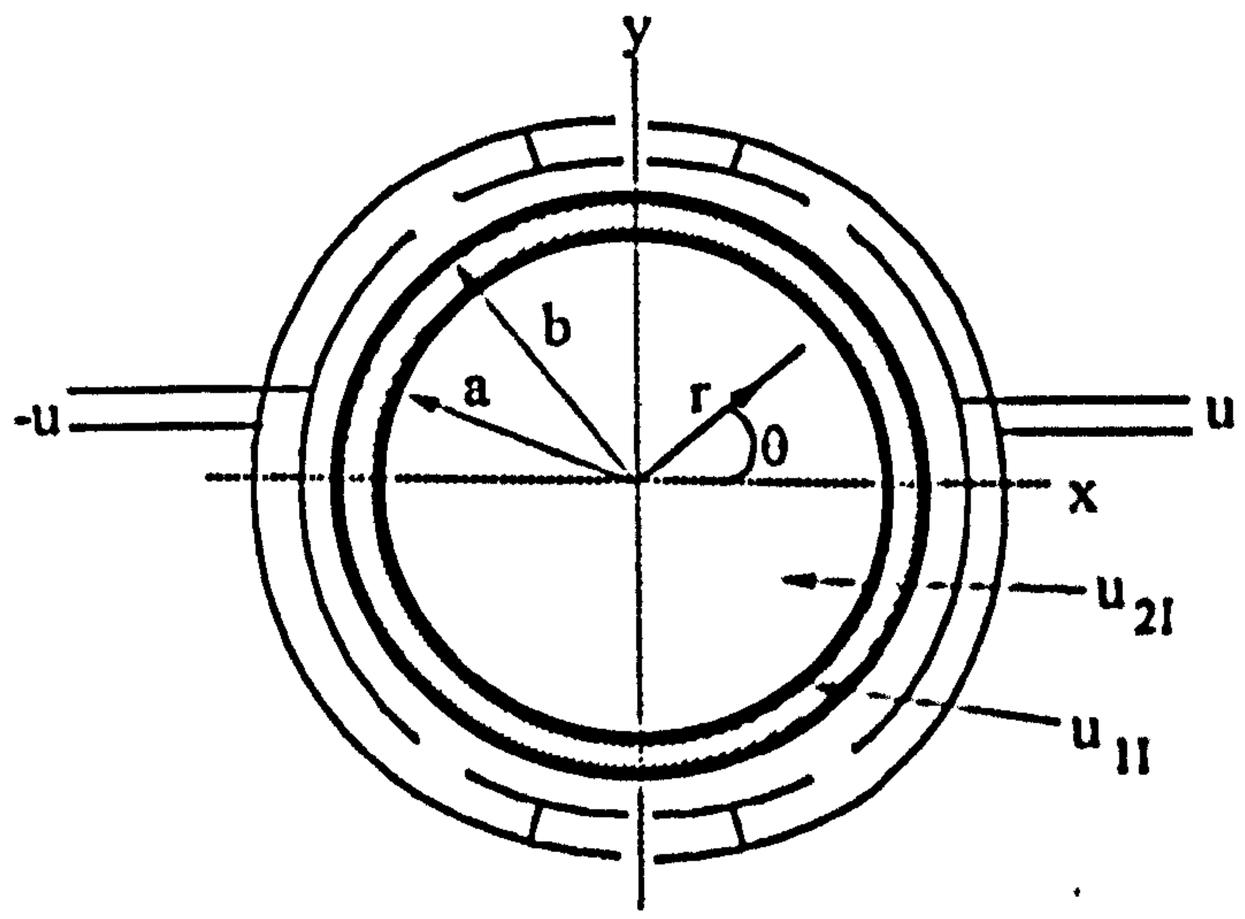

Figure 8.2: Schematic diagram with electrodes at a potential ± u volts and no flow (case I).

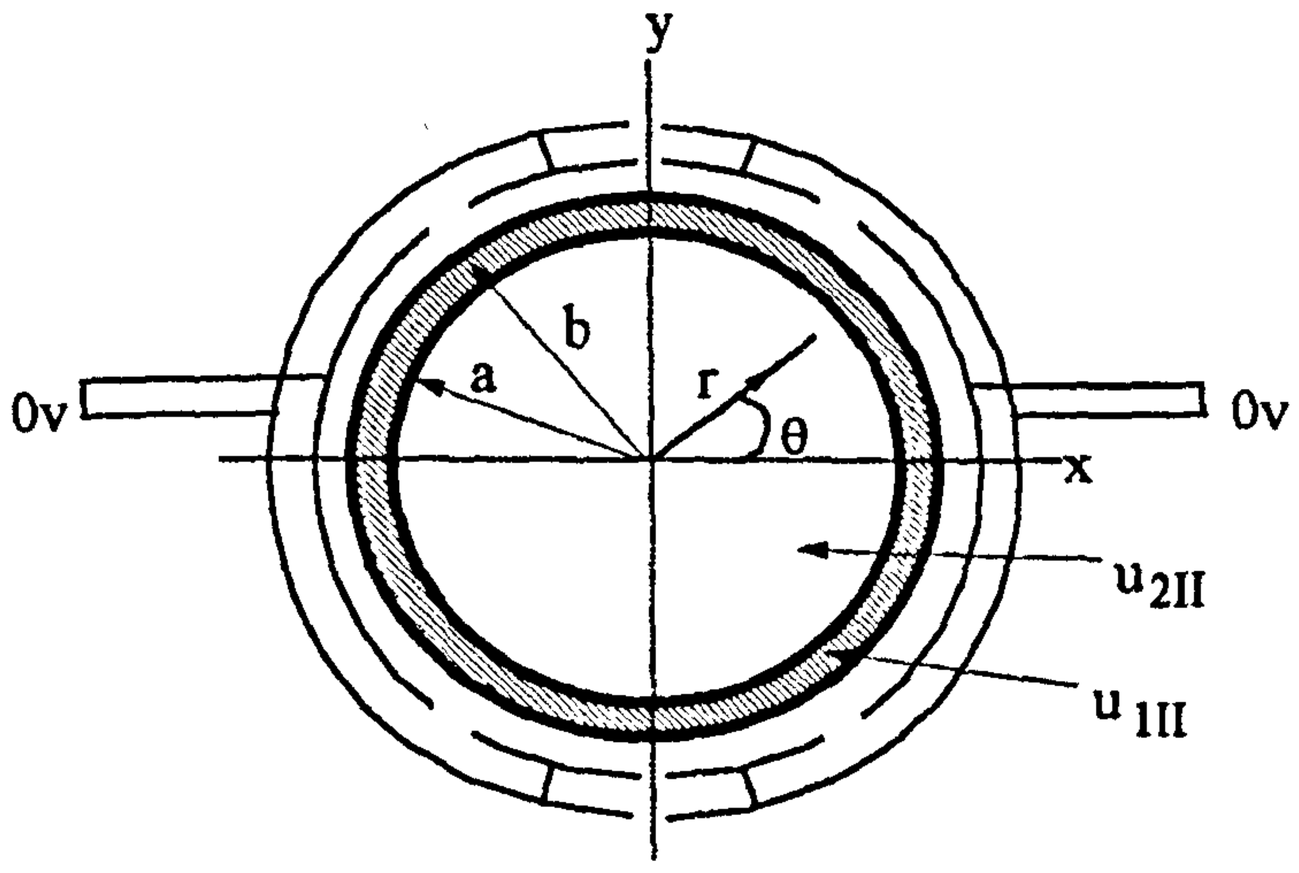

Figure 8.3 : Schematic diagram with electrodes at zero potential and flow induced potential present (case II).

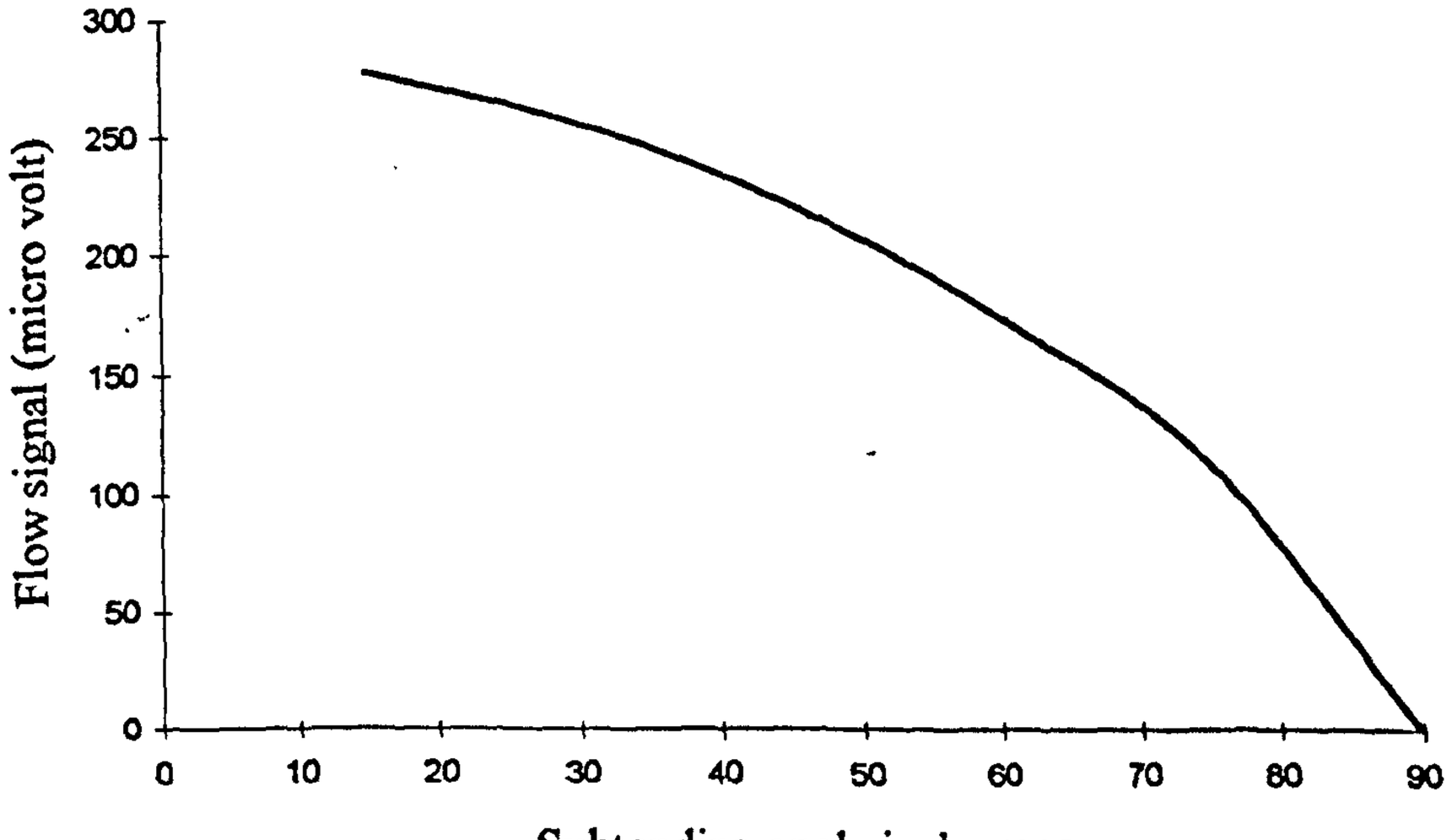

Figure 8.4: Sensitivity of the meter at different subtending angles.

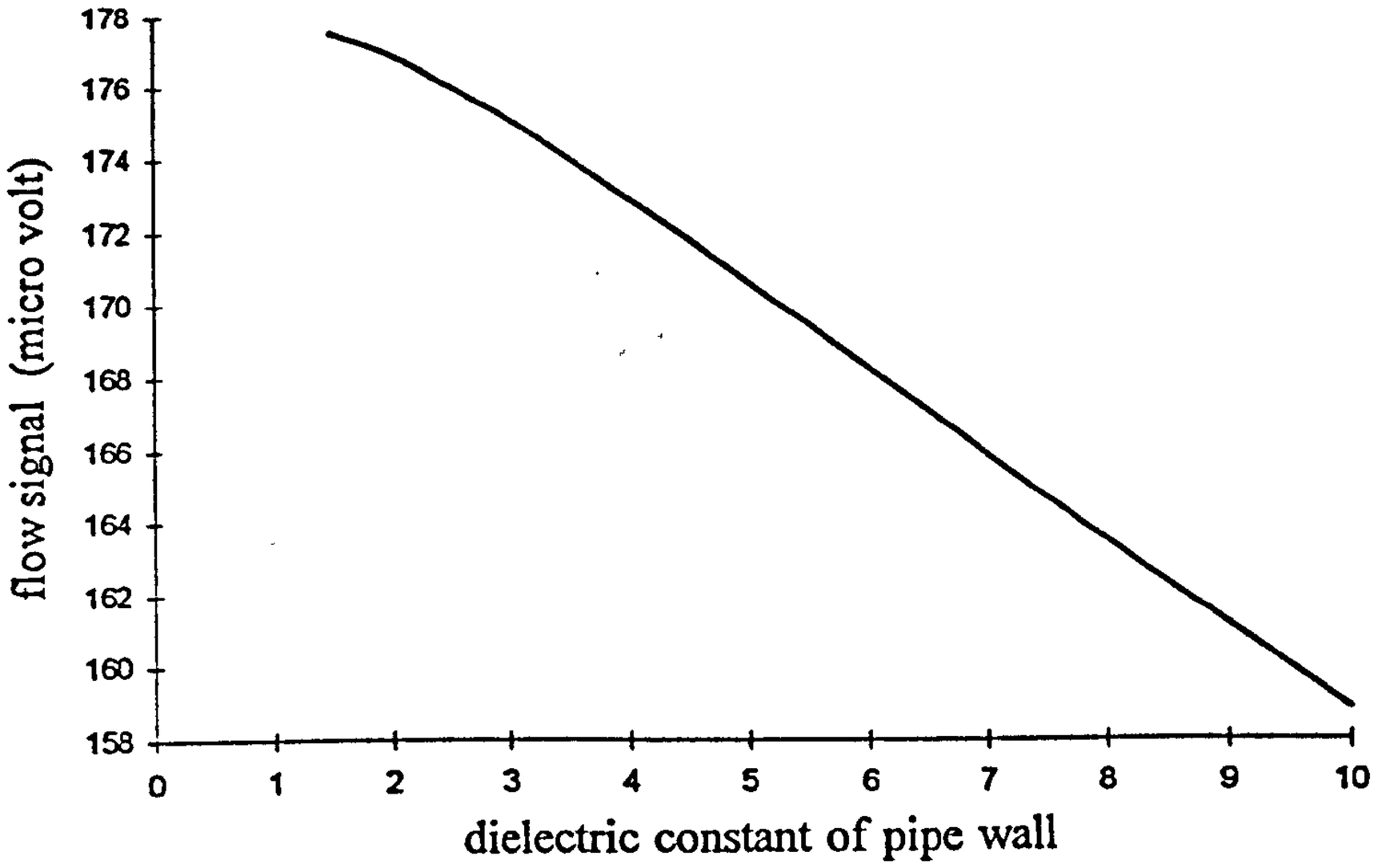

Figure 8.5: Sensitivity of the meter for various pipe wall dielectric permittivity.

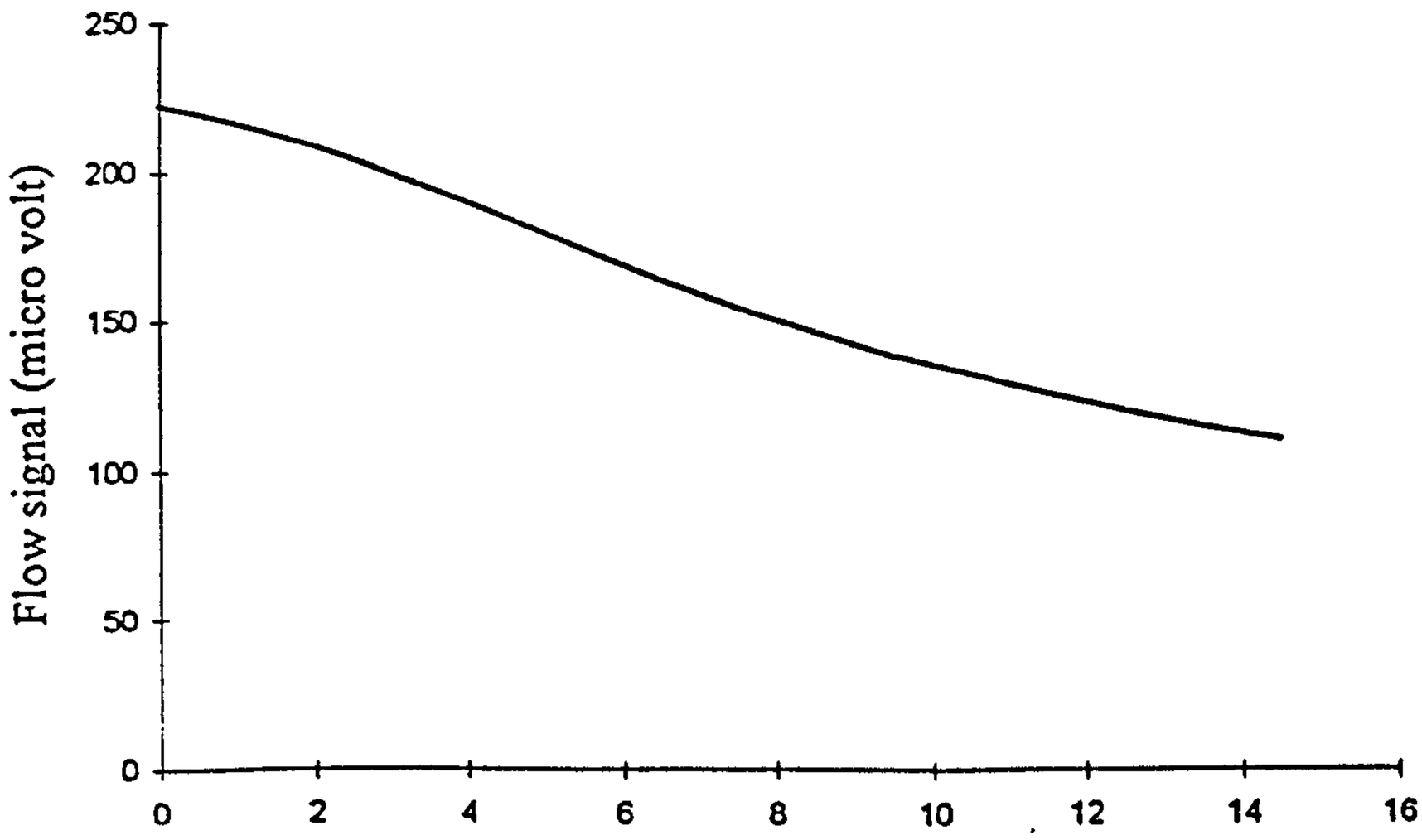

Figure 8.6: Sensitivity of the meter for various pipe wall thickness.

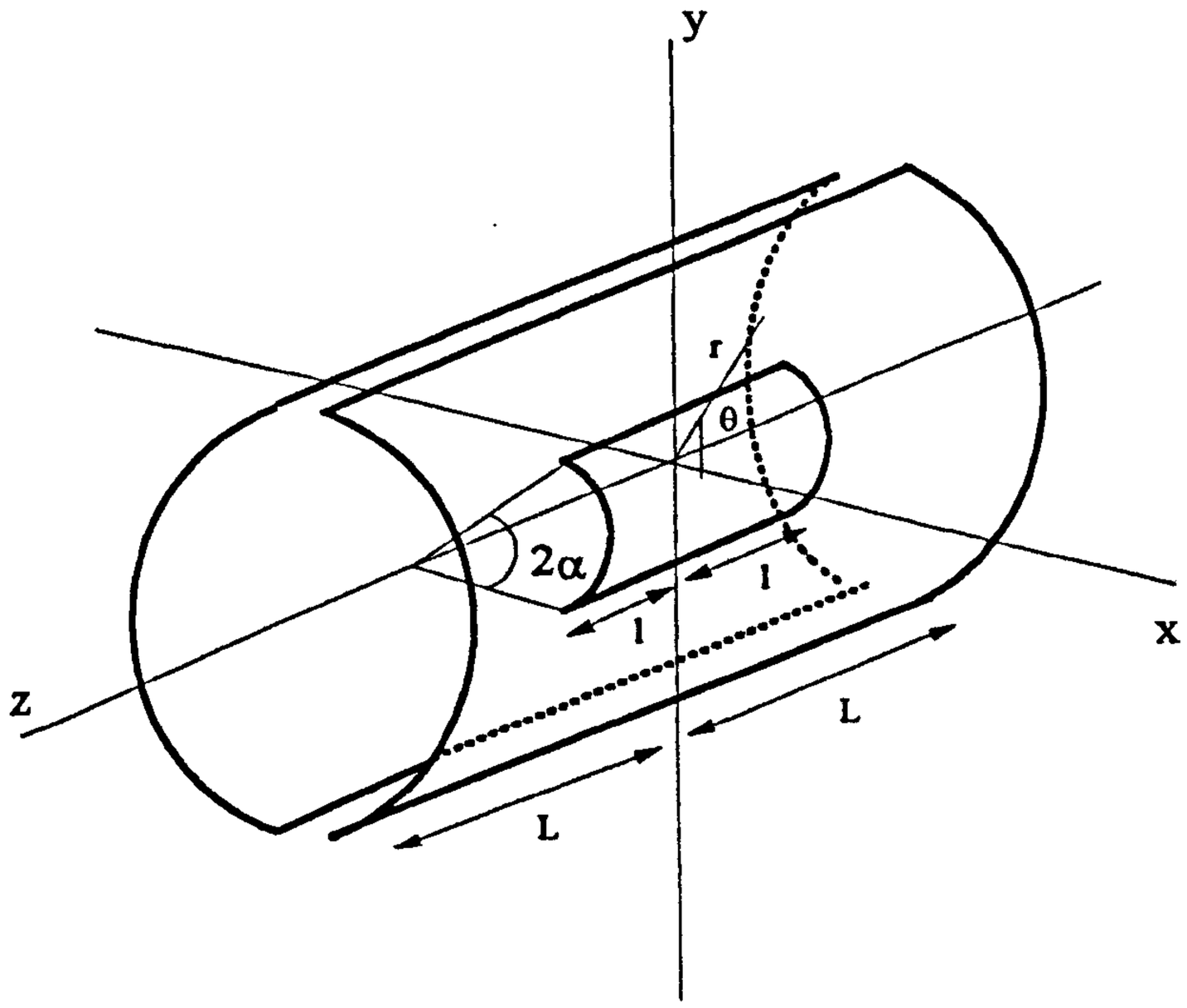

Figure 8.7 : Schematic diagram for end-effect analysis

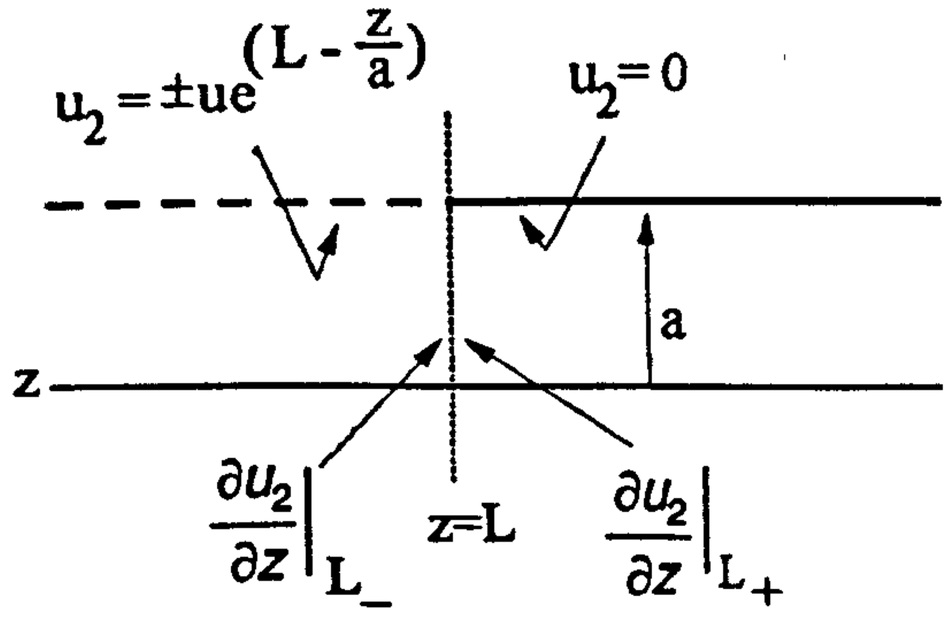

Figure 8.8: Boundary conditions for end-effect analysis.

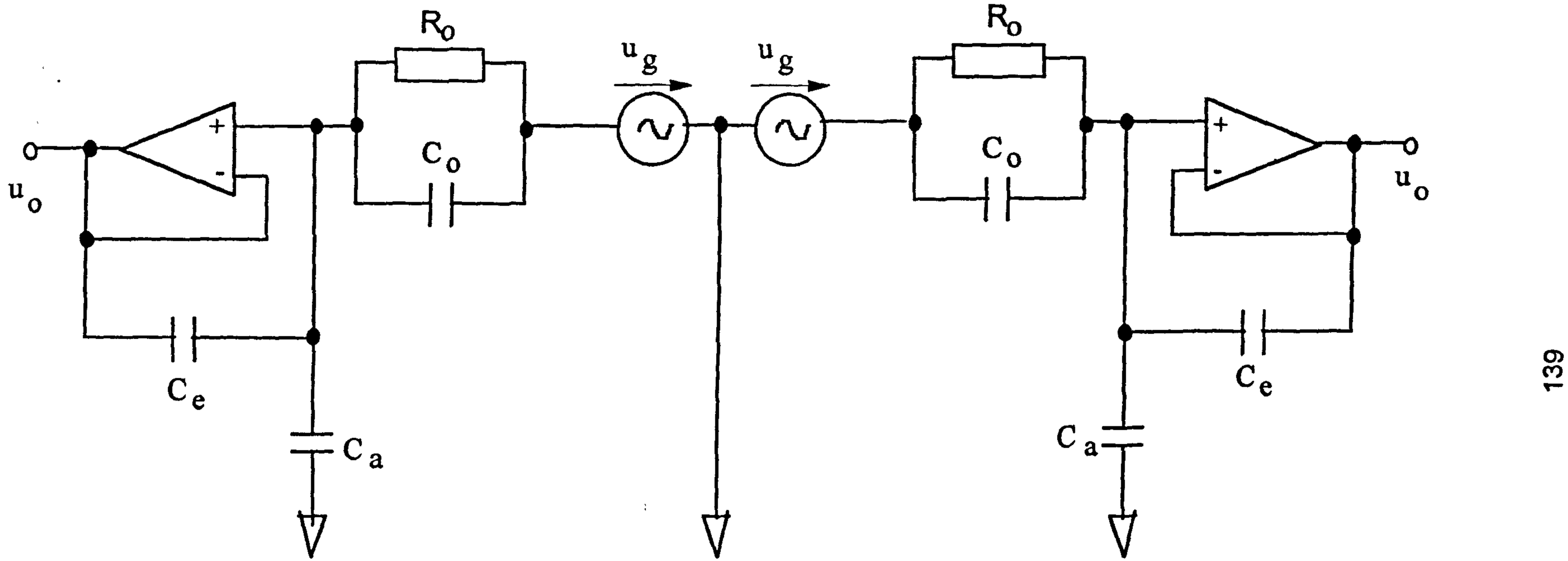

Figure 8.9 : Equivalent circuit of the flowmeter together with follower amplifiers.

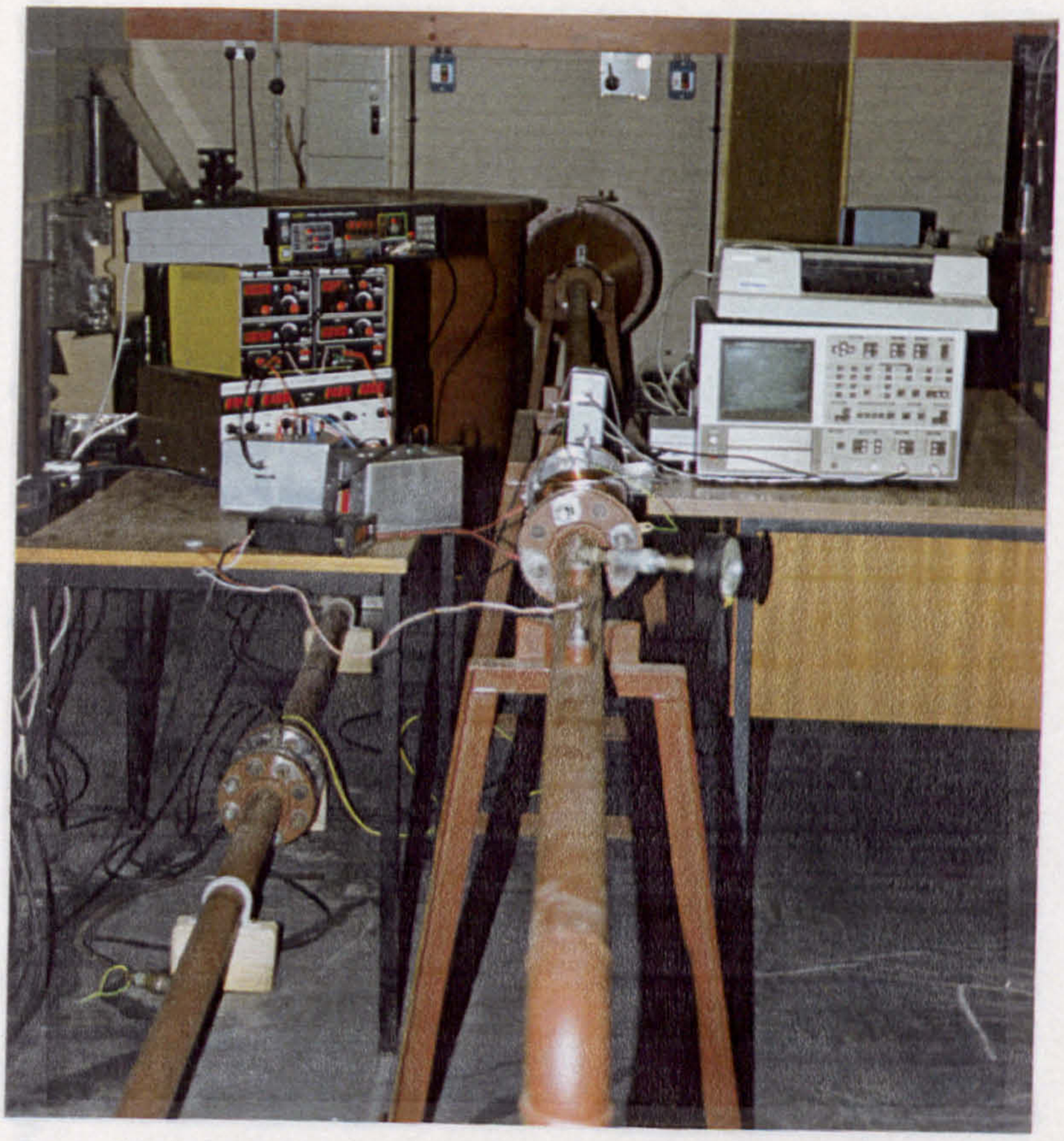

Figure 9.1 (a): End-on view of the BP180 oil flow rig in use.

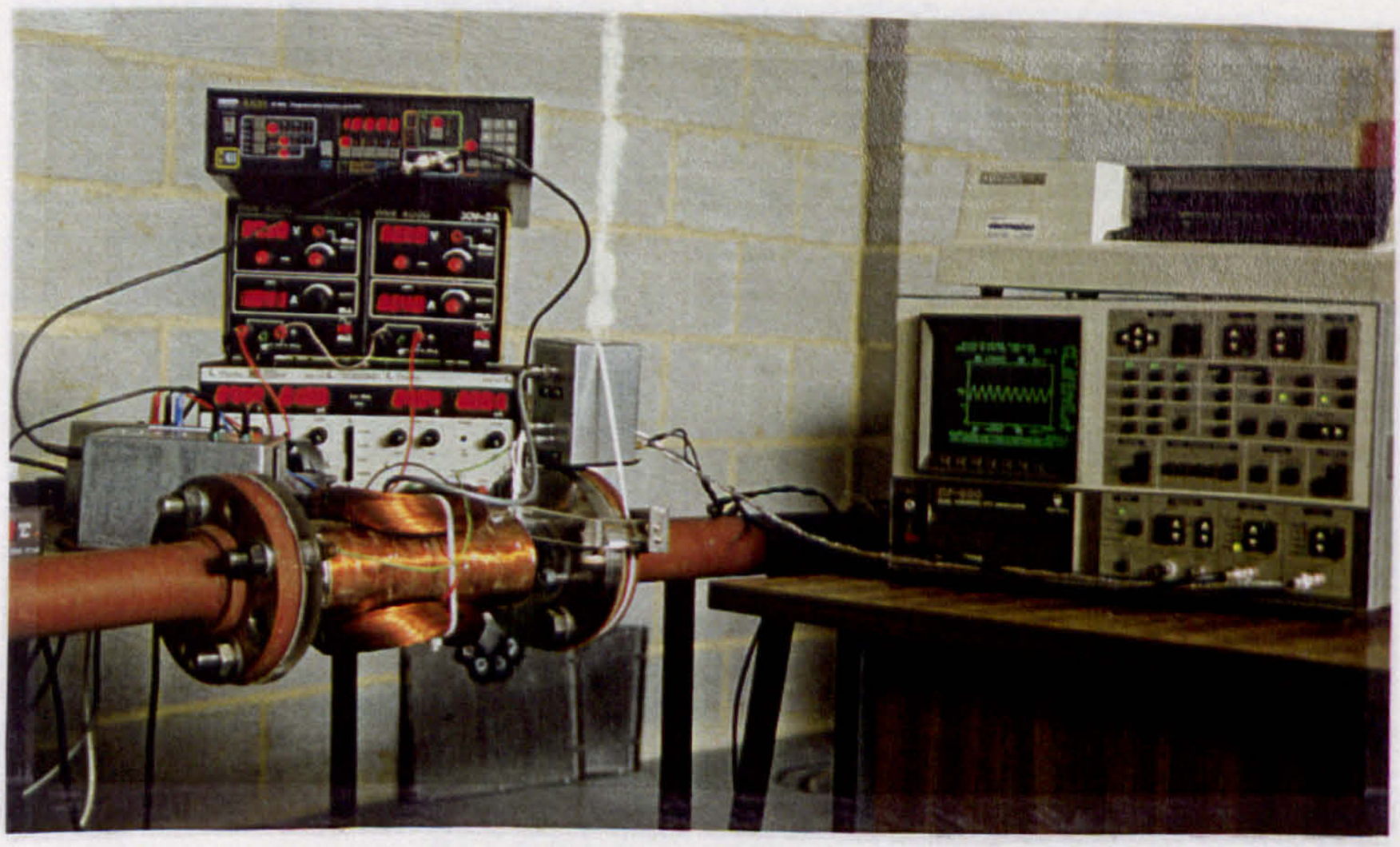

Figure 9.1 (b): The electromagnetic flowmeter in use on BP180 oil.

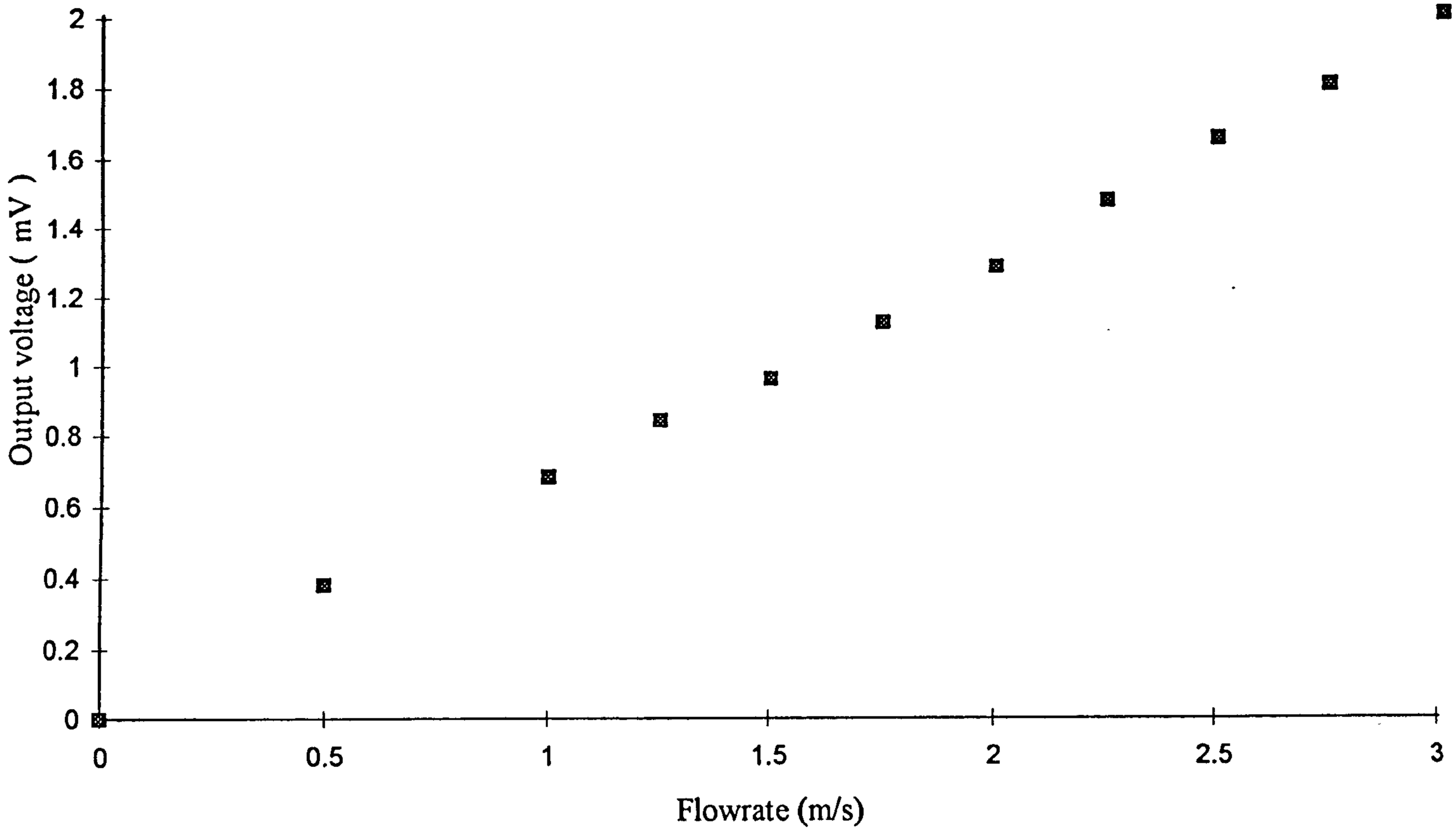

Figure 9.2: Output voltage of the electromagnetic flometer for BP180 at 20 degrees Celsius

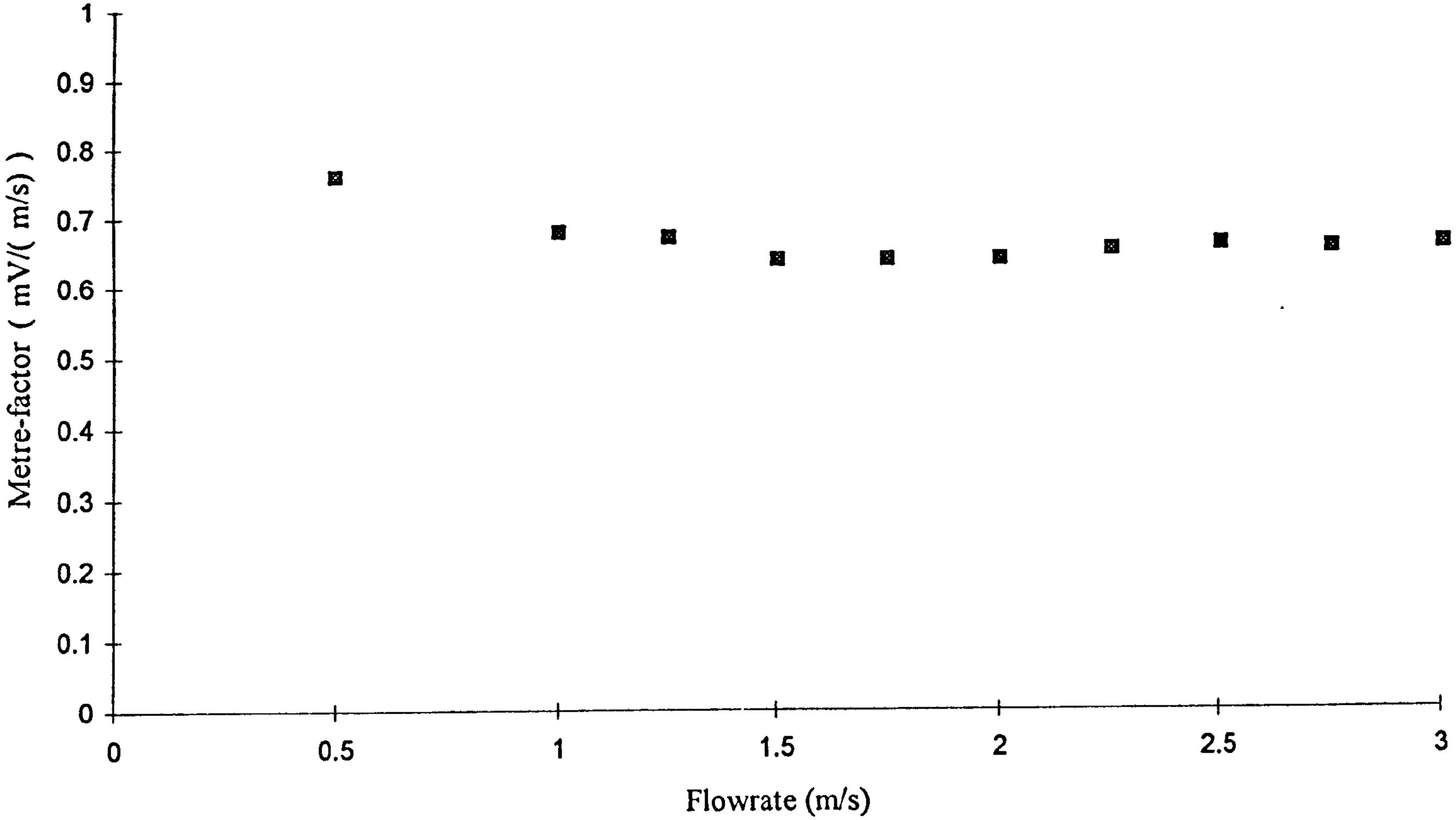

Figure 9.3 The meter-factor of the electomagnetic flowmeter for BP180.

● NOT TO SCALE

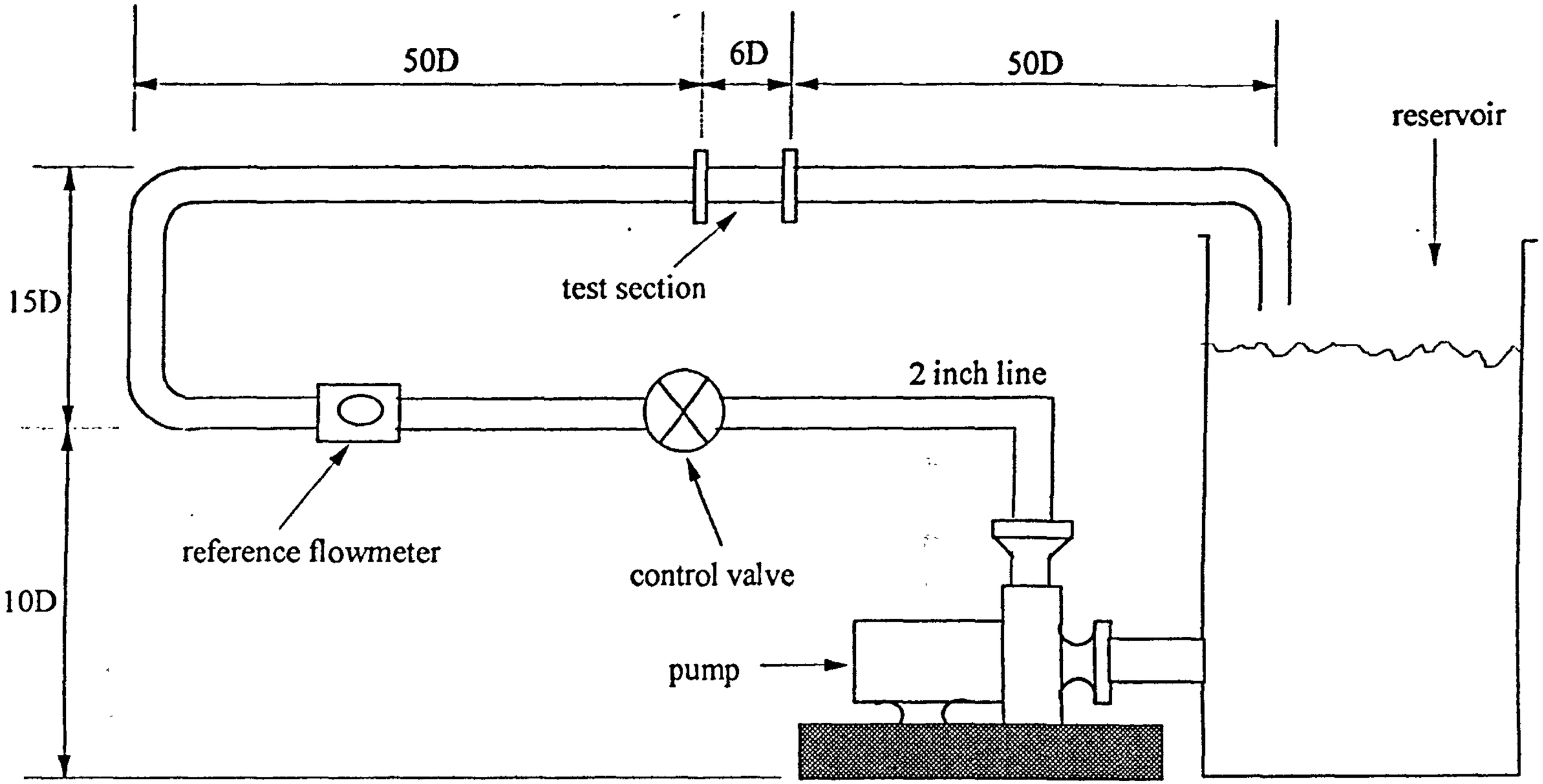

Figure 9.4: Simplified schematic diagram of the flow loop used in the experiment to measure the flowrate of water.

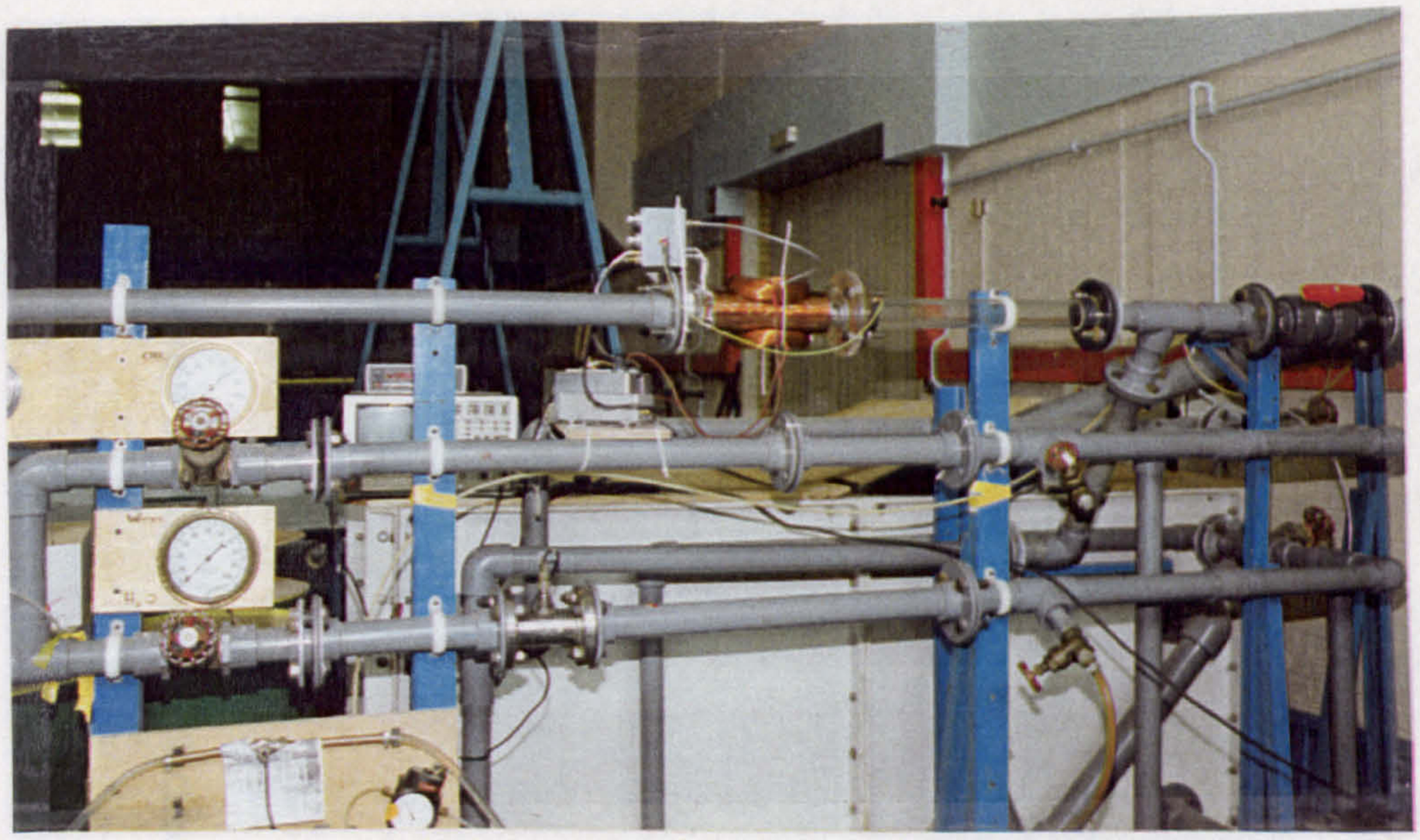

Figure 9.5 (a): Side view of the multi-purpose water flow rig in use.

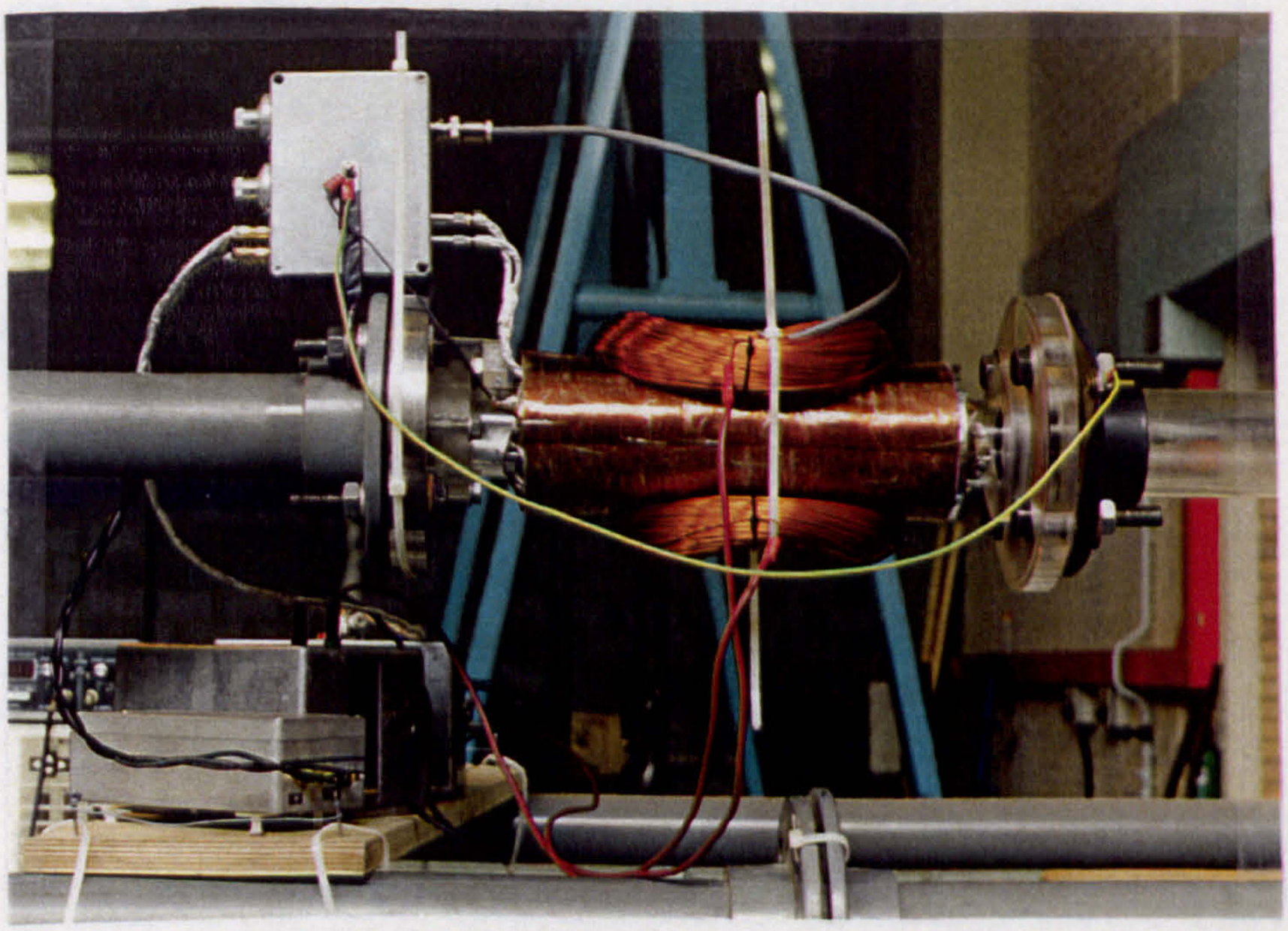

Figure 9.5 (b): The electromagnetic flowmeter in use on water.

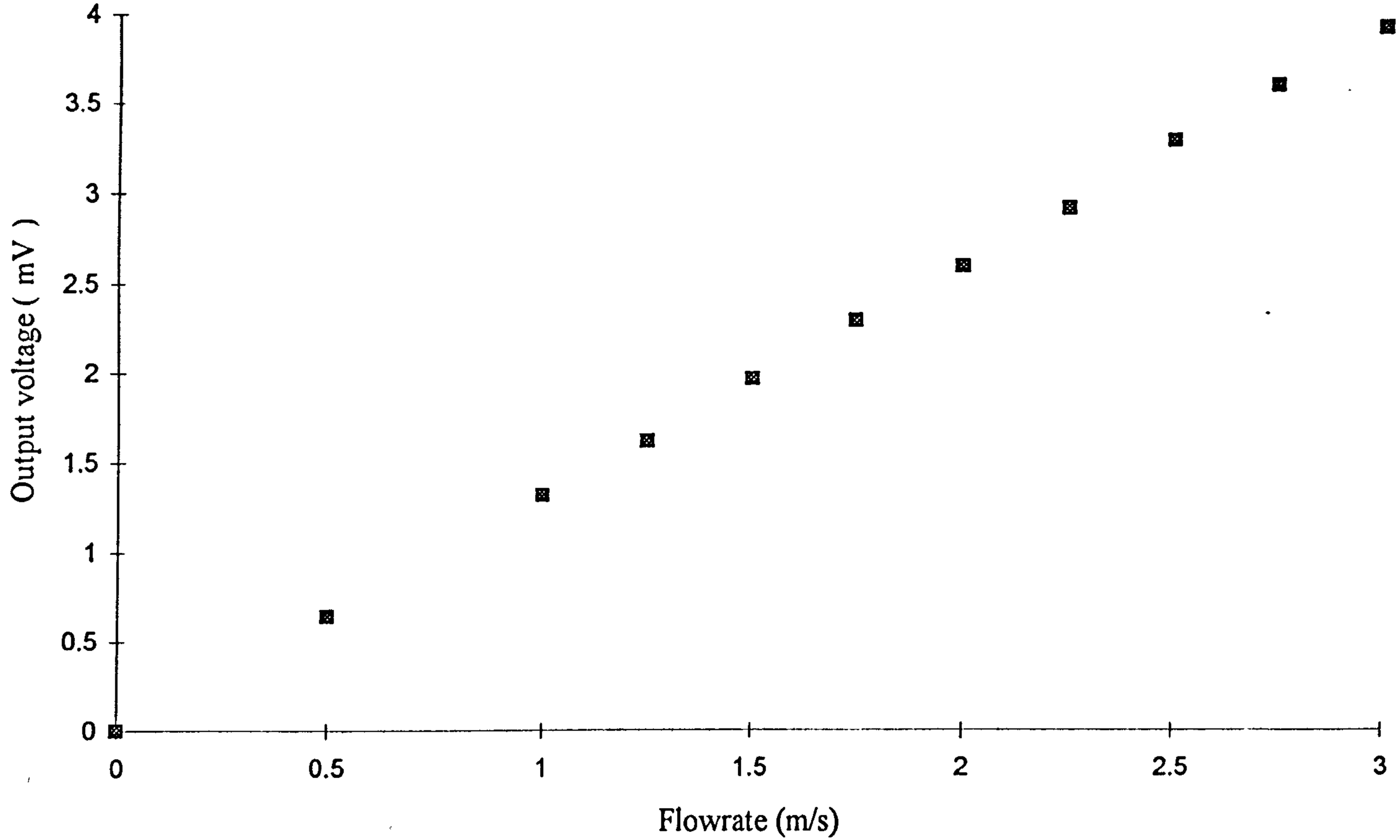

Figure 9.6: Output of the electromagnetic flowmeter for tap-water at 20 degrees Celsius

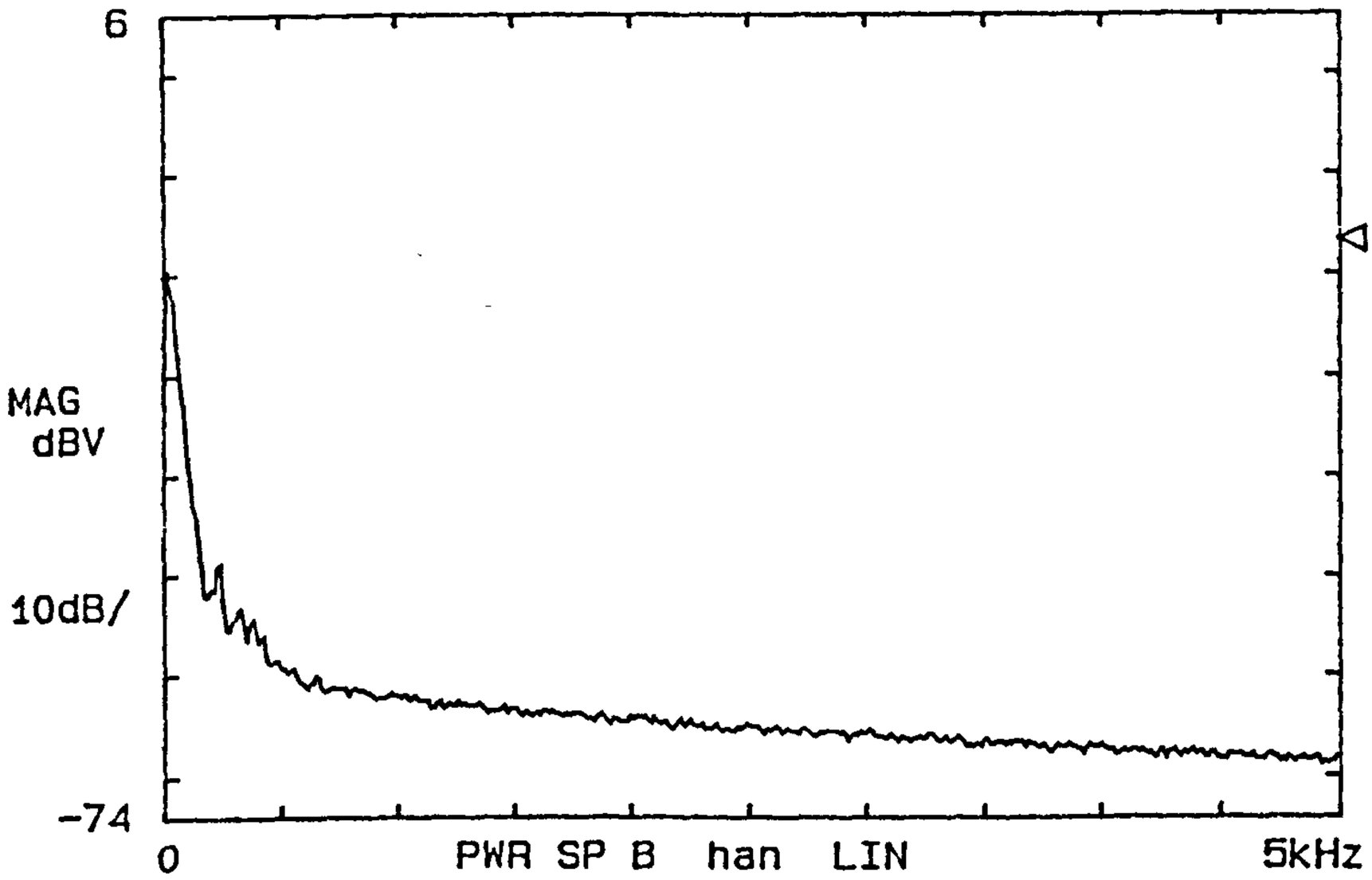

Figure 9.7 (a): Frequency spectrum of the charge distribution at a flow velocity of 1 m/s without the relaxation tank in the flow rig.

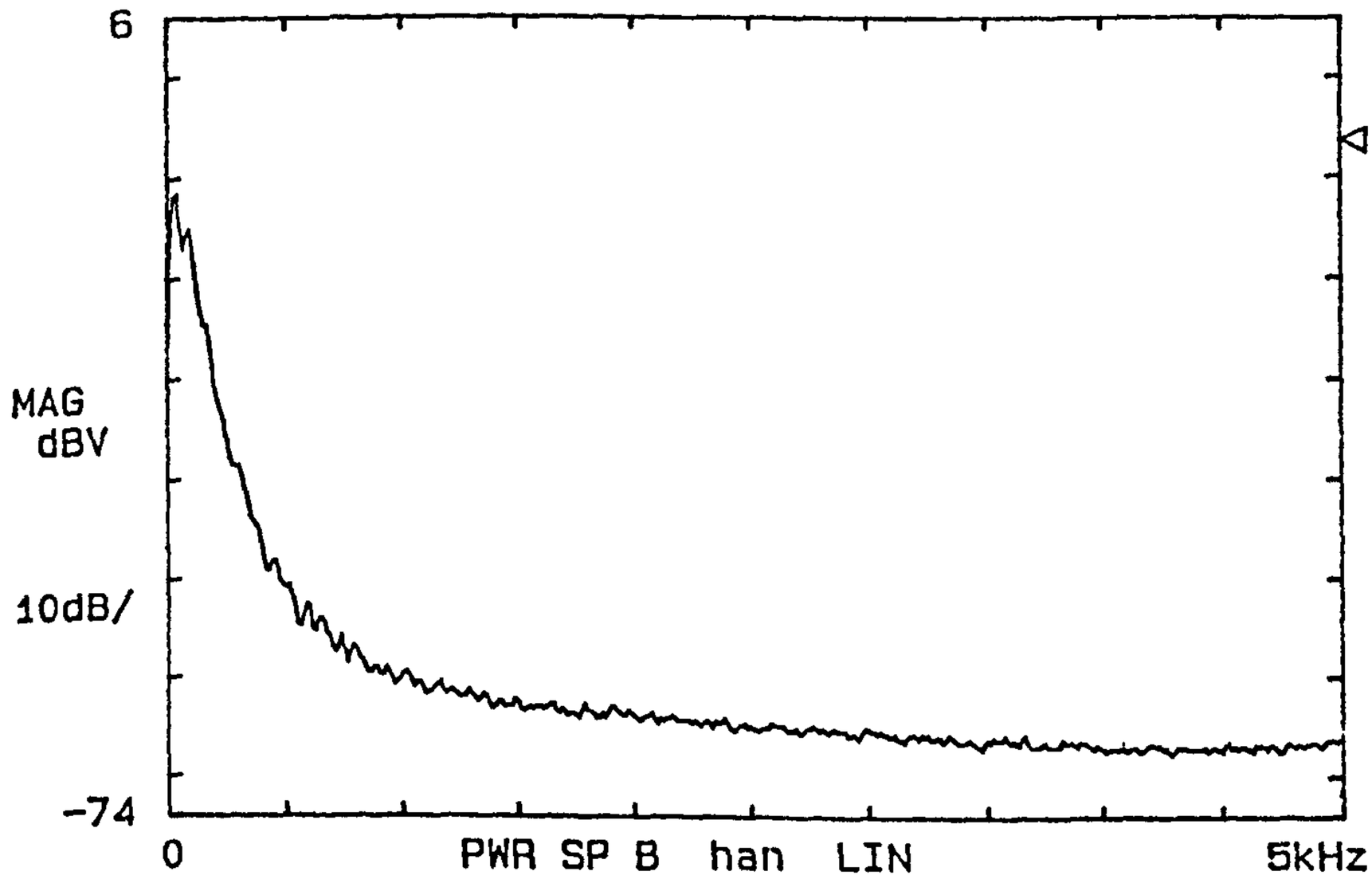

Figure 9.7 (b): Frequency spectrum of the charge distribution at a flow velocity of 3 m/s without the relaxation tank in the flow rig.

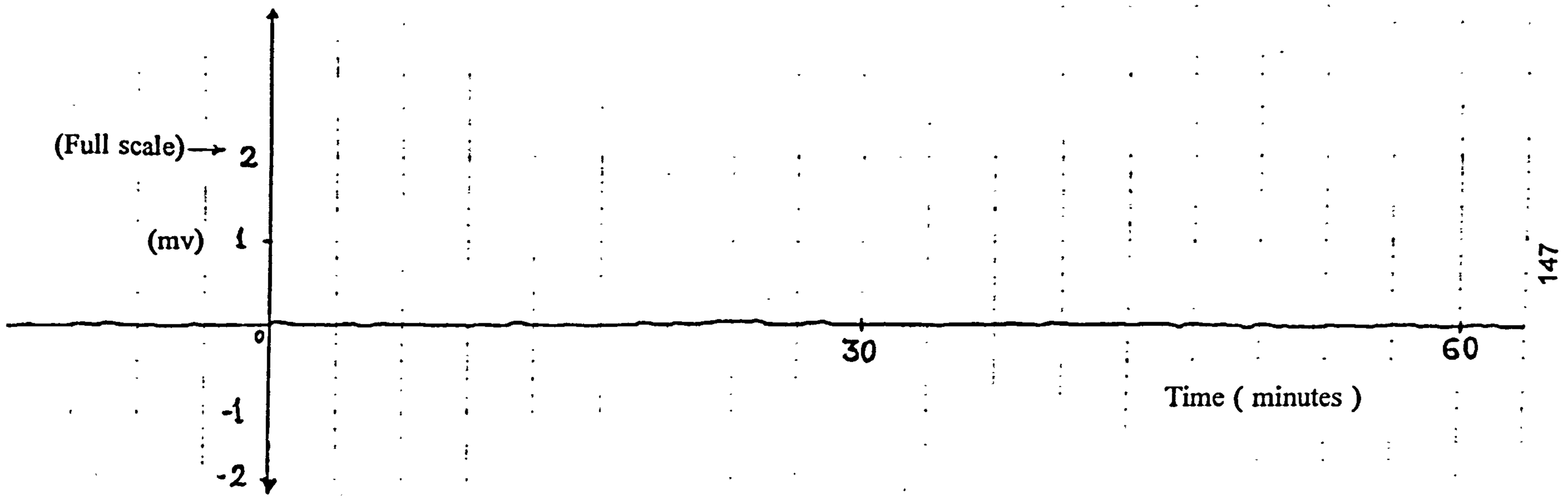

Figure 9.8: The chart record of the zero stability of the meter
(chart recorder type: OMNISCRIBE B5216-2).

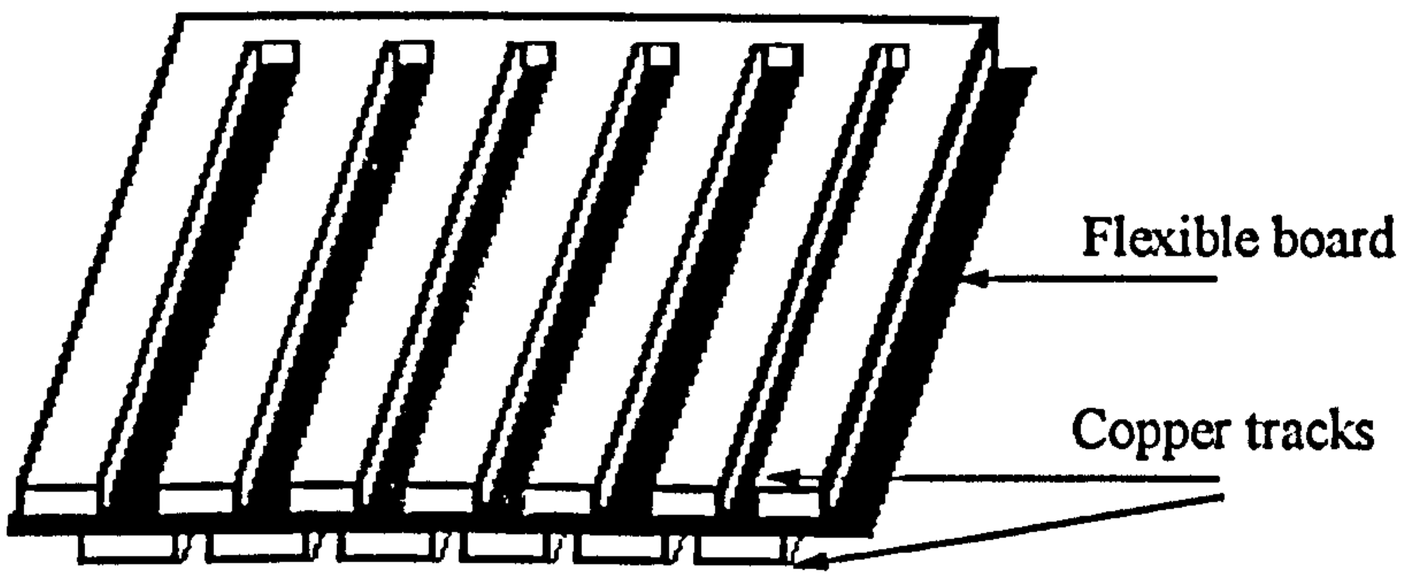

Figure 10.1: Schematic of the recommended pcb design for improved eddy current free electrostatic shield

APPENDIX A

COVERING LETTER AND QUESTIONNAIRE FOR MARKET SURVEY

14th December 1993

(Address as per-envelope)

Dear Sir,

I am currently undertaking a PhD in the above department at Cranfield Institute of Technology. The project I am involved in is concerned with the development of an Electromagnetic Flowmeter for "non-conducting" or insulating liquids.

The enclosed questionnaire is concerned with the types of flowmeter used in industry to measure the flowrate of insulating and moderately conducting liquids.

As I am interested only in the information you provide, identification of your company is not necessary. However, I would be more than happy to make the findings of this survey available to you if you require them. All findings distributed up on request will be anonymous.

If you have any queries or comments I can be contacted on Bedford (0234) 750111 Ext. 5414.

May I thank you in advance for your cooperation.

Yours faithfully

Ted Amare

Enc.

FLOWMETERS MARKET SURVEY

This questionnaire is divided in to two sections. Section **I** contains only two questions about your company and product whereas section **II** refers to your flowmeters.

Please tick the box to indicate your answer. If there is more than one answer for a particular question, please tick appropriately. You may tick **"Other"** and write down your answer on the space provided if it is not one of the choices given.

I About your company and product

1 Please indicate what sector of industry you are in ?

Petroleum/oil/gas ☐

Food/drink ☐

Chemical ☐

Water ☐

Mineral ☐

Other _____ ☐

2 Please give an indication of the types of liquids for which you monitor the flowrate;

Hydrocarbons (petroleum products) ☐

Cryogenics or liquified gases ☐

Vegetable/animal oil ☐

Water ☐

Milk ☐

Other _____ ☐

II About your flowmeters

Please note the letters that identify the type of flowmeter you use in question 1 below, and just write down the letter when answering the rest of the questions.

1 Please indicate the types of flowmeters used by your company;

A - Differential pressure (DP) ☐

B - Positive displacement ☐

C - Turbine or Rotary inferential ☐

D - Fluid Oscillatory ☐

E - Ultrasonic ☐

F - Mass ☐

G - Electromagnetic ☐

H - Other _____ ☐

2 Please fill in the following table for your flowmeters; if it is difficult to give the exact figures please give an estimate or range of values.

Flowmeter and Liquid type	Quantity	Flowrate (l/s)	Pipe diameter (inch)	Age (years)	Frequency of maintenance (months)	Purchase cost (£)	Annual running cost

3 Is maintenance conducted by in house personnel?

Yes ☐ No ☐

If yes please indicate the level of competence required to complete the work;

Flowmeter type	skilled	semi-skilled	un-skilled

4 Please give an estimate of the following features for your flowmeters using the notation below; the bracketed ones are for the last column (Ease of operation).

Very Low	(Very difficult)	1
Low	(Difficult)	2
Medium	(Not difficult)	3
High	(Easy)	4
Very high	(Very easy)	5
Don't Know		6

Flowmeter type	Accuracy	Reliability	Confidence	Ease of operation

5 Please rate the following factors in your order of importance when purchasing a new flowmeter;

1 = Low **6** = High

Accuracy ☐

Brand loyalty ☐

Price ☐

Maintenance ☐

Recommendation ☐

Reliability ☐

Other _____ ☐

Thank you for completing the questionnaire.

Please tick box if you would like a copy of the results of this survey. ☐

APPENDIX B

THEORY OF ELECTROMAGNETIC FLOWMETERS

Equations to describe the dynamics of an *electromagnetic flowmeter can be derived* from the general equations governing the electrodynamics of a moving medium. The basis of these general equations are Maxwell's equations which are:

$$\nabla \cdot \underline{B} = 0 \qquad (1)$$

$$\nabla \cdot \underline{D} = \rho \qquad (2)$$

$$\nabla \times \underline{E} = -\frac{d\underline{B}}{dt} \qquad (3)$$

$$\nabla \times \underline{H} = \frac{d\underline{D}}{dt} + \underline{J} \qquad (4)$$

The constitutive equations when the medium is at rest are assumed to be

$$\underline{D} = \varepsilon\varepsilon_o \underline{E}, \qquad \underline{B} = \mu \underline{H}, \qquad \underline{J} = \sigma \underline{E} \qquad (5)$$

where ε , μ and σ are constants. The constitutive equations when the medium is moving with a velocity v and $v^2/c^2 \ll 1$ or $v^2/c'^2 \ll 1$ (where $c = 1/\sqrt{(\varepsilon_o \mu_o)}$ and $c' = 1/\sqrt{(\varepsilon\varepsilon_o\mu)}$) are

$$\underline{D}=\varepsilon\varepsilon_o\underline{E}+K\underline{v}\times\underline{H} \qquad 6$$

$$\underline{B}=\mu\underline{H}-K\underline{v}\times\underline{E} \qquad 7$$

$$\underline{J}=\sigma(\underline{E}+\underline{v}\times\underline{B})+\rho\underline{v} \qquad 8$$

$$K=\varepsilon\varepsilon_o\mu-\varepsilon_o\mu_o \qquad 9$$

For derivation of equations 6 to 8 refer to Panofsky and Phillips (1955) and also Al-Rabeh, Baker and Hemp (1978).

If polarization P and magnetization M are defined by

$$\underline{P}=\underline{D}-\varepsilon_o\underline{E} \qquad 10$$

$$\underline{M}=\left(\frac{1}{\mu_o}\right)\underline{B}-\underline{H} \qquad 11$$

and are rearranged to give D and H respectively, then from equation 4

$$\nabla\times\underline{B}=\mu_o\left(\underline{J}+\frac{d\underline{P}}{dt}+\varepsilon_o\frac{d\underline{E}}{dt}+\nabla\times\underline{M}\right) \qquad 12$$

However, if low conductivity liquids are assumed to have $\mu=\mu_o$, then from equations

6, 7, 9, 10 and 11

$$\underline{M}=\underline{P}\times\underline{v}+\frac{1}{\varepsilon}(\varepsilon\varepsilon_o-\varepsilon_o)\underline{v}\times(\underline{v}\times\underline{B}) \qquad 13$$

Since the magnitude of the term $\frac{\mu_o}{\varepsilon}(\varepsilon\varepsilon_o-\varepsilon_o)\underline{v}\times(\underline{v}\times\underline{B})$ in equation 13 is much less than

B in equation 12, it can be ignored. Therefore equation 12 can be rewritten as

$$\nabla\times\underline{B}=\mu_o(\underline{J}+\frac{d\underline{P}}{dt}+\varepsilon_o\frac{d\underline{E}}{dt}+\nabla\times(\underline{P}\times\underline{v})) \qquad 14$$

which is the starting point for Cushing's analysis.

Taking the divergence of equation 14 and substituting for J and P gives

$$\nabla\cdot(\sigma(\underline{E}+\underline{v}\times\underline{B})+\rho\underline{v}+\varepsilon_o(\varepsilon-1)\frac{d(\underline{v}\times\underline{B})}{dt}+(\varepsilon\varepsilon_o+\varepsilon_o)\frac{d\underline{E}}{dt})=0 \qquad 15$$

If v is steady, E and B are sinusoidal in time with angular frequency ω and the fluid is incompressible (*i.e.* $\nabla\underline{v}=0$ so $\nabla\cdot(\rho\underline{v})=0$ in the two-dimensional case), equation 15 can be written in complex terminology (after rearrangement):

$$\nabla\cdot((\sigma+j\varepsilon_o\varepsilon\omega)\underline{E})=-\nabla\cdot((\sigma+j\varepsilon_o(\varepsilon-1)\omega)\times(\underline{v}\times\underline{B})) \qquad 16$$

where $j = \sqrt{-1}$.

To prescribe a definite flowmeter configuration, the following assumptions are made:

(1) - The flow pipe is circular with an interior radius a ;

(2) - The rms value of the magnetic field B is constant both in magnitude and direction;

(3) - The flow profile is symmetrical with respect to the axis of the pipe, and the direction of flow is everywhere parallel to the axis of the pipe (thus $v_z = v(r)$), also $v(a) = 0$;

(4) - The electrical properties of the fluid are homogeneous with dielectric constant of ε and conductivity of σ ;

(5) - The idealized detecting electrode configuration will be such that the electrodes contact the fluid along the lines $(r, \theta) = (a, 0)$ and $(r, \theta) = (a, \pi)$.

Because of the symmetry of this case, we have a two-dimensional problem (refer to figure 3.2). The flow is everywhere in z direction and there is no gradient of any quantity in the z direction. Hence, equation 16 simplifies to

$$\nabla \cdot \underline{E} = -Z \nabla \cdot (\underline{v} \times \underline{B}) \qquad 17$$

where Z is as defined in equation 3.2 to 3.4 (chapter 3).

Expressing E as a negative gradient of potential u , expanding $\nabla \cdot (\underline{v} \times \underline{B})$ (Kolin, 1945) and noting that in this configuration $\underline{B} \cdot (\nabla \times \underline{v}) = B \frac{dv(r)}{dr} \cos\theta$ leads to the general expression for the flow signal of an electromagnetic flowmeter as given in equation 3.1.

APPENDIX C

THE SOURCE CODE FOR THE C-PROGRAM FOR ANALYSIS OF THE DESIGN OF CIRCUILAR COILS.

```
/*  start  */

#include <stdio.h>
#include <math.h>

#define   PI  3.14159

main()
{
 float x,y,z,d,g,a,f,b,r;
 FILE *afile,*bfile;

if((afile = fopen("a:\\dis.vl","w+")) == NULL)
 {
   printf("fopen failed 1 \n");
   exit(0);
 }

if((bfile = fopen("a:\\sum.bvl","w+")) == NULL)
{
   printf("fopen failed 2 \n");
   exit(0);
```

```
}


r=0.0;
x = 2.0*PI*1.5*pow(10.0,-7.0);
z = pow(0.055,2.0);

for(a=0.033;a<=0.1;a=a+0.001)
  {
     fprintf(afile,"%1.3f\n",z);


      y=pow(a,2.0);
      d=z+y;
       g=pow(d,3.0);
       f=sqrt(g);

      b=(x*y)/(f);
      r=r+(30*b);


      fprintf(bfile,"%1.4f\n",b);
  }

fclose(afile);
fclose(bfile);

printf("\n\n\n\nWire diameter = 1mm\n\n");
printf("Number of turns on each coil = 2000 \n\n");
printf("Applied current = 1.5A\n\n");
```

```
    printf("For Z = 0.055m \n\n");
    printf("Field strength for one coil = %fT\n\n",r);
   r=2*r;
   printf("Field strength for two coils = %fT\n\n\n",r);

}
```

APPENDIX D

THE SOURCE CODE FOR THE C-PROGRAM TO ANALYSE THE SENSITIVITY FORMULA OF THE METER.

```
/*  start  */

#include <stdio.h>
#include <math.h>       /* compiler functions declearation */

#define  PI  3.141592
#define  eo  8.854e-12
#define  Eoi 2.0        /* Dielectric constant of oil */
#define  Soi 5.6e-11    /* Conductivity of oil */
#define  B   0.01       /* magnetic field in Tesla */
#define  a   0.0215     /* Inside pipe radius */
#define  V   2.0        /* Velocity of flow */
#define  N   10000      /* Number of sum elements */

double z_cal(double w1);
double R_cal(double w2,double s,double e);       /* function declearation */
double sum(double ew,double b1,double angle);

main()
  {
    double w,Ew,Sw,f1,Z,R,S,A,F,b;
    double q,g,h,Vo;
```

```
    int c1,c2;

     c1=1;

do
     {
       printf("Please type wall Diel. constant =\n");
      scanf("%lf",&Ew);

      printf("\nPlease type wall conductivity =\n");
      scanf("%lf",&Sw);

      printf("\nPlease type the frequency =\n");
      scanf("%lf",&f1);

       printf("\nPlease type outside radius =\n");
       scanf("%lf",&b);

       printf("\nPlease type the Angle in radians =\n");
       scanf("%lf",&A);

      w=2*PI*f1;       /* angular frequency and flowrate calculation */
       F=PI*a*a*V;

       Z=z_cal(w);
       R=R_cal(w,Sw,Ew);  /* Z and R calculation */

            S=sum(Ew,b,A);    /* summation result */
```

```
q=(F*B*Z)/(2.0*b);
 g=(a/b)*(a/b)*(R-1);
 h=R/((R+1)-g);

 Vo=q*h*S*sin(PI/A);     /* output voltage calculation */

    printf("Output Voltage = %g mv\n\n",(Vo*1000));

    printf("Do you want to repeat ?  (1 or any)\n");
    scanf("%d",&c2);
    if(c2!=1)
      c1=2;

}while(c1<2);

   }

/* Function to calculate Z */

double z_cal(double w1)
    {
       double bet,bo,bot;
       double alph,z5;
       struct complex z7;

       bet=(w1*eo)/Soi;
       bo=(w1*eo*Eoi)/Soi;
```

```
bot=bo*bo;
z7.y=bet/(1+bot);

alph=(bet*bet)*Eoi*(Eoi-1);
z7.x=(1+alph)/(1+bot);
z5=cabs(z7);
        printf("z5=%f \n",z5);
        return(z5);
    }

/* Function to calculate R */

double R_cal(double w2,double s,double e)
     {
double x1,x2,r;
double y1,y2,z1,z2;

x1=Soi*Soi;
y1=Eoi*eo*w2;
y1=y1*y1;
z1=x1+y1;

x2=s*s;
y2=e*eo*w2;
y2=y2*y2;
z2=x2+y2;
```

```
  r=sqrt(z1/z2);

  printf(" R=%f\n",r);
  return(r);

}
/* Function to calculate the summation */

double sum(double ew,double b1,double angle)
  {
     double x,y,u,v,s1,s;
     int m,n;

     m=0;
     s1=0;

do
  {
     n=(2*m)+1;

     x=pow((a/b1),((double)n*2))*(ew-Eoi);
     y=((ew+Eoi)-x)/((ew+Eoi)+x);
     v=(1/(double)n)*sin((double)n*(PI/2))*sin((double)n*(PI/angle));
     u=y*v;
     s1=s1+u;
     m=m+1;
```

```
    }while(m<N);

    s=1/s1;
    printf("sum= %g\n",s);
    return(s);
}
```